Technical Progress Report: Year 3

Targeting Reserve Growth Opportunities in the Northern Gulf of Mexico Basin: Transferring Secondary Gas Recovery Technology to the Offshore Environment

by
L. J. Wood, H. Zeng, M. V. DeAngelo, T. F. Hentz, M. H. Holtz, K. Chan, A. Badescu, C. Kilic, C. Rassi, and D. Zhou

prepared for
National Energy Technology Laboratory
U.S. Department of Energy
P.O. Box 10940, 626 Cochrans Mill Road
Pittsburgh, PA 15236-0940

Bureau of Economic Geology
Scott W. Tinker, Director
The University of Texas at Austin
Austin, Texas 78713-8924

October 2001

CONTENTS

TABLES

FIGURES

16. Root-mean-squared (RMS) amplitude map from the F Sand interval extracted from the 3-D seismic data set over the study area. The thin orange lines are down-to-the-southeast normal faults. Several stratigraphic incised distributary-channel leads are pointed out, including the Lead 3 opportunity. This accumulation (bright red) is limited on its west side by shaly (dark) facies. Seismic section A–A' shown in figure 14.

17. Gamma-ray and resistivity log from Well 206 drilled by Texaco in 2001 to test the Lead 3 stratigraphic trap. Note the sharp-based upward-fining signature of the stacked channel-fill sands and the high resistivity in the top of the unit denoting gas saturation.

18. Root-mean-squared (RMS) amplitude map of the B sand reveals subtle stratigraphic features in Starfak field that may be associated with a large incised-valley system. Tiger Shoal field indicates that there is little or no sand associated with this reservoir interval. Farther to the east of the study area, there are clear indications of incised-valley sands and incised-valley-fill sands; however, most have been penetrated by previous drilling.

19. Root-mean-squared (RMS) amplitude map of the G sand interval depicting a depositional environment dominated by shales. No leads were generated from this map.

20. Root-mean-squared (RMS) amplitude map of the H sand interval depicting an incised-valley system that dominates the saddle area between Lighthouse Point field and Mound Point field. Additional valley-fill sands are evident throughout the eastern half of the study area. Starfak field has amplitudes indicative of shale-dominated sequences.

21. Root-mean-squared (RMS) amplitude map of the J sand interval illustrating few features of interest. One prospect was identified on this map, a fault-bounded graben with a significant strong amplitude anomaly in the North Lighthouse field. Tiger Shoal field is interpreted to be dominated by deep marine sediments at this interval.

22. Root-mean-squared (RMS) amplitude map of the L sand illustrating a prominent lowstand incised-valley system traversing Lighthouse field and the saddle area between Starfak and Tiger Shoal fields. In addition, several sinuous features in the east portion are interpreted to be remnants of an ancient fluvial system. Tiger Shoal shows little evidence of reservoir-quality sand deposits. Two structural prospects are associated with deeper "rollover" features on the downthrown (hanging wall) side of a first-order growth fault.

23. Root-mean-squared (RMS) amplitude map of the M sand revealing a large lowstand incised valley system dominating the Tiger Shoal field and the adjacent saddle area to the west, providing two excellent prospects missed by previous drilling programs. Similar features pervade the Mound Point field; however, these features have already been exploited. Starfak field has several sinuous features that meander through the area. Each of these features needs to be examined closely for hydrocarbon potential.

24. Root-mean-squared (RMS) amplitude map of the N sand interval illustrating massive depositional sequences dominating the northern two-thirds of the study area. Syndepositional subsidence along the first-order growth faults probably contributed to the creation of accommodation for the thick, lowstand-deltaic sands.

25. Root-mean-squared (RMS) amplitude map of the O sand interval depicting a dominant highstand systems tract that caused significant deposition of sand units through most of the study area. Several prospect were identified in the Tiger Shoal field.

26. Root-mean-squared (RMS) amplitude map of the Q sand interval showing predominantly shale rich environment. The southeastern Amber Complex has several possible deposits (slope fan?) that may prove to be productive.

27. Root-mean-squared (RMS) amplitude map of the R sand interval that may depict the beginnings of a highstand systems tract sequence. Note the "ripples" in the eastern portion of the study area. This feature is indicative of "lap-out" depositional sequences common in this type of depositional environment.

28. Root-mean-squared (RMS) amplitude map of the S sand reservoir system. The depositional environment is indicative of an early highstand systems tract. Note the "rippling" on the eastern extremity of the study area. These features are commonly associated with progradational/retrogradational depositional systems and should be examined carefully for stratigraphic target potential.

29. Root-mean-squared (RMS) amplitude map of the T sand reservoir. Note the incised valley system cutting through Tiger Shoal field. The high amplitudes (red) correspond to thick incised-valley-fill sands, which have already been heavily exploited. However, several additional prospects were located by analysis of this map. The eastern half of the study area is interpreted to dominated by deepwater shales.

30. Root-mean-squared (RMS) amplitude map of the U-sand interval illustrating a late lowstand, incised-valley system that caused deposition of the U-sand in Lighthouse and Tiger Shoal fields. Areas outside this incised valley represent the underlying shaly transgressive sequences incised by this valley.

31. Root-mean-squared (RMS) amplitude map of the V sand that successfully illuminated a prospect in the Tiger Shoal field missed by previous drilling. The strong (red) amplitude characteristics associated with the western half of the study area may outline the extent of the ancient paleoshelf at that time.

32. Root-mean-squared (RMS) amplitude map of the X sand reservoir interval illustrating chaotic depositional patters indicative of a highstand/transgressive systems tract, perhaps at its maximum seaward extent. Amplitudes indicate thick sand sequences in the saddle area between Lighthouse and Mound Point fields. Tiger Shoal appears to have some reservoir-quality sands on the eastern flank. Starfak field, however, is dominated by shale. Significant sands should be encountered in the saddle area between Starfak and Tiger Shoal fields.

33. Root-mean-squared (RMS) amplitude map of the Y sand. Strong amplitudes (red) along the hanging wall (downthrown) are associated with rollover structural features and are excellent prospect targets. The remainder of the study area is pervaded by deepwater shale at this interval.

PLATE (in pocket)

EXECUTIVE SUMMARY

The Bureau of Economic Geology's Offshore Secondary Gas Recovery program is a multi-fiscal year project funded by the U.S. Department of Energy, whose goals are to research new techniques and methods in defining the structure, stratigraphy, and hydrocarbon character in a mature area in the northern Gulf of Mexico and to utilize those multidisciplinary techniques and methods to identify additional gas resources, as well as predict regional trends in hydrocarbon accumulation. PHASES 1 and 2 of the project work plan (PROJECT PREPARATION and DATA GATHERING AND LOADING, respectively) have been completed. PHASE 3 of the plan (DATA ANALYSIS) is ongoing. All key chronostratigraphic surfaces have been mapped in logs, cross sections have been generated, and total thickness and isolith maps have been completed for all systems tracts in the reservoir units within the study area. **Targets for resource additions have been identified and classed into target types, and preliminary resources have been calculated for these targets.** Root-mean-squared amplitude maps have been used to better define opportunities within the internal architecture of larger stratigraphic features. Seven play types recognized within the study area have had their architecture and anatomy detailed. Previous work in the Offshore Gulf of Mexico (Hentz and others, 1997; Seni and others, 1997) defines the regional distribution of these same plays. Integration of project results with these previous DOE/GRI/BEG publications has begun and will lead to understanding of the broader implications of the detailed resource additions assessment done within the study area. The process of transforming the seismic attribute volume into a three-dimensional petrophysical volume is progressing, with excellent results. Development of a fourth-order reservoir flow model has begun within the T sand, a large contributor to resources in the fields. Continual communication between the BEG and the staff of our industry partner, Texaco, has facilitated the exchange of information and ideas to the mutual benefit of both parties, and a jointly authored abstract resulting from this collaboration will be presented at the 2002 Annual Meeting of the American Association of Petroleum Geologists. **The project scientists have submitted several resource addition targets to Texaco for testing, two of which have proven successful.** The project is on track with its projected time line, and it has spawned many research directions beyond its originally defined scope that we believe will add much value to the overall results. The team's 2002 work plan will focus on quantifying the total new resources that exist in, between, or immediately outside the fields of study, sensitivity

testing of several methods for populating the reservoir modeling grid with petrophysical data, evaluating the stratigraphic and deep potential across the area, seismic mapping of third- and fourth-order unconformities, generating an impedance volume from the seismic data to aid in examination of the relationship between seismic attributes and petrophysical properties, generating a detailed 3-D reservoir flow model for the T sand in Starfak field, and **assessing the play types in the study area within the context of the larger play group across the Northern Gulf of Mexico.**

INTRODUCTION

Summary of Project Objectives and Key Accomplishments

The Offshore Secondary Gas Recovery (OSGR) project began October 1998 as a 4-year joint research venture between the Bureau of Economic Geology (BEG), The University of Texas at Austin, and the U.S. Department of Energy (DOE). The project is an outgrowth of a previous DOE-sponsored BEG project that produced the *Atlas of Northern Gulf of Mexico Gas and Oil Reservoirs, Volumes 1 and 2* products (Hentz and others, 1997; Seni and others, 1997). The OSGR project is focused on practical application of products from the Atlas study and providing owners of offshore Gulf of Mexico leases a process road map to increase hydrocarbon reserves and their asset base. Among the multifold goals of the OSGR project are to conduct research in new techniques and methods in defining the structure, stratigraphy, and hydrocarbon character in a major field in the northern Gulf of Mexico and to utilize those multidisciplinary techniques and methods to identify additional gas resources, as well as to predict regional trends in hydrocarbon accumulation. The specific objectives of the project are to (1) increase reserves, (2) prioritize newly identified prospects and development opportunities, (3) develop and apply new technologies, (4) create transferable knowledge, and (5) achieve these objectives with high-quality products in a timely fashion. The objectives of the project will be achieved through completion of a nine-phase work plan and the tasks associated with that work plan (fig. 1 and pl. 1).

The two fields under study are Tiger Shoal and Starfak fields in Vermilion and South Marsh Island Areas, northern Gulf of Mexico (fig. 2). Although originally designed to look at data from a single field, the project has evolved to encompass two fields in detail, as well as to consider surrounding fields of Mound Point, Lighthouse Point, and Amber. This evolution

reflects the desire to consider more regional applicability of research results, to move from the postage-stamp application of research results from a single field to the broader distribution of observations throughout the Gulf of Mexico Miocene. Phases 1 (PROJECT PREPARATION) and 2 (DATA GATHERING AND LOADING) of the project plan have been completed. Principal DATA ANALYSIS (Phase 3) involving mapping of key horizons in seismic and well logs and the outgrowth of new play concepts and ideas in reservoir architecture has also been completed. However, data analysis will continue as production and fluid information are integrated into the design of a reservoir flow simulation for the T1 sand. Stratal slice technology (Zeng and others, 1998a, 1998b, 2001) has proved to be a quick-look tool of great value when bright-spot prospecting for valley fills, a major resource-addition target across the study area. Root-mean-squared amplitude maps have provided a level of stratigraphic detail within these valley fills that has helped reduce the uncertainty in well placement and resulted in the drilling of one very successful well and the proposal of several additional stratigraphic resource addition targets. We are currently constructing approaches to quick-map reservoir bodies within this data volume and generate 3-D visualization of the reservoir/seal system. Ongoing interactions with Texaco's development team resulted in several successful development well proposals and successfully drilled prospects, and our Texaco team members actively participated in our 2000 year end review meeting in Morgantown, West Virginia. Our ongoing interaction has resulted in co-authored publications to be presented at the upcoming 2002 American Association of Petroleum Geologists Annual Meeting in Houston.

The team has achieved our Year-Three project objectives and provided a portfolio of reserve growth opportunities to Texaco to facilitate development of the Starfak and Tiger Shoal fields. Two wells to date have targeted two different reserve growth target classes—

saddle-perched traps and incised channel stratigraphic traps—both of which were successful. A summary of preliminary structurally oriented resource-growth opportunities was included in last year's report. Additional compilation of stratigraphic opportunities is included in this year's report. We have calculated preliminary estimates of resources to be provided by these targets. Biostratigraphic work has shown these targets occurring in seven play types previously defined by Seni and others (1997). Data from the Atlases (Hentz and others, 1997; Seni and others, 1997) are being used to examine the nature of these play types within our study area versus their regional character and, if feasible, to extrapolate many of the resource target types and additions found within our detailed study area to the larger region.

The chart shown in Plate 1 illustrates the current status of technical assessment of the study areas. We have completed definition of the sequence framework down to a fourth-order scale, as well as mapped all the faults observable on seismic and integrated with well data. Net-sand maps have been generated, and production, pressure, and petrophysical analysis has been performed on the T1 interval and used to design and populate a full-scale reservoir model of this productive interval. In addition, all wells have been examined for potential recompletion targets and possible bypassed pay. **Forty-eight resource addition targets have been defined, two of which have been successfully tested by our industry partner, Texaco, proving the viability of these resource addition targets.** Fault-seal analysis has been initiated to add tangible transmissibility information to the 3-D reservoir flow simulation model being built using Roxar software. Several successful approaches have been developed for transforming petrophysical information from the seismic data and importing those data into the grid cells of the developing reservoir model. Biostratigraphic data have been analyzed to frame the existing research results into plays and chronozones that can be translated across a broader regional area using the

existing information contained in the Atlases (Hentz and others, 1997; Seni and others, 1997). Overpressure has been mapped in anticipation of looking at deep resource potential across the study area and making observations that can impact resource potential of deep reservoirs across the northern Gulf of Mexico.

We have compiled specific resource growth opportunities associated with specific play trends unique to Miocene-age systems in the northern Gulf of Mexico. A series of producing-horizon-focused root-mean-squared amplitude maps document the stratigraphic resource addition targets. Resource additions are summarized and will be further assessed in terms of uncertainty and classed accordingly. In addition, **we will commit increasing time to evaluating the upside potential that exists in the deeper strata and deep-water depositional facies of the area.** Modeling has begun in earnest and will define interfield opportunities for resource additions in the T1 sand interval, a incised valley play type in a fourth-order sequence, characteristic of the study area.

GEOLOGIC SUMMARY OF THE AREA

Study Area

Starfak and Tiger Shoal fields are located in offshore Louisiana immediately north of the Salt Deformation Province. Although the area's large-scale structural folds are a product of deep salt movement, geologic conditions in the area are structurally simple compared with the complex diapiric deformation that occurs to the south (fig. 3). The fields are associated with several subregional normal faults and associated antithetic faults that cause additional structural partitioning within these two large fields. The primary foci of this study, Starfak and Tiger Shoal fields, have been owned and operated by Texaco Exploration and Production, Inc., since the late 1950's. Current resource-in-place estimates for Starfak are approximately 316 Bcf gas and 13.3

MMbbl oil, and for Tiger Shoal, estimates are 3.1 Tcf gas and 35.9 MMbbl oil. Reservoirs are Miocene-age facies of coastal plain, shelf, slope, and basin-floor depositional systems stacked in an overall upward-shallowing succession 20,000 ft thick. Sinuous, digitate, and lobate geometries associated with the system's depositional elements are readily apparent on regional horizontal seismic-attribute slices. Abundant wells across the fields (155 total) provide ample quantitative petrophysical, production, and engineering data for constraining seismic and flow-unit correlations, assessing the influence of fluid, lithology, and pressure on seismic and well-log response, and accurately modeling past and future reservoir performance.

Regional Structural Context

Starfak and Tiger Shoal fields are located in the Oligocene-Miocene Detachment Province of the northern Gulf Coast continental margin (Diegel and others, 1995). This region is generally characterized by large-displacement, dominantly down-to-the-basin listric growth faults that sole on a regional detachment zone above the Oligocene section. Either regional deformation is a product of salt mobilization from the level of the autochthonous Jurassic Louann Salt, or the detachment zone for the growth faults represents a salt weld that formerly contained a thick, allochthonous salt body (Diegel and others, 1995). A characteristic feature of this province is the great thickness of deltaic and other on-shelf sediments above the detachment zone, typically exceeding 3 mi. This remarkable stacking of deltaic/shelf sandstone reservoirs helps make this province one of the world's great petroleum provinces.

Regional Stratigraphic Framework

Starfak and Tiger Shoal fields produce hydrocarbons from sandstones in most of the Miocene Series (upper lower to upper Miocene), which in the two fields forms a dominantly regressive, progradational succession as much as 10,000 ft thick (fig. 4). The lower part of the

reservoir-bearing interval (upper lower Miocene) is characterized by approximately 3,000 ft of mostly slope and basinal depositional facies: lowstand basin-floor fan, slope-fan, and lowstand-deltaic-wedge depositional facies. Shale-dominated slope-fan deposits, each as much as about 1,000 ft thick, compose the major portion of this lower zone. At about 13,000 ft, this succession is overlain by a 7,000-ft-thick upper zone of mostly on-shelf and significant, but volumetrically minor, off-shelf lowstand depositional facies that exhibits grossly increasing abundance of sandstone upward (middle and upper Miocene). Cyclic distal highstand, distal transgressive, and lowstand prograding-wedge and distal incised-valley-fill facies in the basal part of this upper zone grade upward into progressively more proximal, cyclic highstand, transgressive, and incised-valley-fill facies. A thick succession of aggradational fluvial coastal plain deposits occurs only a few hundred feet above the reservoir-bearing study interval. This upward-shallowing trend of depositional facies coincides with that of the entire Miocene interval in the offshore northern Gulf of Mexico (Seni and others, 1997).

Further details of the sequence stratigraphic and structural framework, depositional systems, resource distributions, seismic sedimentology, and well-log data conditioning and analysis are contained in the OSGR 1999 Year End Report (Hentz and others, 1999) and OSGR 2000 Year End Report (DeAngelo and others, 2000). **It is the intent of this report to build on the foundation of the previous 2 years** and to discuss the details of integrating the chronostratigraphy and regional atlas results to define play types and examine resource distribution within different plays, to detail ongoing resource addition target work being performed on stratigraphic traps, to document initial resource calculations from preliminary intrafield and infield resource addition targets, to discuss preliminary results in structural and

flow modeling of key reservoir architectures, and to discuss the results of research into seismic-transform-derived petrophysical reservoir properties.

INTEGRATION OF LOCAL AND REGIONAL STRATIGRAPHIC SEQUENCES

Detailed reservoir architecture, resource distribution, and possible resource growth have been the subject of the past 3 years of this current OSGR project. Biostratigraphic analysis completed in the past year has allowed the team to place the strata of this study area and the research conclusions and observations in a regional context using chronozones and play types previously defined in Seni and others (1997). Such understanding broadens the application of these research ideas beyond the immediate study area and can significantly increase their impact on regional resource growth.

Biostratigraphic Analysis for Age and Environmental Determination

We have reexamined the details of the Texaco paleontological reports to (1) more precisely define the range limits of prominent regional extinction horizons and (2) glean all available paleobathymetric data from the comprehensive lists of benthic fossils. The paleontological reports from 15 wells in both fields indicate that the ~10,000-ft section from the oldest reservoir (*Robulus* L-8 sand) at the base of the study interval to the Pliocene/Miocene boundary just above the uppermost reservoir (A sand) represents ~11.2 m.y. of deposition and ranges in age from latest early Miocene (~17.3 m.y.) to the end of the Miocene (~6.1 m.y.). These figures are revised from those previously reported in Hentz and others (1999) and DeAngelo and others (2000). Ages of regional biozones in our study were initially derived from Lawless and others (1997), who used the time scale of Berggren and others (1985); we have now converted these ages to the updated chronology of Berggren and others (1995).

We identify 14 regional Gulf of Mexico foraminiferal biozones (Picou and others, 1999) within the study interval, ranging from the *Cibicides* "38" and *Robulus* "L" zones (~16.5 m.y.) in third-order Cycle 9 to the *Robulus* "E" zone (~6.1 m.y.) at the top of the Miocene Series (figs. 5 and 6). No regional biozones occur in Cycle 10. However, lower Miocene strata in deep wells in nearby North Light House Point and Mound Point fields (fig. 2) record the regional *Operculinoides* zone (extinction horizon of *Robulus* "54-B"), the next oldest regional Gulf of Mexico biozone (at ~18.0 m.y.), occurring ~600 to 700 ft below the base of third-order Cycle 10. In most instances, each biozone is chronostratigraphically well constrained in Starfak and Tiger Shoal fields (figs. 6–8), with ~40 to 100 ft of vertical variance for the position of each zone within the 15 wells having fossil data. However, these zones commonly extend across, or terminate at, the same third- and fourth-order maximum flooding surfaces and the same portions of thick slope-fan and highstand shales within the 15 wells. The regional *Cibicides opima* and *Bigenerina* "B" biozones, both of which extend vertically across third-order sequence boundaries 7 and 2 (Fig. 1), respectively, are not as well constrained, most likely because of changing depositional/environmental conditions coinciding with pronounced basinward shifts in depositional facies above the two major unconformities (Figs. 7 and 8). However, occurrences of both taxa above their "common" zones may also be a result of reworking and redeposition of fossils above these unconformities (= "rare" zones). Because of this uncertainty of the positions of the extinction horizons, these biozones are depicted within chronostratigraphic ranges in figure 5.

A comprehensive list of key paleobathymetric indicator fauna (Picou and others, 1999) enabled reconstruction of water depths during deposition of reservoir-scale fourth-order systems tracts (Table 1). Several of the Texaco paleontological reports include the complete faunal-count

Table 1. Characteristic paleobathymetric indicator fossils (foraminifera) in the Miocene section of Starfak and Tiger Shoal fields (Picou and others, 1999).

Marginal marine
- *Ammonia beccarii*
- *Elphidium* spp.

Inner neritic (0–60 ft)
- *Bifarina vicksburgensis*
- *Buccella hannai*
- *Buccella mansfieldi*
- *Cibicides concentricus*
- *Eponides* spp.
- *Nonionella* spp.
- *Reusella* spp.

Middle neritic (60–300 ft)
- *Bolivina floridana* (rare)
- *Cancris sagra*
- *Cibicides carstensi*
- *Cibicides floridanus*
- *Gyroidina hannai*
- *Uvigerina peregrina* (rare)

Outer neritic (300–600 ft)
- *Ammobaculites nummus*
- *Bolivina floridana* (common to abundant)
- *Chilostomella* spp.
- *Cibicides opima*
- *Gaudryina atlantica*
- *Gyroidina scalata*
- *Liebusella* spp.
- *Pullenia salisburyi*
- *Textularia barretti*
- *Uvigerina altacostata* (rare)
- *Uvigerina carapitana*
- *Uvigerina howei*
- *Uvigerina lirettensis*
- *Uvigerina peregrina* (common to abundant)
- *Valvulinaria* spp.

Upper bathyal (600–1,500 ft)
- *Anomalina alazanensis*
- *Cibicides matanzanensis*
- *Cyclammina cancellata*
- *Liebusella pozonensis*
- *Planulina harangensis*
- *Uvigerina altacostata* (common to abundant)

lists recorded by the well-site paleontologists. Samples were recorded every 30 ft in each well; these lists provide a detailed accounting of fossil assemblages, abundances of individual species in each well, and the major faunal "floods" within the study section. Indicator fossils, which are benthic organisms that lived within narrow ranges of water depth, can then be used to estimate the paleobathymetric conditions under which the sediments containing the fossils were deposited. The vertical distribution of indicator fossils in the study interval (Fig. 9) indicates that deepest water depositional conditions (>600 ft, upper bathyal) are recorded within lowstand slope-fan and basin-floor deposits near the base of the interval in Cycles 9 (Fig. 6) and 10, and within the thick *Cristellaria* "I" and *Bigenerina humblei* shales at and immediately above the two maximum flooding surfaces in the third-order highstand systems tract (HST) in upper Cycle 7 (fig. 8). The indicator fossils show a general upward-shallowing trend, coinciding with the overall regressive stacking pattern of the study interval. Information provided by the indicator fossils also supports our previously reported interpretations of systems tracts and genetic framework (DeAngelo and others, 2000). For example, stacking patterns of HST's and lowstand slope-fan and overlying prograding-wedge sections both comprise thick shales overlain by progradational sandstone intervals. Fossil data indicate that the HST's, deposited on the shelf, accumulated in waters depths less than 600 ft deep—the approximate depth of the shelf edge/top of slope. Slope-fan deposits, however, contain indicator fauna representing significantly deeper water environments (>600 ft).

We have also been able to reasonably approximate water depths recorded by shale intervals within individual fourth-order systems tracts by using a shale-decompaction equation that was derived from the work of Baldwin and Butler (1985):

$$t_d = [(d + t_c)^{1.1575} - (d)^{1.1575}]^{0.86395},$$

where t_d = decompacted thickness of shale, d = depth of shale unit, and t_c = compacted thickness of shale unit.

The equation considers two variables that enable reasonable reconstruction of original mud thickness from present shale thickness: current depth of burial (d) and thickness of the shale unit (t_c). Only the thicknesses of shale units within progradational genetic units (systems tracts) were considered because they represent most of the accommodation space (sea floor to sea level) that was filled primarily by muddy sediments. Possible effects on calculations of paleobathymetry by the volumetrically minor sandstone units that cap the progradational cycles (HST's and slope-fan/prograding wedge complexes [SF/PW]) were not considered. Shale thickness was measured from the marine condensed section to the base of the deltaic/shoreface sandstones of HST's and from the base of the slope-fan deposits (sequence boundary) to the base of the prograding-wedge sandstone of SF/PW's. Because these shale units within genetic depositional cycles represent relatively continuous deposition that was uninterrupted by major fluctuations in relative sea level, they are reasonably accurate records of paleobathymetry.

Calculations of original mud thickness (= approximate paleo-water depth) throughout the study interval generally coincide with water depths recorded by the indicator fossils found within the basal marine condensed section. As an example, a 250-ft-thick HST shale at the top of Cycle 7 (10,100 to 9,850 ft) in Starfak field (Fig. 8) decompacts to an original mud thickness of 469 ft. The marine condensed section forming the base of the shale unit contains outer neritic indicator fossils (table 1). Both lines of evidence suggest water depths between 300 and 600 ft during initiation of this fourth-order HST. Similar calculations made within other portions of the study interval also generally show good agreement, thus supporting our initial interpretations of the genetic framework of the Miocene succession.

Mapping of Systems Tracts

The high-resolution sequence-stratigraphic framework that has been constructed for the Miocene succession in Starfak and Tiger Shoal fields (DeAngelo and others, 2000) allows the precise mapping of individual reservoir-scale (fourth-order) systems tracts. In our study, the characterization of reservoir geometry and thickness, areal distribution, and internal heterogeneities has been one of the primary focuses of the project. Toward this end, we have constructed a series of isochore and net-sand maps for the most productive intervals in the two fields to deduce what depositional controls influenced sand distribution, the nature of sandstone compartmentalization, and the character of potential sealing horizons, such as sequence boundaries (unconformities).

All maps were constructed digitally, and values of interval thickness and net-sand percentage were calculated using an algorithm designed to interface directly with the project's database. The database contains the subsea elevations of all key sequence-stratigraphic surfaces delineated in our genetic framework. Maps depict the thickness and content of reservoir-quality sandstones within systems tracts, not lithostratigraphic (nongenetic) units. This is a key distinction because the integration of the chronostratigraphic bounding surfaces of systems tracts into the mapping process enables the scrutiny of depositionally controlled geometries and internal heterogeneities within reservoirs, thus adding a firmly predictive aspect to reservoir analysis. Isochore maps (unit-thickness maps as measured from well logs in which the structural dip of bedding is not known) were only constructed for lowstand systems tracts (LST's) and highstand systems tracts (HST's) because they contain the only significant accumulations of sand. In HST's, these maps represent the total thickness of the systems tract measured between the maximum flooding surface at the base and the capping sequence boundary. In LST's

(incised-valley fills, prograding wedges), the interval is measured between the sequence boundary at the base and the transgressive surface at the top. In the construction of net-sand maps, we measured sand thickness and quality on all well logs using a 50-percent shale volume (V_{sh}) cut-off value. We generated V_{sh} curves for each well log by standard integration of spontaneous potential and gamma-ray curves and of all sidewall-core petrophysical data.

We have focused on mapping the LST's and HST's within the most productive zone in the study section, the third-order LST in Cycle 7 (fig. 8) to define probable reservoir-scale controls on resource distribution. The map depictions of fourth-order systems tracts are remarkably accurate, as shown by their comparison with amplitude stratal slices (Zeng and others, 2001) of the same stratal zones (fig. 10). **Maps of incised-valley fills exhibit a high degree of variation in sandstone thickness within the valley systems, where sandstones are generally thickest in aligned trends coinciding with the inferred valley axes (fig. 11). Three-way stratigraphic traps form at the updip margin of sandstone thicks where they abut shalier sands.** Lead 3 (see fig. 16) is an example of such a reservoir. Moreover, **the updip margins of valley systems where valley sandstones contact older shaly HST delta-plain strata across unconformities (sequence boundaries) also form a potential trapping mechanism.** Such traps are only revealed by mapping systems tracts. Figures 12 and 13 depict a lowstand prograding wedge and associated incised valley, and the underlying HST into which some of these lowstand deposits are incised, respectively. In some instances, the transition from incised valley to the proximal portion of the equivalent prograding wedge (lowstand delta) appears to form a barrier, perhaps diagenetic, to fluid flow and forms a trap. Note the positioning of producing wells at this transition in figure 12. However, compartmentalization of thick prograding-wedge sandstones within shaly interdeltaic deposits, all overlain by widely

distributed transgressive shales, probably contributes to most hydrocarbon accumulation in these deposits. Underlying HST sandstones (fig. 13) generally form separate reservoir compartments. They are typically more widely distributed and exhibit less sandstone-thickness variability than the LST sandstones. Structural traps appear to form the dominant control on reservoir occurrence in fourth-order HST's. An additional value of net-sand and isochore maps is that they enable us to more precisely calculate reservoir thickness and the areal dimensions of reservoirs within areas of well control, and thus total reservoir volume.

RESERVE GROWTH OPPORTUNITIES

Mapping Methods for Resource Addition Target Analysis

Previous research (Zeng and others, 2001) applied "stratal-slicing" techniques to enhance stratigraphic imaging of complete reservoir containers (for example, valleys) associated with this study area. The **stratal-slicing method can be used for quick reconnaissance of stratigraphic elements imbedded within the 3-D seismic volume** by automating the generation of proportionally spaced surfaces between a few manually picked surfaces. This process can also generate surfaces that are diachronous. Consequently, when attributes (amplitude) are extracted from these surfaces, subsequent attribute maps may not reflect time-equivalent elements and facies. In areas having complex structural and stratigraphic relationships, a more precise interpretation is warranted. **"Stratal-surface" methods are a more targeted approach to resource-addition identification and rely on many carefully picked chronostratigraphic surfaces that pervade the study area.**

Stratal-surface methods

Stratal-surface interpretation techniques were used to determine the spatial distribution of sandstone reservoirs throughout the study area. Stratal surfaces are visibly distinctive,

chronostratigraphic, sheetlike rock units, whose seismic signature parallels the acoustic impedance boundary associated with surrounding rock. Maximum flooding surfaces, typically pervasive throughout the study area, served as excellent "stratal surfaces." These surfaces were subsequently used to define upper and lower extents of stratal-bounded seismic analysis windows (fig. 14). Facies-sensitive seismic attributes were extracted from between the mapped maximum flooding surfaces to generate paleolithologic maps, showing spatial lithological relationships within a specified vertical (geologic time) zone of interest.

RMS amplitudes and prospective areas

Seismic reflection amplitude information can be useful in identifying unconformities, reefs, channel and deltaic sands, lithology, and gas/fluid accumulations. Amplitude anomalies may also be attributed to constructive or destructive interference (tuning effect) caused by two or more closely spaced reflectors as well as to variations in net sand within a thin-bed unit. Root-mean-squared (RMS) amplitudes are calculated as the square root of the average of the squares of the amplitudes found within an analysis window. These **RMS amplitudes are sensitive to sandstone-bearing depositional systems tracts within the reservoir-bearing successions** and help define the spatial distribution of genetically related depositional successions. **RMS amplitude maps may image stratigraphic leads that have been missed by previous exploitation programs.**

Calculating RMS amplitudes between two bounding maximum flooding surfaces generated a map illuminating several depositional elements (fig. 15) associated with the D-Sand, LST reservoir. On this map, a large incised-valley system can be seen traversing the middle portion of the study area. Available well data indicate that this feature has been heavily exploited. The Mound Point field, however, has two promising leads previously overlooked by

exploitation programs. The northernmost lead (lead 1) has a strong amplitude anomaly located on the downthrown block of a second-order growth fault. The associated faults have more than 100 ft of throw, which is most likely sufficient to seal any hydrocarbon accumulations. The second lead (lead 2) is a sinuous feature interpreted to be remnants of an ancient fluvial system. Its strong amplitudes are on the upthrown block and truncate abruptly against a second-order growth fault.

A second RMS amplitude map (fig. 16) of the F sand reservoir interval identified three possible additional leads. A strong amplitude anomaly (lead 3) positioned on the downthrown block of a first-order growth fault is an excellent target. The sand body is interpreted to "shale-out" or terminate before it reaches the first-order growth fault. A prominent dark-blue lineation flanks the west edge of this anomaly and is interpreted to be a shale plug. To the immediate south of lead 3, an additional lead (lead 4) was identified. This lead is characterized by a strong amplitude anomaly bounded to the north by a second-order growth fault. Lead 5 is located in Mound Point field. It is characterized by a strong amplitude anomaly located on a graben feature. This sinuous feature is flanked on the north and south by second-order growth faults.

Testing Stratigraphic Resource Addition Targets

Through an integrated process of sequence stratigraphy, stratal slicing, and stratal-surface analysis, the team developed many opportunities for Texaco to consider as tests for the viability of smaller, incised-distributary, statigraphic traps across the study area. The opportunity titled **lead 3 (fig. 16) was chosen as a drill location for Texaco's 2000 development program.** The lead was initially visible on stratal slices as a low-sinuosity, high-amplitude anomaly thought to terminate updip at the northern-bounding first-order growth fault. However, RMS amplitude mapping better defined the internal geomorphology and imaged a shaly portion of the fill,

limiting the updip extent of the reservoir prior to the fault, thus defining a true stratigraphic trap. **Well results at the amplitude depth indicate a sharp-based, upward-fining, gamma-ray signature interpreted to represent a 50-ft-thick package of basal fluvial fill overlain by an upper portion of estuarine fill (fig. 17). The upper 21ft of the reservoir interval was gas filled, producing 3,500 Mcf/d with no condensate.** Volumetrics subsequent to drilling indicate that the reservoir extent is truly limited to the north and west by lithologic pinch-out, suggesting that RMS amplitude maps are an accurate indicator of reservoir extent. **Total resources for this stratigraphic trap are calculated at 6.4 Bcf oil and gas in place and probable reserves of 5.7 Bcf.**

A series of RMS amplitude maps were generated for key reservoir unit horizons to identify possible stratigraphic traps associated with these producing intervals. These maps are detailed in figures 18 through 35. They show more than 20 new stratigraphic resource addition targets.

Resource Additions

Many preliminary resource addition opportunities were identified and detailed in the 2000 Year End Report for Offshore Secondary Gas Recovery (DeAngelo and others, 2000). These targets include rollovers, bright spots terminated against faults, flat spots, untested fault blocks, faulted anticlines, and pure stratigraphic traps. The 2001 focus was on additional deep structural/stratigraphic combination resource addition targets and stratigraphic potential for untapped resources across the region. **Twenty-four additional opportunities have been added to the portfolio, bringing the total number of opportunities to 47.** Table 2 shows the size and depth of resource addition opportunities currently identified within the study area. Average net reservoir thickness shown on the right-hand side of the table was measured using an estimated

Table 2. Resource addition opportunities within the study area.

Target #	Unit	Size (acres)	Estimated Depth (ft)	Average Net Pay (ft)	At-Certainty Estimate OGIP (Bcf)
19A	B	110	6130	30	2.4
18	Y	120	12350	35	3.2
8	Y	215	12200	50	8.1
42	Y	280	12200	45	9.5
10B	V	45	11180	55	1.9
41	V	60	11160	55	2.5
7	T	195	10340	60	9.0
10A	T	90	10380	65	4.5
3	Robl2/4	85	14250	40	2.6
44	Robl 8	500	14150	40	15.4
6	Robl 6	60	14100	40	1.8
43	Robl 4	130	13180	40	4.0
4	Robl 4	65	14400	30	1.5
9	Robl 4	120	14500	30	2.8
12	Robl 2	215	12300	25	4.1
17	Robl 2	390	12500	30	8.9
16	Robl 2	420	13400	50	16.1
5	Robl 2	250	14150	30	5.8
21	Q	395	11080	40	12.0
15	Q	295	9590	20	4.6
35	Q	112	11180	40	3.4
2	Q	50	11230	20	0.8
36	Q	145	11260	30	3.3
34	Q	65	11810	30	1.5
32	O	125	9380	45	4.3
31	O	255	9590	45	7.8
11	O	430	9340	45	14.9
33	O	240	11150	35	6.4
30	N	220	10480	25	4.2
29	N	300	9375	35	8.1
28	M	142	9750	45	4.9
27	M	315	8180	40	9.7
26	M	145	8220	40	4.5
25	L	250	7970	30	5.8
1	L	550	7680	20	8.4
14	L	155	8720	40	4.8
13	L	50	8765	30	10.9
19B	J	130	7750	20	2.0
39	H	60	7560	20	0.9
40	H	100	7715	25	1.9
24	F2	665	8550	45	23.1
23	F1	410	7080	30	9.3
22A	F1	385	7240	30	8.8
38	D	490	6880	30	11.1
22B	D	300	6925	30	6.8
37	D	83	7000	30	1.9
20	12000a/b	85	14550	20	1.3
					291.7 Bcf Total

thickness from the seismic data. **Resource additions calculated at certainty for these defined targets total more than 291 Bcf.** Ongoing work will continue identifying additional targets, as well as assessing the technical risk associated with these opportunities.

"PLAY-TYPE" CLASSIFICATION FOR UPSCALING RESEARCH RESULTS

The Gas and Oil Atlases of the northern Gulf of Mexico (Hentz and others, 1997; Seni and others, 1997) examine productive areas in the northern Gulf of Mexico to evaluate reservoirs by grouping them into play types. Grouping reservoirs into play types offers several advantages. Because of their relatively similar geological, engineering, and production characteristics, **reservoirs within the same play tend to have similar production and ultimate recovery growth (URG) patterns**. These patterns of better known, mature reservoirs may be extrapolated with relative confidence to newly discovered reservoirs within the same play. Moreover, production and URG responses to technology may be determined for a representative reservoir and results readily transferred to the larger family of reservoirs that constitute the play. Additionally, knowledge gained from plays can assist in the future exploration for similar reservoirs (Galloway and others, 1983). The Offshore Secondary Gas Recovery research attempts to apply these principles by examining the internal anatomy and production characteristics of several play types, examining their similarities and differences, identifying nontraditional targets associated with them and pinpointing those characteristics that affect reserve distribution and ultimate recovery from them. These observations can then be upscaled through the hierarchy of play types developed in the 1997 atlases.

Play Types in the Study Area

On the basis of the atlases of the northern Gulf of Mexico (Hentz and others, 1997; Seni and others, 1997), we can classify reservoirs in Starfak and Tiger Shoal fields into several play types.

As defined in these atlases, **plays are broad groupings of reservoirs based on depositional style from gross stacking pattern (aggradational, progradational, retrogradational) and the chronozone in which the reservoirs occur**. This approach is necessary to aggregate basinally distributed reservoirs having broadly similar characteristics within a manageable organizational scheme. This process enables the observations and processes defined within a smaller study area to be more broadly applied to regional resource addition issues.

The 10,000-ft upper-lower through upper Miocene succession in the two fields comprises seven middle and upper Miocene plays, five progradational and two retrogradational (table 3). Rock successions in the progradational plays, typically several thousand feet thick, consist of repeating upward-coarsening intervals representing primarily regressive depositional systems. In contrast, backstepping progradational intervals grouped into a broadly upward-fining succession characterize the retrogradational plays, which are typically several hundred feet thick. These successions are further divided into chronozones based on key extinction horizons within the middle and upper Miocene section (table 1). Primarily fourth-order onshelf highstand and lowstand incised-valley sandstones form the framework of the progradational plays in the two fields (2,000 to 6,000 ft). The much thinner (100 to 500 ft) and more localized retrogradational plays are successions of third-order LST's and overlying transgressive systems tracts (TST's) that collectively grade upward from thick fourth-order lowstand-wedge and incised-valley sandstones to thinner and finer grained strandplain/deltaic sandstones. Thick shales of third-order TST's and overlying HST's form regional sealing units across the fields, significantly influencing hydrocarbon distribution. Hydrocarbons reside in fourth-order LST's, TST's, and HST's in all plays within the two fields, although **about 93**

percent of total hydrocarbons have been produced from third-order LST's (DeAngelo and others, 2000).

Table 3. Play types within Starfak and Tiger Shoal fields based on play designations of Hentz and others (1997) and Seni and others (1997). Note that the two fields share four plays in four different chronozones.*

Starfak

UM1 P.1B	Lower Upper Miocene Eastern Progradational Sandstone
MM9 P.1B	Upper Middle Miocene Central Progradational Sandstone
MM7 P.1B	Middle Middle Miocene Eastern Progradational Sandstone
MM4 P.1	Lower Middle Miocene Progradational Sandstone

Tiger Shoal

UM3 R.2	Upper Upper Miocene Eastern Retrogradational Sandstone
UM3 P.1B	Upper Upper Miocene Eastern Progradational Sandstone
UM1 P.1B	Lower Upper Miocene Eastern Progradational Sandstone
MM9 P.1B	Upper Middle Miocene Central Progradational Sandstone
MM7 R.1B	Middle Middle Miocene Eastern Retrogradational Sandstone
MM7 P.1B	Middle Middle Miocene Eastern Progradational Sandstone
MM4 P.1	Lower Middle Miocene Progradational Sandstone

*Biostratigraphic limits of chronozones:

UM3: extinction horizons of *Discorbis* "12" (base) and *Robulus* "E" (top).
UM1: extinction horizons of *Bigenerina* "2" (base) and *Discorbis* "12" (top).
MM9: extinction horizons of *Bigenerina humblei* (base) and *Bigenerina* "2" (top).
MM7: extinction horizons of *Amphistegina* "B" (base) and *Bigenerina humblei* (top).
MM4: extinction horizons of *Discorbis* "B" (base) and *Amphistegina* "B" (top).

Hydrocarbon Distribution within Plays

Detailed sequence-stratigraphic analysis clarifies the reservoir framework of these plays and enables a focused strategy of exploitation, particularly in mature fields such as Starfak and Tiger Shoal. Hydrocarbons that have been produced from the fields reside is a variety of different traps

(DeAngelo and others 2000); most of these are structural in nature, being the easiest to image using seismic data. We believe that abundant **undiscovered resources will lie in stratigraphic traps formed by (1) updip pinch-outs of incised-valley sandstones within shaly highstand strata, (2) local diagenetic pinch-outs of late highstand sandstones that are capped by tight (sealing) zones formed by possible pedogenic cementation formed during lowstand exposure, (3) a variety of potential subregional sandstone pinch-outs within lowstand prograding wedges, (4) updip pinch-outs of lowstand basin-floor-fan sandstones within slope-fan shales, and (5) updip pinch-outs of locally well-developed sandstones within channel-levee complexes of thick lowstand slope-fan successions.** It is significant that no lower Miocene plays are defined for the Starfak/Tiger Shoal study by Seni and others (1997) for this interval even though many of the recent exploration efforts have been concentrated in those deep (>15,000-ft) strata. This observation is consistent with data recently compiled by the Minerals Management Service (2001) that show that only 5 percent of all wells drilled on the Gulf of Mexico shelf have penetrated strata below 15,000 ft, in which there is an estimated 10.5 Tcf of deep-gas recoverable resources.

FY2002 will compare the characteristics of plays found in the research area with the characteristics of the same play in the larger northern Gulf of Mexico area utilizing regional information compiled in the Atlases. These observations will form the foundation for uncertainty in extrapolation of play types, trends, and resource addition results derived within the study area.

RESERVOIR CHARACTERIZATION OF STARFAK T1 RESERVOIR

The Starfak T1 reservoir is being studied to broaden our understanding of Miocene water-drive gas reservoirs. This reservoir is composed dominantly of sandy facies and is located just below a thick regionally extensive shale. This stratigraphic position is optimal to

ensure rigorous, high-certainty correlation and definition of the T1 interval, both in well logs and in seismic data.

The Starfak T1 reservoir represents a reservoir that has undergone a complete production history. As of October 2001, production has been terminated in this reservoir. This means that the **cumulative production from the reservoir is equivalent to the ultimate commercial production,** implying that the ultimate recovery efficiency can be deduced from studying this reservoir. Additional detailed study could result in a determination of the volumetric sweep efficiency due to the aquifer drive.

Determining Reservoir Architecture

The architecture of the Starfak T1 reservoir is defined by the spatial position of faults and stratigraphic surfaces. The detailed position of faults has been interpreted from the integration of 3-D seismic, well-log curves, and fluid levels. The initial study-area-wide interpretation of first-order faults was built upon to interpret smaller scale second- and third-order faulting that can significantly affect reservoir production behavior. An amplitude stratal slice map was integrated with a map of initial fluid levels to identify possible sealing faults within the T1 reservoir. Fluid-flow communication was interpreted to be nonexistent among wells where fluid levels were inconsistent between the wells. Fluid-flow boundaries where drawn on the fluid-level map as a result of this interpretation. This map was then overlain by an amplitude stratal slice map of the T1 interval. Amplitude striations, or boundaries shown on this map, were investigated for compatibility with previous fluid-flow boundaries interpreted from the fluid-level map. Anomalies common to the two maps were then analyzed and classed into fault boundaries or depositional architecture boundaries. Fault boundaries identified were then used to check the accuracy of fault picks in the seismic and were sometimes used to extend the fault reach

upsection beyond the resolution of the seismic. This approach led to an ability to extend the fault interpretation beyond the reach of conventional seismic using an integrated approach that incorporated the engineering production data.

The T1, 3-D reservoir model is being constructed in three stages: (1) building the fault model, (2) generating structural surfaces, and (3) integrating the faults and surfaces to construct a 3-D, geocellular structural model. Below is a detailed, stage-by-stage description of the procedures for building this model, using the IRAP RMS reservoir modeling software provided by Roxar.

3-D Fault Modeling

The first step in constructing the 3-D structural model is building a consistent fault model. In IRAPRMS, the fault model consists of a set of fault surfaces along with their associated fault lines. The aim of fault modeling in this program is to build a fault model in which all structural surfaces are consistent with the fault surfaces and each pair of fault lines match the upthrown and downthrown side of the corresponding structural surface. The following inputs and procedures were used to build a consistent fault model for all the various faults that penetrate the maximum flooding surface 30 (MFS30) to maximum flooding surface 32 (MFS32) stratigraphic intervals within the Starfak study area. The resulting fault model was (1) first used to ensure proper stratigraphic modeling of the T1 and T2 structural surfaces in the faulted areas and (2) later incorporated into the 3-D modeling grids to allow accurate reservoir volume calculation.

Input

Three-dimensional fault modeling requires preparation of three input data sets. First, the MFS30 and MFS32 well picks for the 47 wells within the Starfak study area were loaded into the

Landmark OpenWorks database. Second, MFS30 and MFS32 depth surface grids that honor both seismic data and well observations were created in and subsequently exported from Landmark Z-MAP Plus. Third, the fault segments for fault EW4, D2, D3, D15, D20 created in Landmark SeisWorks were converted into depth fault sticks and stored in the OpenWorks database. The input data used in the fault-modeling step thus consist of the following:

- MFS30 and MFS32 depth surface picks.
- 2-D depth surface grids of MFS30 and MFS32.
- Five sets of depth fault sticks.

Modeling steps

The following paragraphs document the step-by-step process flow involved in building the 3-D T1 reservoir model. They are listed in their order of occurrence from first to last.

- Import 2-D depth surface grids (500 by 500 ft grid in Z-MAP Plus *ascii* format) for MFS30 and MFS32 into IRAP RMS.
- Reduce lateral extent of the imported surfaces to that of the RMS project.

  (for this project Xmin = 1717500 ft; Xmax = 1747500 ft; Ymin = 269150 ft; Ymax = 299150 ft)
- Load MFS30 and MFS32 depth surface picks into the RMS project directly from Landmark OpenWorks database.
- Load depth fault sticks of EW4 (as shown in fig. 36), D2, D3, D15, and D20 into IRAP RMS directly from Landmark OpenWorks database.
- Display and edit the fault sticks as necessary, using the 3-D line editor in IRAPRMS.
- Grid the fault surfaces based on the fault sticks (gridding algorithm = smooth; grid increment = 500 ft).
- Generate the MFS30 fault lines for EW4, D2, D3, D15, and D20, using the IRAPRMS Fault Modeling tool, which is illustrated in figure 37. This tool creates a pair of parallel cutoff lines located on opposite sides of the fault and arrives at the MFS30 upthrown and downthrown fault lines by extrapolating both cutoff lines onto the fault surface(algorithm = smooth extrapolation; cutoff line's distance to fault = 500 ft).
- Use the same method to generate the MFS32 fault lines for all the faults.
- Display and edit the fault lines as necessary, using the Fault Editor tool and 3-D Line Editor in IRAPRMS.
- Re-grid the fault surfaces based on the modified fault lines and fault sticks

  (gridding algorithm = horizontal; grid increment = 100 ft).
- Re-grid MFS30 and MFS32 surfaces using the Mask Method gridding algorithm

(grid size = 100 by 100 ft; total grid nodes = 301 column * 301 rows = 90601).

- Re-generate the MFS30 and MFS32 fault lines for EW4, D2, D3, D15, D20, using the new fault surfaces and structural surfaces

  (algorithm = horizontal extrapolation; cutoff line's distance to fault = 500 ft).
- Truncate fault D2 against the older and larger fault, EW4, as depicted in figure 38

  (adjust radius = 500 ft).
- Adjust MFS30 and MFS32 surfaces to the EW4, D2, D3, D15, D20 fault lines

  (influence radius = 1000 ft).
- Use the Surface Editor in IRAPRMS to manually edit the inconsistent surface grids near the faults.
- Adjust the resulting faulted surface grids to the corresponding depth surface picks of the 47 wells within the Starfak study area.
- Use the Horizon Administration tools in IRAPRMS to check whether MFS30 and MFS32 surfaces overlap with each other (especially at the fault planes) and, if necessary, adjust them to be internally consistent.

Output/results

The main product of the fault-modeling step is a consistent fault model of the EW4, D2, D3, D15, D20 fault surfaces and their associated fault lines. In addition, this step also results in revised MFS30 and MFS32 structural surfaces (see fig. 39) that are consistent with both the fault model and the top picks from well logs.

Surface Modeling

The second step in constructing the T1 3-D reservoir model is generating the T1 structural surface (defines the top of the 3-D structural model) through the use of stratigraphic modeling tools in IRAPRMS. In essence, stratigraphic modeling in IRAPRMS is a process by which seismically interpreted surfaces and geologically modeled isochores are amalgamated together for a perfect fit and then become the stratigraphic framework of the reservoir. This process uses *interpreted* horizon surfaces (such as MFS30 and MFS32), geological isochores, and/or surface picks from well logs as the main input. In addition, it also takes into account the generated fault model (as discussed in the previous section) to ensure accurate architectural

modeling in the faulted areas. The results are new *calculated* horizon surfaces, which result from the addition and/or subtraction of isochores from the associated interpreted horizons.

A top surface for the T1 reservoir was built. All well-log T1 picks were reviewed and refined to be consistent with the top of the reservoir interval. Kelly-Bushing heights were reviewed and adjusted. Deviation surveys on nonvertical wells were checked for accuracy. Combining these T1 well picks with the seismically defined MFS30 and MFS32 surfaces resulted in an integrated stratigraphic architectural framework for the T1 reservoir interval.

Surface model input

The surface modeling procedures use two sets of input data. The first set of input data consists of the revised MFS30 and MFS32 *interpreted* horizon surfaces (see fig. 40) and the integrated structural model derived from the previously discussed fault modeling process. The MFS30, T1, T2, MFS32 top picks for 47 wells within the Starfak study area provide the second set of input data that are necessary for modeling the T1 and T2 *calculated* horizon surfaces.

Modeling steps

The following are a series of detailed steps used to model the stratigraphic horizons T1 and T2.

- Use the Horizon administration tools in IRAPRMS to insert an empty T1 calculated horizon between the MFS30 and MFS32 interpreted horizons.
- Use the same tool to insert an empty T2 calculated horizon between MFS30 and MFS32.
- Load the T1 top and T2 well-log top picks into IRAPRMS directly from the Landmark OpenWorks database.
- Run the Stratigraphic Modeling process in IRAPRMS to calculate and build T1 and T2 horizon surfaces, using the following settings:
    - ❖ Select MFS30 to MFS32 as the interval to be modeled.
    - ❖ Specify the T1 top and T2 top surface picks as part of the main input used in stratigraphic modeling.

- ❖ Set isochore correction method = correct proportional.
- ❖ Toggle "use well correction" ON, setting algorithm = cosine expansion.
- ❖ Toggle "use fault" ON, to allow accurate stratigraphic modeling in the faulted areas.

- Examine the resulting T1 and T2 structural surfaces in RMS 3-D display window and, if necessary, use RMS Surface Editor to manually edit the inconsistent surface grids near the faults.
- Use RMS Horizon Administration tools to check whether MFS30, T1, T2, and MFS32 surfaces overlap with one another (especially at the fault planes) and, if necessary, adjust them to be internally consistent.

Output/results

The surface modeling procedures described above result eventually in the final MFS30, T1, T2, MFS32 structural surfaces that, as shown in figure 41, are consistent with both the structural model and the corresponding well-top picks.

Quality control measures

To ensure the accuracy of the final T1 surface, the T1 top pick of each well was carefully scrutinized for accuracy and consistency before being loaded into IRAPRMS. Following stratigraphic surface modeling, the final stratigraphically *calculated* T1 surface was contrasted with an equivalent seismically *interpreted* T1 surface to show how well they match with each other and thereby provide a second quality check on the well-pick-based interpolated surface.

The T1 seismic surface used to triangulate the stratigraphic modeling results was derived from a set of 3-D seismic T1 picks (fig. 42) that honored both the well observations and the seismic trend throughout most of the study area. Since, as figure 43 indicates, the T1 stratigraphic and seismic surfaces match closely with each other except in areas where there are no seismic data present, the final T1-model-interpolated surface can be considered a reasonably accurate representation of the "real" T1 surface that defines the top of the T1 3-D reservoir model.

Building the 3-D Grid Model

The third step in constructing the 3-D structural model is building the 3-D grids for the T1 reservoir on the basis of the structural model and the final T1 and MFS32 surfaces. These two surfaces will define the 3-D zone inside which all detailed 3-D reservoir modeling is done. The 3-D grids thus created describe the 3-D reservoir volume and provide the framework for Year 4 modeling of petrophysical and facies parameters to populate grid cells.

Input

The 3-D modeling of the T1 reservoir structure uses output from the previous two modeling steps as input. Specifically, this modeling step requires as input both (1) the final T1and MFS32 surfaces resulting from the surface interpolation process and (2) the consistent structural model created in the fault modeling step.

Modeling steps

The following paragraph provides a step-by-step description of the process by which a three-dimensional grid model is built. The steps from first to last are

- Use the Create Zone tools in RMS to create a new 3-D zone bounded between the T1 and MFS32 surfaces
- Use the Create Modeling Grid tool in RMS to build the 3-D grids that describe the volume within the 3-D zone defined above, using the following settings:
  - ❖ setting T1 as the top reference surface and MFS32 as the bottom reference surface.
  - ❖ grid type = corner point; rotation = 0.
  - ❖ grid X increment = 100 ft; grid Y increment = 100 ft; cell thickness = 2 ft.
  - ❖ set cell truncation = truncate cells against bounding surfaces.
  - ❖ Toggle on "Use faults" and activate "incorporate fault throw in 3D grid."
- Examine the resulting 3-D structural grids in IRAPRMS 3-D display window and use the IRAPRMS Show/edit Cell Content utility to display and/or edit the x, y, z values of the 3-D grids.

Output/results

The final result of the above modeling steps is a 3-D geocellular structural model of the reservoir volume bounded by the T1 and MFS32 surfaces. In this model, the T1 reservoir structure is represented as a 300 rows × 300 columns × 171 layers 3-D volume, composed of more than 10 million 100 × 100 × 2 ft 3-D cells. Because the 3-D grid cells bordering the fault planes are regularized cells that retain their rectangular shape in the modeling process, the resulting fault planes in the 3-D model look like a set of slanted staircases overlying the original smooth surfaces of the input fault model.

Plans in Year 4 of the Offshore Secondary Gas Recovery project are to explore various methods for deterministically populating grid cells with petrophysical and facies data, to add more stratigraphic complexity to the grid framework, and to explore the impact of varying transmissibilities on the flow structure.

ENGINEERING WATER-DRIVE RESERVOIR: CASE STUDY OF THE T1 SAND

Water-Drive Gas Reservoirs

Water-drive gas reservoirs, such as the T1 Reservoir, are by their very nature plagued throughout their life by water encroachment. Water that maintains reservoir pressure will migrate toward or "encroach" upon production wells, often trapping residual gas behind the invading waterfront. These effects reduce the volume of gas that will be produced, as compared with conventional pressure depletion. Also, as water volume flowing into the well bore increases, loading can eventually occur, which will effectively kill the free flow of gas, resulting in down time, sporadic well production, costly well maintenance, and ultimately, abandonment of the well. Additionally, high volumes of produced water can increase disposal costs, rendering a well

uneconomic. Careful planning, design, reservoir characterization, and well handling are needed to maximize gas recovery when aquifer encroachment occurs.

Aquifer encroachment decreases ultimate recovery in gas reservoirs. Typical gas reservoir pressure depletion can have recovery efficiencies ranging from 0.75 to 0.9, whereas aquifer-drive recovery efficiencies are typically in the range of 0.5 (MacKay, 1994, Grab and Smith, 1987). Ancell and Manhart, 1987, reported a recovery factor of 0.65 in a 9,100-ft Texas Frio reservoir, and Hower and others (1992) reported a 0.489 recovery for a Gulf of Mexico Miocene reservoir.

U.S. gas reservoir production trends display a similar character of lower recovery efficiency for aquifer-drive reservoirs. For all pressure-depletion-drive reservoirs in the United States the mean ultimate recovery efficiency is approximately 0.74 (fig. 44), according to data compiled by the Department of Energy's Gas Information System (GASIS). The distribution of ultimate recovery displays a tail ending at around 0.5 with some outliers at 0.1 and 0.2. These outliers are probably due to data busts within a public database, as they lie outside the 5 percent delimiting range. In contrast to the pressure-depletion distribution, the aquifer-drive gas reservoirs display a mean ultimate recovery efficiency of 0.67 (fig. 45). The distribution is bimodal with a group centered around 0.5 and another around 0.9. The high-recovery grouping is interpreted to be due to incorrectly distinguishing between aquifer drive and pressure-depletion drive in the public database or from underestimating the original gas in place.

Aquifer and hydrocarbon reservoir characteristics and production history govern water encroachment, and understanding these factors is critical to optimizing oil and gas recovery. The main aquifer attributes that influence hydrocarbon recovery are aquifer size, pressure, and geologic character. Size and pressure characteristics affect the pressure support

transmitted to the hydrocarbon reservoir. The larger the aquifer size relative to the hydrocarbon reservoir (dimensionless radii), the greater and longer the pressure support and the lower the recovery efficiency. A greater pressure differential between the aquifer and a depleting gas reservoir can reduce ultimate recovery. Recovery efficiencies for gas reservoirs and aquifers at lower initial pressures will be less affected by aquifer encroachment, whereas higher pressure systems may result in more rapid water encroachment (Agarwal and others, 1965). Permeable and homogeneous aquifer/gas reservoir systems undergo more rapid water encroachment at higher reservoir pressures and thus have lower gas recovery efficiency. Also, higher residual gas saturation resulting from pore geometry and higher relative permeability to water will lead to lower recovery efficiency. High residual oil saturation occurs when pressure depletion is not uniform in the oil leg and when the oil has high viscosity relative to the encroaching water. Overall, characteristics that promote water influx and decrease a reservoir's incremental pressure cause lower recovery efficiency.

Production history also influences aquifer encroachment. An increased gas production rate can result in an increased recovery of gas (Agarwal and others, 1965; Matthes and others, 1973; Lutes and others, 1977). An increased production rate often leads to greater pressure depletion before wells water out and thus results in greater gas recovery. The performance parameters proposed by Hower and Jones (1991) illustrate the interrelationship between gas flow rate and reservoir characteristics. High production rates, however, must be designed so that no coning or fingering occurs. Relative permeability and residual gas saturation are important considerations in the effectiveness of higher production rates. Permeability, relative permeability, and residual gas saturation characteristics affect the broadness of the pressure gradient between gas reservoir and aquifer. A broad pressure gradient will increase the water-

invaded zone and result in a larger volume of trapped gas. Oil recovery is increased when reservoir pressure depletion is uniform. Uniform pressure depletion reduces water fingering and, thus, bypassed oil as the aquifer water front encroaches.

T1 Reservoir Production Character

The production history of the T1 reservoir displays the strong influence of aquifer influx. The **reservoir has undergone four pulses of production as wells have been completed and produced in separate fault blocks within the reservoir** (fig. 46). Each production pulse is characterized by declining gas production rate along with a contemporaneous water production increase. The first pulse of production came from wells 50 E1, 50 B2, and 50 B1. These wells produced from the southernmost fault block in the reservoir and produced for an average of 6 years from 6/1/78 to 6/7/84. Water production steadily increased after 1 year of production and essentially killed any steady gas production after 3 years.

The next pulse of production came from wells producing in the next fault block north. These wells, including 31-19 and 31-1, produced for about 7 years. These wells also experienced a steady gas production decline and a steady water production increase. A third pulse came from well 31-11 producing at the high point on the "31" fault block. Well 31-11 experienced a short production life of less than 2 years with steady gas production decline and water production increase. The fourth and last pulse of production came from well 30-5 positioned in a fault block farthest to the north up against a major regionally extensive, first-order normal fault. This well saw just over 2.5 years of declining gas production and increasing water production. **It is clear from the production history of relative reservoir pressure depletion that aquifer encroachment is controlling production character.** This conclusion infers that **it is likely that only slightly more than half of the original gas in place has been produced, leaving a large**

gas resource behind. Ongoing reservoir modeling is designed to enhance production of these bypassed resources and provide a process by which future development can be designed to mitigate such bypass.

POPULATING RESERVOIR MODELS WITH PETROPHYSICAL PROPERTIES

Designing petrophysical models is the first task in integrating reservoir architecture and fluid-flow trends. Salient petrophysical properties include porosity, permeability, residual gas/oil saturation, capillary pressure, formation resistivity factor, wettability, relative permeability, and initial water saturation. The goal in designing petrophysical models is to devise methods for determining storage capacity, flow capacity, and hydrocarbon pore volume at the smallest common geological scale. Several methods for populating reservoir grid designs with petrophysical properties are being considered by the team, and their efficiency and accuracy are being researched.

The Modeling Approach

Petrophysical properties are interdependent. Porosity has been related to residual gas saturation, permeability, capillary pressure, and relative permeability such that all petrophysical properties are interrelated. This interrelationship will be applied in the 3-D geocellular model such that each petrophysical property will have the proper value relative to another for each cell in the model. In the following description the models to calculate properties are described, as well as their interrelationship with porosity.

Residual gas saturation controls the volume of gas trapped in the portion of the reservoir that has experienced water encroachment. As water moves into a rock volume filled with gas, the water displacement of the gas is incomplete. The water fills pores and pore throats, causing capillary pressure and relative permeability effects to stop the flow of gas and allow only

water to pass through the rock volume. This results in gas being trapped behind the encroaching water front as residual gas. The volume and location of the residual gas is controlled by the distribution of the petrophysical properties. To determine how to minimize the residual gas saturation in water-drive gas reservoirs, reservoir simulation is being performed on the Starfak T1 sandstone reservoir.

A robust model of residual gas saturation was developed from field and published data. A strong relationship is documented between increasing porosity and decreasing residual gas saturation (fig. 47). The trend is linear, and the best fitting equation is given below in Equation 1

Equation 1: $S_{or} = -0.9696\phi + 0.5473$

Where Sor = Residual gas saturation (fraction)
ϕ = porosity (fraction)

The relationship between porosity and permeability was determined by generating a best-fit equation between the two properties. A conventional crossplot of porosity vs. permeability displays a strong exponential fit with less than one order-of-magnitude variation (fig. 48). Permeability ranged up to a high end of 1 Darcy at 0.3 porosity and a low end of 1 millidarcy (md) at 0.14 porosity. Permeability can be predicted from Equation 2:

Equation 2: $k = 0.0027e^{41.794\phi}$

Where k = permeability (md)
ϕ = porosity (fraction

Capillary pressure character displays a consistent change with permeability. As permeability increases the capillary pressure, entry pressure decreases, the curves become more convex, and the irreducible water saturation decreases (fig. 49).

The limited capillary pressure data can be grouped into high-, medium-, and low-permeability categories. Averaging the capillary pressure data on the basis of their permeability values derives the following reservoir-quality groups. The capillary pressure curve representing less than 10 md became the lowest rock-quality group, followed by curves averaged between 10 and 100 md making up the medium-rock-quality group, and finally, curves representing greater than 100 md making up the high-rock-quality group. The resultant average capillary pressure curves are illustrated in Figure 50.

Such rock-quality grouping allows end-point saturations to be determined for the range of rock quality. Table 4, shown below, summarizes the petrophysical properties of each defined group. Porosity was calculated from the aforementioned porosity–permeability relationship applying an average permeability for the rock group. Residual gas saturation was determined from the porosity–residual gas saturation relationship and initial water saturation was obtained from the average capillary pressure curves.

Table 4. Petrophysical properties for the three rock-quality groups defined in this study.

Rock quality class	Porosity average (fraction)	Permeability (md)	Residual gas saturation (fraction)	Initial water saturation (fraction)
Low	**0.17**	**<10**	0.382468	0.46
Medium	**0.225**	**10 – 100**	0.32914	0.24
High	**0.28**	**>100**	0.275812	0.14

The key to a detailed understanding of the salient petrophysical properties in water-drive gas reservoirs is the character of the gas-water, two-phase flow. The gas-water, two-phase flow is dictated by the relative permeability. Because we do not have relative permeability measurements from any T1 reservoir samples, relative permeability curves have been developed by initial water saturation and residual gas saturation end points. These end points were used in a relative permeability model (Cory model) to generate relative permeability curves.

From the end-point saturations and established relative permeability models, high-, medium-, and low-reservoir-quality groups were established for relative permeability. A set of gas relative permeability (krg) and water relative permeability values were then generated for each of the rock groups (fig. 51a, b, c).

Seismic Transform Approach

Quantitative transform of 3-D seismic data into log property volumes can greatly improve sequence-stratigraphic interpretation and reservoir model building. In the Gulf Coast region, however, there are two important issues that need to be addressed before a good log-property inversion can be achieved.

One practical issue is the poor quality of sonic and density logs for most of the Tertiary formations in the region. The unconsolidated nature of sandstone/shale sequences causes serious bole-hole damage that prevents the logging tools from recording correct velocity and density values of the rocks. The problem is especially damaging for old fields like Starfak and Tiger Shoal, where most wells were drilled and logged long before the more advanced logging tools were developed in recent years. **Without high-quality velocity/density data, wavelet extraction would be difficult and unreliable, and an accurate link between acoustic impedance (AI) and log properties is hard to define.** Alternative inversion schemes without wavelet extraction and AI estimation become important and necessary.

The other issue, which is more fundamental for the general inversion problem, is the seismic tuning effect. **Tuning is a major source of ambiguity in the interpretation of poststack seismic data.** For a seismically thin bed ($<\lambda/4$), top and bottom traveltimes cannot be resolved, and independent thickness information is lost (Sengbush, 1961). Numerous publications have discussed using a tuning (amplitude versus thickness or AVTh) curve to

calculate thin-bed thickness (for example, Meckel and Nath, 1977; Neidell and Poggiagliolmi, 1977; Schramm and others, 1977), but the methodology has its limitations because of the required assumption of constant AI contrasts, which implies consistent rock properties (most commonly, porosity). More realistically, amplitude is a function of impedance × thickness. Solving for AI and thickness separately from amplitude is an underdetermined problem. For example, to solve for AI in any poststack inversion scheme, a priori information on thickness is needed. Ambiguity is merely translated to uncertainty in guessing the thickness between wells. Additional, independent data are needed to reduce the degree of freedom within the problem.

Neural Network-Assisted Multiattribute Analysis

One of the promising developments in reservoir-property inversion in recent years is the use of **a multiattribute transform to predict log properties** (Schultz and others, 1994; Russell and others, 1997; Zeng and Kerans, 2000; Zeng and others, 2000; Hampson and others, 2001; Zeng and others, 2001). Directly exploring the correlation between a log property (for example, porosity) and multiple seismic attributes at well locations, shown by the following equation:

$$\text{Log property} = C_1*\text{Attribute}_1 + C_2*\text{Attribute}_2 + \ldots + C_n*\text{Attribute}_n,$$

where $C_1 \ldots C_n$ are constants, has many advantages over conventional inversion procedures. Directly exploring the correlation between a log property (for example, porosity) and multiple seismic attributes at well locations. This method has many advantages over conventional inversion procedures. It can be used to map log properties without previous knowledge of impedance; it makes use of far more seismic measurements (attributes) beyond a single amplitude trace; and there is no need to extract a seismic wavelet. A multiattribute transform can be built either as a linear, multivariable regression problem or as a nonlinear, neural-network problem. The **neural-network approach is preferred because it can achieve**

higher resolution with smaller error. After multiple tests, a generalized forward-feed model was selected as the neural-network training model (fig. 52). The training was conducted by using NeuroSolutions (commercial software from NeuroDimension, Inc.).

Amplitude-versus-Frequency-Based Detuning

A new seismic attribute, **amplitude versus frequency (AVF), can be used to reduce the tuning effect in log-property inversion** (Zeng and Kerans, 2000; Zeng and others, 2000; Zeng and others, 2001). Conventional approaches of inversion and attribute analysis only make use of the dominant frequency of seismic data, other frequency components (both low and high frequencies) being mostly masked and unused. In a synthetic example (fig. 53) of a thin-wedge model, only one amplitude tuning curve (AVTh) can be observed for a wavelet of fixed dominant frequency. Expanding the relationship to include multiple wavelets having different frequencies creates multiple AVTh's having different tuning points, making it possible to view the relationships from a different angle (AVF). **AVF reveals the relationship between dominant frequency (filter) and reflection amplitude for a certain thickness, which is an extension and supplement to AVTh.** In synthetic study, instantaneous attributes are also controlled by both thickness and frequency.

In practice, **AVF data can be achieved by panel-filtering in the effective frequency range of seismic data that separates different frequency components.** Applying panel-filtering to amplitude and instantaneous attribute traces generates multiple attributes for a single reservoir (fig. 54). Assisted by neural-network training, we make dynamic use of frequency spectra to release additional, independent information in the attributes for seismic data detuning, thus helping to reduce the degree of freedom of any thin-bed inversion problem.

Results

Thirty-five wells in Starfak field were selected for neural-network training. The log property chosen for inversion is volume of shale (V_{sh}, or percentage shale) that is calculated from gamma-ray/spontaneous potential logs in the wells. Volume of shale is an excellent indicator of lithology in the study area because it easily distinguishes clean sandstone (small V_{sh}) from shaly sandstone (intermediate V_{sh}) and shale (large V_{sh}). Volume of shale is also a good indicator of reservoir quality by showing a linear relationship to effective porosity: the smaller V_{sh}, the larger the porosity and the better the reservoir quality. **By exploring directly the relationship between V_{sh} and seismic attributes using a neural network, we avoided wavelet extraction and AI calibration that require accurate velocity/density data, as in a conventional inversion.**

As an example, the result in the A-H sand section in the Miocene Starfak field is shown in figure 55. With nine wells tied to the seismic section, we observed that in the original data (fig. 55a) most sandstones are tied to amplitude trough (red) in character. However, thickness of the sandstones and shales is not very well defined because of tuning. Some very thin sandstones (15 ft or thinner) are simply unresolved. Because of tuning, amplitude is not a good indicator of V_{sh} and shows a very low correlation between the two (R = 0.29 in 35 wells). The inversion (fig. 55b) dramatically improves the result by showing (1) much less tuning effect and more vertical and horizontal thickness changes, (2) higher resolution for very thin sandstones that are otherwise unresolved in the original data, and (3) much better fit between V_{sh} and seismic data (R = 0.72 in 35 wells).

We have conducted similar procedures for the I-M sand, N-O sand, T1-T2 sand, and U-W sand sections, all of which generated satisfactory results that show significant improvement in

reservoir delineation and high-frequency sequence-stratigraphic definition. Future work will be focused on (1) integrating the inversion results to the reservoir modeling in the T1 interval, and (2) reinterpreting some of the high-frequency sequences and systems tracts for better reservoir geometry mapping and risk analysis.

MAPPING THE TOP OF GEOPRESSURE VIA SEISMIC ATTRIBUTES

The Northern Gulf of Mexico has numerous deep reservoir fluid compartments that are overpressured (geopressure), typically characterized by a pressure gradient that exceeds 0.5 psi/ft. Such overpressured conditions in the reservoir have a significant impact on diagenesis of the reservoir rocks, production characteristics of the units, seal qualities, seismic data interpretation, log quality and the overall economics of drilling and production. These compartments are formed when rapid deposition of sediments overtakes the ability of in situ fluids to escape, effectively trapping the fluids that in turn act as support of the surrounding rock matrix. Geopressured formations can be extremely hazardous when abnormally high fluid pressures invade the borehole unexpectedly, potentially leading to loss of control of the drilling process. These **transition zones are identifiable on sonic and density logs as a distinct decrease in velocity and rock matrix density, respectively.** Within the transition zone itself the density and velocity are relatively stable. The characteristics associated with the geopressured formations make it possible to map these transition zones using seismic data. **A variety of seismic attributes can be applied to try to map the sudden change in acoustic impedance (density $\times$ velocity) at the top of geopressure,** which is characterized by strong amplitudes, and the associated "passive" reflectivity expected within the zone of geopressure. One of the tasks in the coming project year will be to expand on our initial efforts to map geopressure using seismic data.

FY 2002 WORK PLAN

The team was very successful in 2001, completing or making significant progress on those tasks outlined in the 2000 Year End Report (DeAngelo and others, 2000). A library of maps, including structure, amplitude, coherency, interval isopach, and net sand, was been created for key reservoir horizons and associated systems tracts using integrated well and seismic data. Production maps, fluid contact maps, and overpressure depth maps are currently being produced. These maps are being used to examine migration pathways into productive zones, to target bypassed pay and other resource addition targets, to build 3-D fluid-flow models for key horizons, to evaluate fault-seal transmissibility and its influence on resource distribution, and to define sand depositional and bypass fairways.

2002 Work Plan

The team's 2002 work plan will focus on quantifying the total new resources that have been defined in, between, or immediately outside the fields of study, sensitivity testing several methods for populating the reservoir modeling grid with petrophysical data, evaluating the stratigraphic and deep potential across the area, seismic mapping of third- and fourth-order unconformities, generating an impedance volume from the seismic data to aid in examining the relationship between seismic attributes and petrophysical properties, generating a detailed 3-D reservoir flow model for the T sand in Starfak field, and assessing the play types in the study area within the context of the larger play group across the Northern Gulf of Mexico. In the course of completing this work plan we will address issues in fault seal and transmissibility, quality of stratigraphically deep reservoirs, seismic inversion, and neural-network-based mapping of depositional elements. We will also examine the broader implication of our research results for regional resource additions in the play types found within our study area.

Deep Reserve Opportunities

A significant section of middle-to-late Miocene deep marine facies across the study area is penetrated by relatively few wells (fig. 4). As part of our complete evaluation of resource addition targets across the study areas we have begun evaluation of the resource potential and trapping mechanisms for gas in these deep (below 15,000 ft subsea) sections. Table 1 shows several identified targets for resource additions in this section. Seni and others (1997) defined no plays for the lower Miocene through this interval, even though many of the recent exploration efforts have been concentrated in those deep (>15,000-ft) strata. Data from the Minerals Management Service (2001) show an estimated 10.5 Tcf of deep gas recoverable reserves may be regionally associated with this interval. **Across the study area, large, deep structures exist below 3.0 s.** First-order normal faults that help form closure on the shallow, large Starfak and Tiger Shoal fields are deep seated. Secondary fault swarms form multiple deep fault traps and untested fault blocks (figs. 56 and 57). The stratigraphically deep reservoir facies within the central planning area are middle to late Miocene-age deep marine fan and slope deposits. **Current research by this team is focused on the controls on the quality of reservoirs below 15,000 ft, trap types, keys to mapping quality reservoir distribution and tools for mapping overpressure from the seismic data.**

Technology Transfer

The goal of the OSGR team in dissemination of research results has been to maximize the exposure of these results through publication in several professional journals and presentation in a variety of formats at multiple meetings to reach as broad an audience as possible. This process has included presentation of oral, poster, and written research results in regional and national/international forums. We have publications or in-press manuscripts and extended

abstracts in three separate refereed journals or volumes that are widely distributed to the geoscience community, including the *Gulf Coast Association of Geological Societies (GCAGS) 2001 Annual Meeting Transactions*, the *Society of Exploration Geophysicists (SEG) 2001 Annual Meeting Transactions*, and the geophysical journal *The Leading Edge*. In 2001 we will deliver oral presentations at the 2001 GCAGS meeting in Shreveport, Louisiana, and 2001 SEG meeting in San Antonio; we have already presented five oral and poster presentations at the 2001 American Association of Petroleum Geologists Annual Meeting in Denver. In addition, we have been invited to present project research results to operators and explorationists at regional associate luncheon's in both Corpus Christi and Houston. To date, this project has resulted in more than 11 oral or poster presentations, 3 extended abstracts, and 3 papers.

Plans for research dissemination in the coming year include the following:

- Teach a short course titled "New Resources from Old Fields: Revitalizing Recovery in the Shelf-Bound Neogene Reservoirs of the Gulf of Mexico," at the 2002 GCAGS Meeting in Austin, Texas, utilizing the visualization facilities at The University of Texas at Austin. This short course will be co-sponsored by the Petroleum Technology Transfer Council.
- Generate summary sheets on key technology applications.
- Complete additional manuscripts for publication in American Association of Petroleum Geologists (AAPG) Bulletin, finalize four student theses from the study area, present three talks at the 2002 AAPG meeting and additional talks at the GCAGS 2002 meeting, and maintain the OSGR Web site.

Offshore Secondary Gas Recovery 2001 publications include the following:

DeAngelo, M. V., and Wood, L. J., 2001, 3-D seismic detection of undrilled prospective areas in a mature province: The Leading Edge, November.

Zeng, H. L., Wood, L. J., and Hentz, T. H., 2001, Stratal slicing of Miocene-Pliocene sediments in Vermilion Block 50-Tiger Shoal Area, offshore Louisiana: The Leading Edge, April.

Zeng, H. L., 2001, From seismic stratigraphy to seismic sedimentology: a sensible transition: Gulf Coast Association of Geological Societies Transactions.

Zeng, H. L., and Zhou, D., 2001, Reducing ambiguity in predicting log properties from multiple seismic attributes by amplitude versus frequency detuning: Society of Exploration Geophysicists Annual Meeting Transactions.

Badescu, A. C., and Zeng, Hongliu, 2001, Integrating 3-D seismic, sequence stratigraphy, and reservoir properties to enhance secondary gas recovery of two major Miocene Gulf of Mexico offshore fields: American Association of Petroleum Geologists Annual Convention, Denver. ***Second-Place Winner in the Student Presentations Session***

Hentz, T. F., Zeng, Hongliu, Wood, L. J., Badescu, A. C., Rassi, Claudia, and Kilic, C. O., 2001, Controls on hydrocarbon distribution within a sequence-stratigraphic framework: a case study from the Miocene of offshore Louisiana: American Association of Petroleum Geologists Annual Convention, Denver.

Rassi, Claudia, and Hentz, T. F., 2001, Production prediction and reservoir characterization of systems tracts of fourth-order sequences in the Miocene offshore Louisiana: American Association of Petroleum Geologists Annual Convention, Denver.

Zeng, Hongliu, Hentz, T. F., and Wood, L. J., 2001, 3-D Seismic expression of high-frequency sequence stratigraphy in Vermilion Block 50-Tiger Shoal Area, offshore Louisiana: American Association of Petroleum Geologists Annual Convention, Denver.

Zeng, Hongliu, Wood, L. J., and Hentz, T. F., 2001, Seismic sedimentology by stratal slicing of fluvial and shallow-marine depositional system in Pliocene, offshore Louisiana: American Association of Petroleum Geologists Annual Convention, Denver.

ACKNOWLEDGMENTS

This publication was prepared with the support of the U.S. Department of Energy, under Cooperative Agreement No. DE-FC26-98FT40136. However, any opinions, findings, conclusions, or recommendations expressed herein are those of the authors and do not necessarily reflect the views of the DOE. As an industry partner, Texaco contributed the well, 3-D seismic and production data. Landmark Graphics Corporation provided software for the basic 3-D seismic interpretation via the Landmark University Grant Program. Roxar contributed the reservoir modeling software.

REFERENCES

Agarwal, R. G., Al-Hussainy, R., and Ramey, H. J., Jr., 1965, The importance of water influx in gas reservoirs: AIME, Journal of Petroleum Technology, Nov., p. 1336–1342.

Ancell, K. L, and Manhart, T. A.,1987 Secondary gas recovery from a water-drive gas reservoir: a case study, SPE paper #16944, Society of Petroleum Engineers, 62d Annual Technical Conference and Exhibition.

Baldwin, Brewster, and Butler, C. O., 1985, Compaction curves: American Association of Petroleum Geologists Bulletin, v. 69, p. 622–626.

Berggren, W. A., Kent, D. V., and Van Couvering, J. A., 1985, Neogene chronology and chronostratigraphy, *in* Snelling, N. J., ed., The chronology of the geologic record: The Geologic Society Memoir No. 10, p. 211–260.

Berggren, W. A., Kent, D. V., Swisher, C. C., III, and Aubrey, M.-P., 1995, A revised Cenozoic geochronology and chronostratigraphy, *in* Berggren, W. A., Kent, D. V., Aubry, M.-P., and Hardenbol, Jan, eds., Geochronology, time scales and global stratigraphic correlation: SEPM (Society for Sedimentary Geology) Special Publication No. 54, p. 129–212.

Chierici, G. L., Pizzi, G., and Ciucci, G. M., 1976, Water drive gas reservoirs: Uncertainty in reserves evaluation from past history: Journal of Petroleum Technology, v. 19, no. 2, p. 237–244.

Diegel, F. A., Karlo, J. F., Schuster, D.C., Shoup, R. C., and Tauvers, R. P., 1995, Cenozoic structural evolution and tectonostratigraphic framework of the northern Gulf Coast

Continental margin, *in* Jackson, M. P., Roberts, D.G., and Snelson, S., eds., Salt tectonics: a global perspective: American Association of Petroleum Geologists Memoir 65, p. 109–151.

DeAngelo, M. V., Hentz, T. F., Wood, L. J., Zeng, Hongliu, and Barba, R. E., Jr., 2000, Targeting reserve growth opportunities in the northern Gulf of Mexico Basin: transferring secondary gas recovery technology to the offshore environment: The University of Texas at Austin, Bureau of Economic Geology, technical progress report: year 2, prepared for U.S. Department of Energy, National Energy Technology Laboratory, under contract no. DE-FC26-98FT40136, 59 p.

Firoozabadi, A., Olsen, G., and Golf-Racht, T. W., 1987, Residual gas saturation in water-drive gas reservoirs. Society of Petroleum Engineers, Paper #16355.

Fishlock, T. P., Smith, B. M., Soper, B. M., and Wood, R. W., 1986, Experimental studies on the waterflood residual gas saturation and its production blowdown: Society of Petroleum Engineers, Paper #15455.

Galloway, W. E., Ewing, T. W., Garrett, C. M., Tyler, Noel, and Bebout, D. G., 1983, Atlas of major Texas oil reservoirs: The University of Texas at Austin, Bureau of Economic Geology, 139 p.

Grab, F. A., and Smith, G. L., 1987, Estimation of oil and gas reserves, *in* Petroleum Engineering Handbook, Society of Petroleum Engineers, P 40-1–40-38.

Hampson, D. P., Schuelke, J. S., and Quirein, J. A., 2001, Use of multiattribute transform to predict log properties from seismic data: Geophysics, v. 66, no. 1, p. 220–236.

Hentz, T. F., Seni, S. J., and Wermund, E. G., Jr., eds., 1997, Atlas of northern Gulf of Mexico gas and oil reservoirs: volume 2. Pliocene and Pleistocene reservoirs: The University of Texas at Austin, Bureau of Economic Geology, 78 p.

Hentz, T. F., Zeng, Hongliu, Wood, L. J., Kilic, Cem, Yeh, J. S., Skolnakorn, Jirapa, and De Angelo, M. V., 1999, Targeting reserve growth opportunities in the northern Gulf of Mexico Basin: transferring secondary gas recovery technology to the offshore environment: The University of Texas at Austin, Bureau of Economic Geology, technical progress report: year 1, prepared for U.S. Department of Energy, Federal Energy Technology Center, under contract no. DE-FC26-98FT40136, 40 p.

Hower, T. L., Bergeson, Intera, Lewis, D. R., 1992, Recovery optimization in a multi-reservoir offshore gas field with water influx: SPE paper #24865, Society of Petroleum Engineers, 67th Annual Technical Conference and Exhibition.

Hower, T. L., and Jones, R. E., 1991, Predicting recovery of gas reservoirs under waterdrive conditions: SPE 1991 Annual Technical Conference and Exhibition, Reservoir Engineering proceedings, SPE #22937, p. 525–540.

Katz, D. L., Legatski, M.W., Tek, M. R., Gorring, L., and Neilsen, R. L., 1966, How water displaces gas from porous media:, Oil and Gas Journal, January 10, p. 55–66.

Lawless, P. N., Fillon, R. H., and Lytton, R. G., III, 1997, Gulf of Mexico Cenozoic biostratigraphic, lithostratigraphic, and sequence stratigraphic event chronology: Gulf Coast Association of Geological Societies Transactions, v. 47, p. 271–282.

Lutes, J. L., Chiang, C. P., Rossen, R. H., Brady, M. M., 1977, Accelerated blowdown of a strong water-drive gas reservoir: Journal of Petroleum Technology, December, p. 1533–1538.

MacKay, Virginia ed., 1994, Determination of oil and gas reserves: Petroleum Society of the Canadian Institute of Mining, Metallurgy and Petroleum, Calgary Section, Petroleum Society Monograph #1 p. 361.

Matthes, G., Jackson, R. F., Schuler, S., and Marudiak, O. P., 1973, Reservoir evaluation and deliverability study, Bierwang field, West Germany: Journal of Petroleum Technology, January, p. 23–30.

Meckel, L. D., Jr., and Nath, A. K., 1977, Geologic considerations for stratigraphic modeling and interpretation, *in* Payton, C. E., ed.: Seismic stratigraphy: American Association of Petroleum Geologists Memoir 26, p. 417–438.

Minerals Management Service, 2001, The promise of deep gas in the Gulf of Mexico: Minerals Management Service, U.S. Department of the Interior, OCS Report MMS 2001-037, 4 p.

Neidell, N. S. and Poggiagliolmi, E.,1977, Stratigraphic modeling and interpretation—geophysical principles and techniques, *in* Payton, C. E., ed., Seismic stratigraphy: American Association of Petroleum Geologists Memoir 26, p. 389–416.

Russell, B., Hampson, D. P., Schuelke, J., and Quirein, J., 1997, Mutiattribute seismic analysis: The Leading Edge, v. 16, p. 1439–1443.

Picou, E. B., Jr., Perkins, B. F., Rosen, N. C., and Nault, M. J., eds., 1999, Gulf of Mexico basin biostratigraphic index microfossils: a geoscientist's guide, foraminifers and nannofossils, Oligocene through Pleistocene: Gulf Coast Section of the Society of Economic Paleontologists and Mineralogists Foundation, Parts I and II, 215 p. + 3 charts.

Schramm, M. W., Jr., Dedman, E. V., and Lindsey, J. P., 1977, Practical stratigraphic modeling and interpretation, *in* Payton, C. E., ed.: Seismic stratigraphy, American Association of Petroleum Geologists Memoir 26, p. 477–502.

Schultz, P. S., Rosen, S., Hattori, M., and Corbett, C., 1994, Seismic guided estimation of log properties, parts 1, 2, and 3: The Leading Edge, v. 13, p. 305–310, 674–678, and 770–776.

Sengbush, R. L., Lawrence, P. L., and McDonald, F. J., 1961, Interpretation of synthetic seismograms: Geophysics, v. 26, no. 2, p. 138–157.

Seni, S. J., Hentz, T. F., Kaiser, W. R., and Wermund, E. G., Jr., eds., 1997, Atlas of northern Gulf of Mexico gas and oil reservoirs: volume 1. Miocene and older reservoirs: The University of Texas at Austin, Bureau of Economic Geology, 199 p.

Zeng Hongliu, Backus, M. M., Barrow, K. T., and Tyler, Noel, 1998a, Stratal slicing, part I: realistic 3-D seismic model: Geophysics, v. 63, no. 2, p. 502–513.

Zeng, Hongliu, Henry, S. C., and Riola, J. P., 1998b, Stratal slicing, part II: real seismic data: Geophysics, v. 63, no. 2, p. 514–522.

Zeng, Hongliu, Hentz, T. F., and Wood, L. J., 2001, Stratal slicing of Miocene-Pliocene sediments in Vermilion Block 50–Tiger Shoal area, offshore Louisiana: The Leading Edge, v. 20, p. 408–417.

Zeng, Hongliu, and Kerans, Charles, 2000, Amplitude versus frequency—applications to seismic stratigraphy and reservoir characterization, part I: model (exp. abs.), *in* 2000 technical program expanded abstracts: SEG International Exposition and Seventieth Annual Meeting, Calgary, August 6–11: Society of Exploration Geophysicists.

Zeng, Hongliu, Kerans, Charles, and Lucia, Jerry, 2000, Amplitude versus frequency—applications to seismic stratigraphy and reservoir characterization, part II: real 3-D data in Abo reservoir, Kingdom field, West Texas (exp. abs.), *in* 2000 technical program expanded abstracts: SEG International Exposition and Seventieth Annual Meeting, Calgary, August 6–11: Society of Exploration Geophysicists.

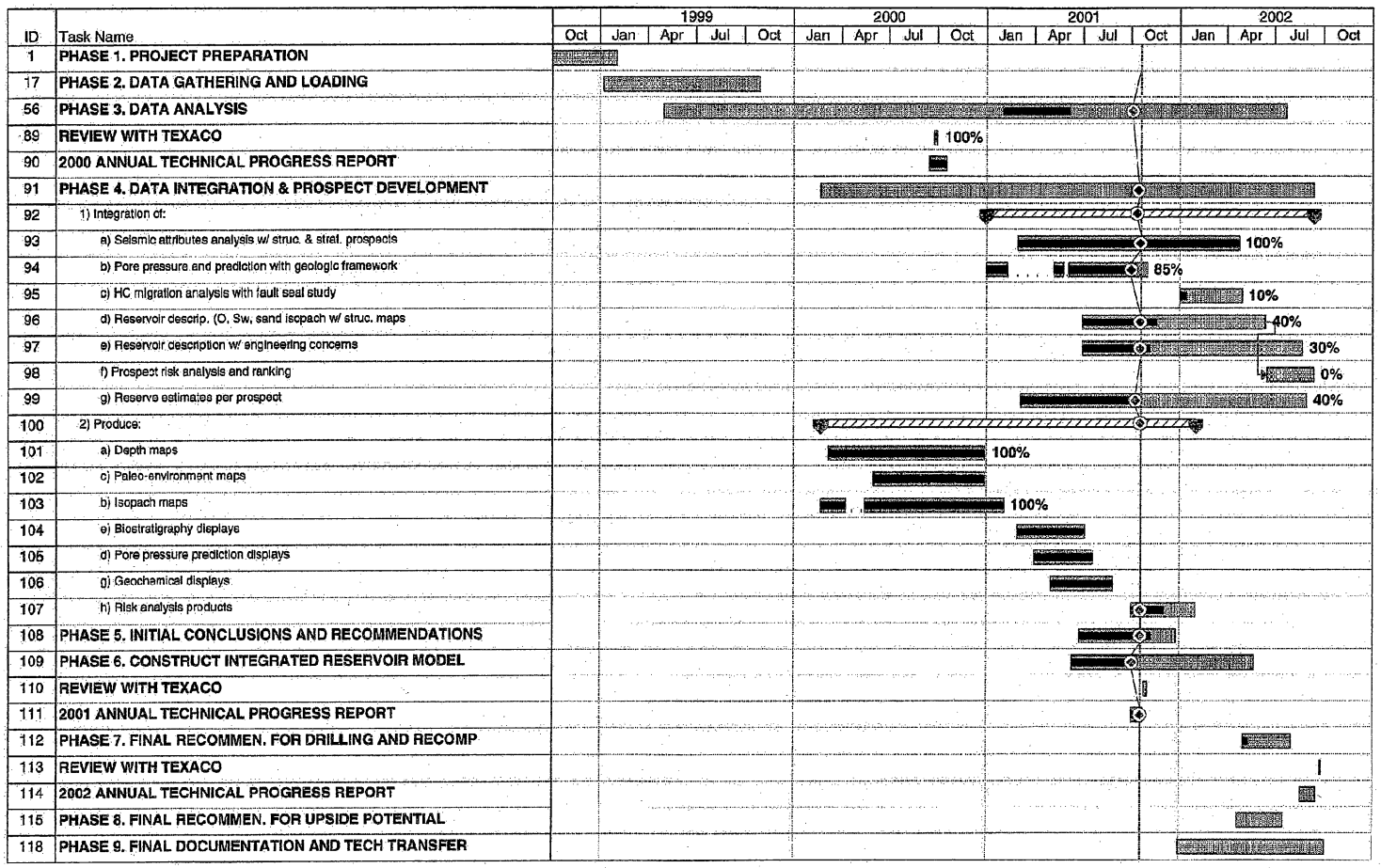

Figure 1. Chart of the project time line showing key project phases and events.

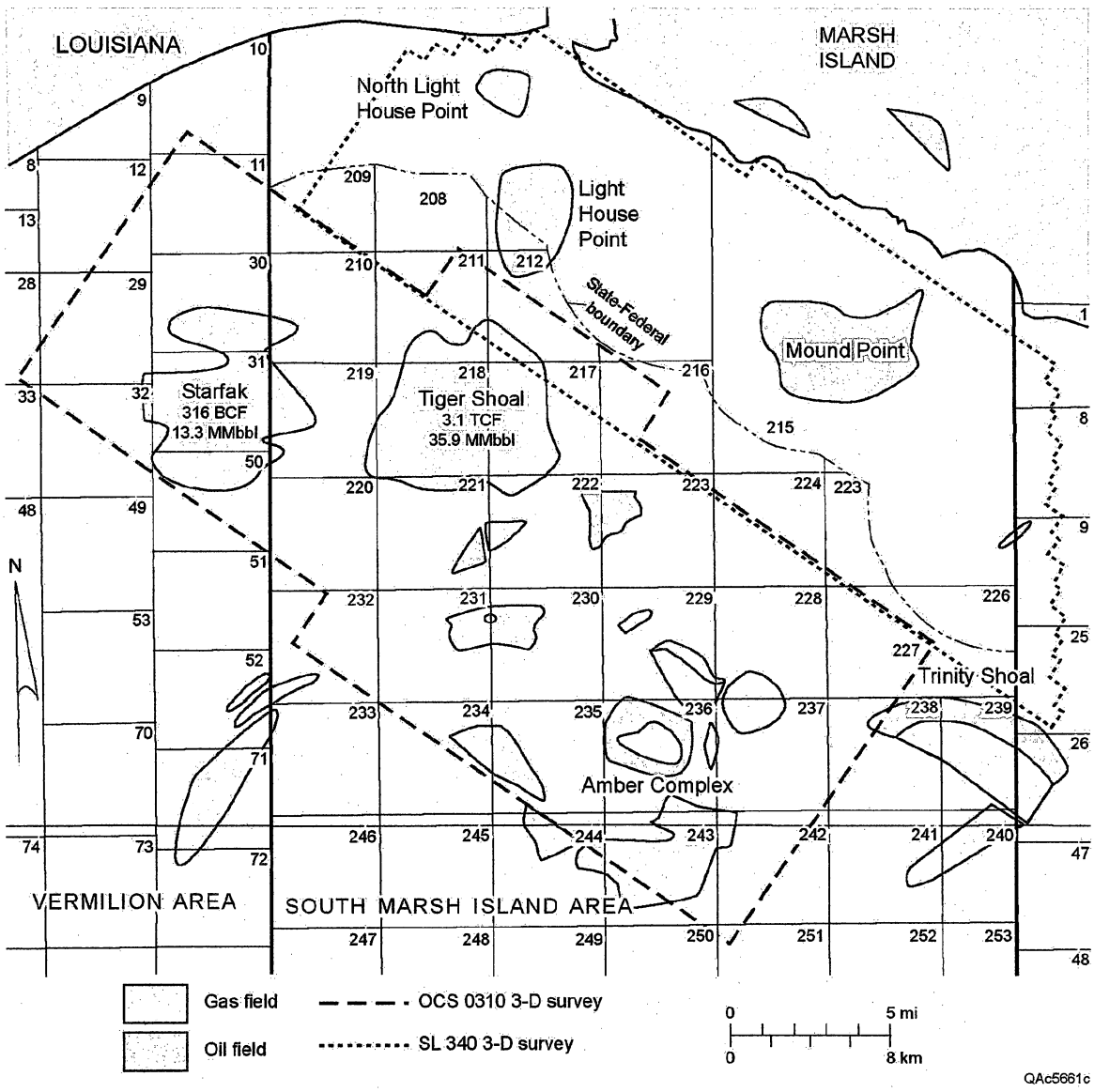

Figure 2. Map of the Vermilion and South Marsh Areas showing the study's primary target fields, Starfak and Tiger Shoal, as well as surrounding fields and the outline of the two major 3-D seismic surveys being used in this resource assessment.

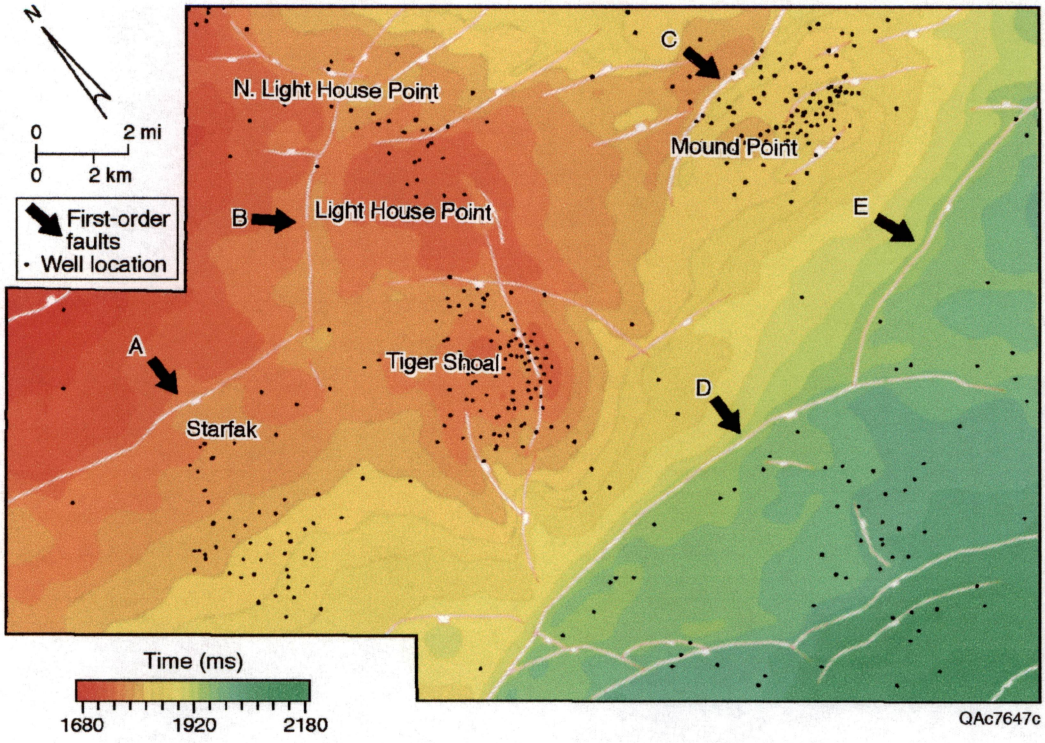

Figure 3. Time-structure map (contour interval = 20 ms) of maximum flooding surface 2 depicting the subsurface topography associated with the five major producing fields. Note the five (A, B, C, D, and E) first-order normal faults.

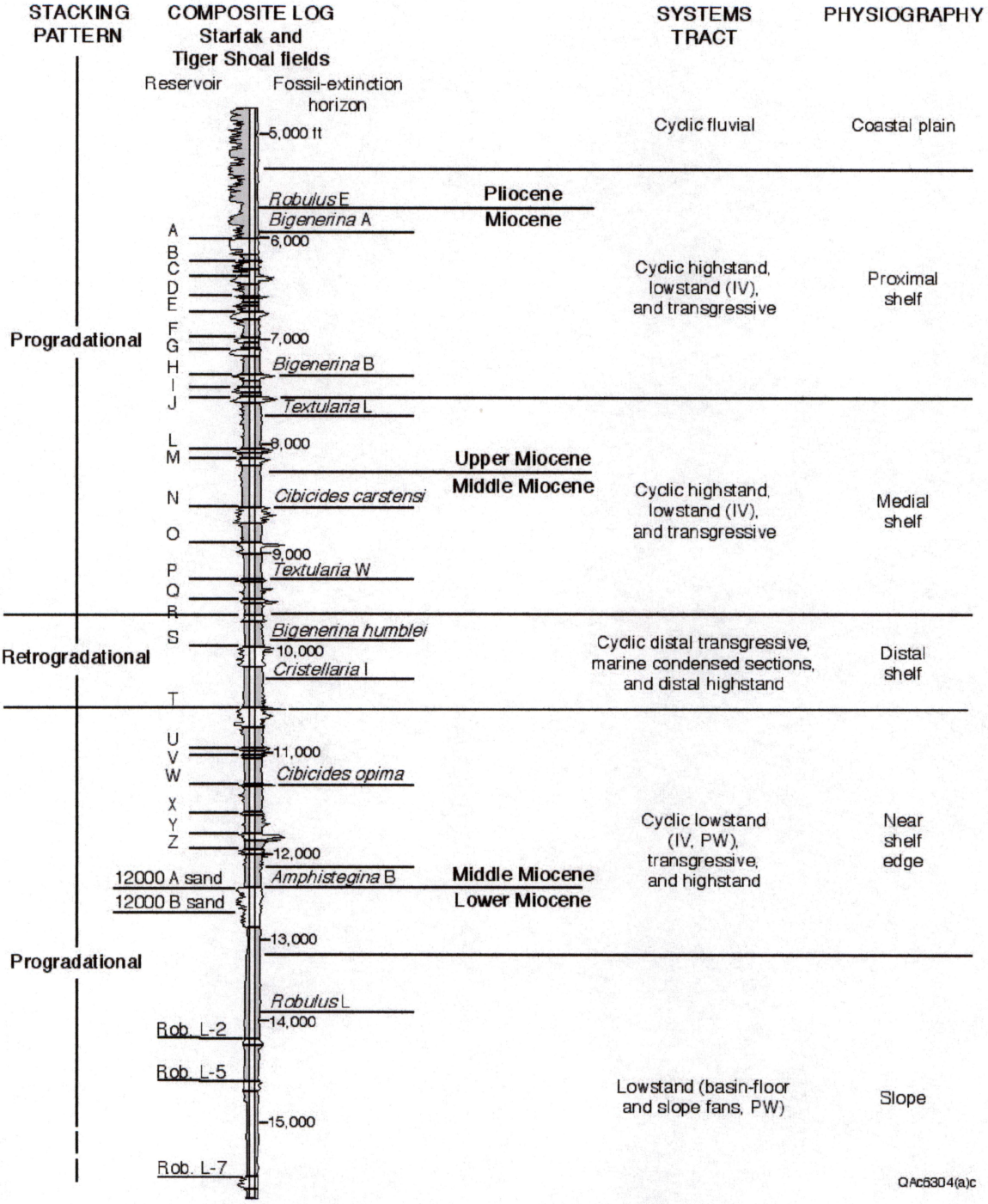

Figure 4. Composite type log of Starfak and Tiger Shoal fields that displays gross stacking patterns, reservoir nomenclature, extinction horizons of invertebrate paleofauna, and stage boundaries . Stage boundaries are approximate and are based on microfossils from several wells in each field. Interpretation of systems tracts and paleophysiography is based on wireline-log facies, inferred lateral facies relationships, facies stacking patterns, and mapping using seismic data (primarily time-depth-structure and isochron maps and amplitude stratal slices).

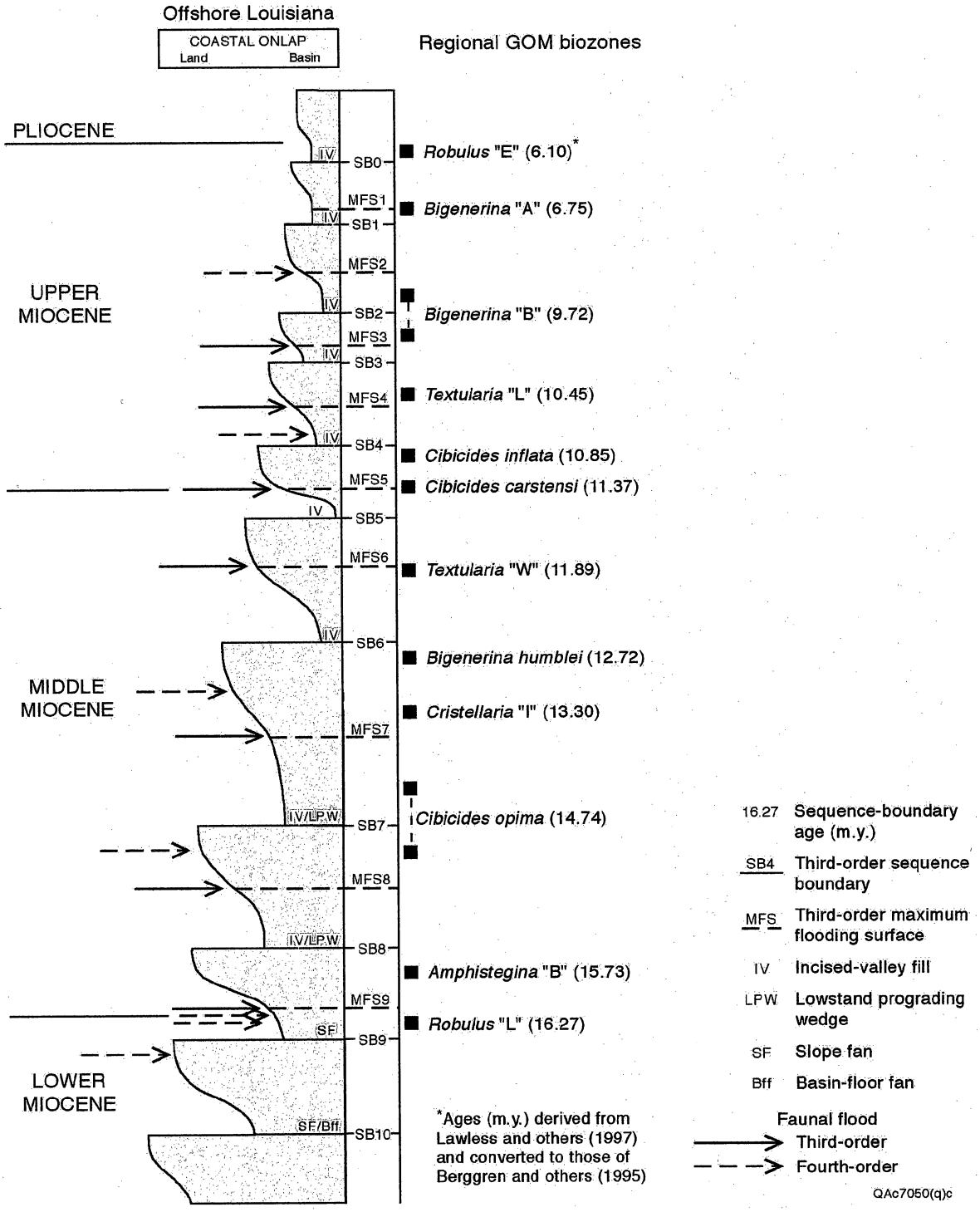

Figure 5. Inferred coastal-onlap curve of the entire Miocene study interval and the relative stratigraphic positions and absolute ages of regional Gulf of Mexico biozones. Third- and fourth-order faunal "floods" are those identified in Texaco paleontological reports.

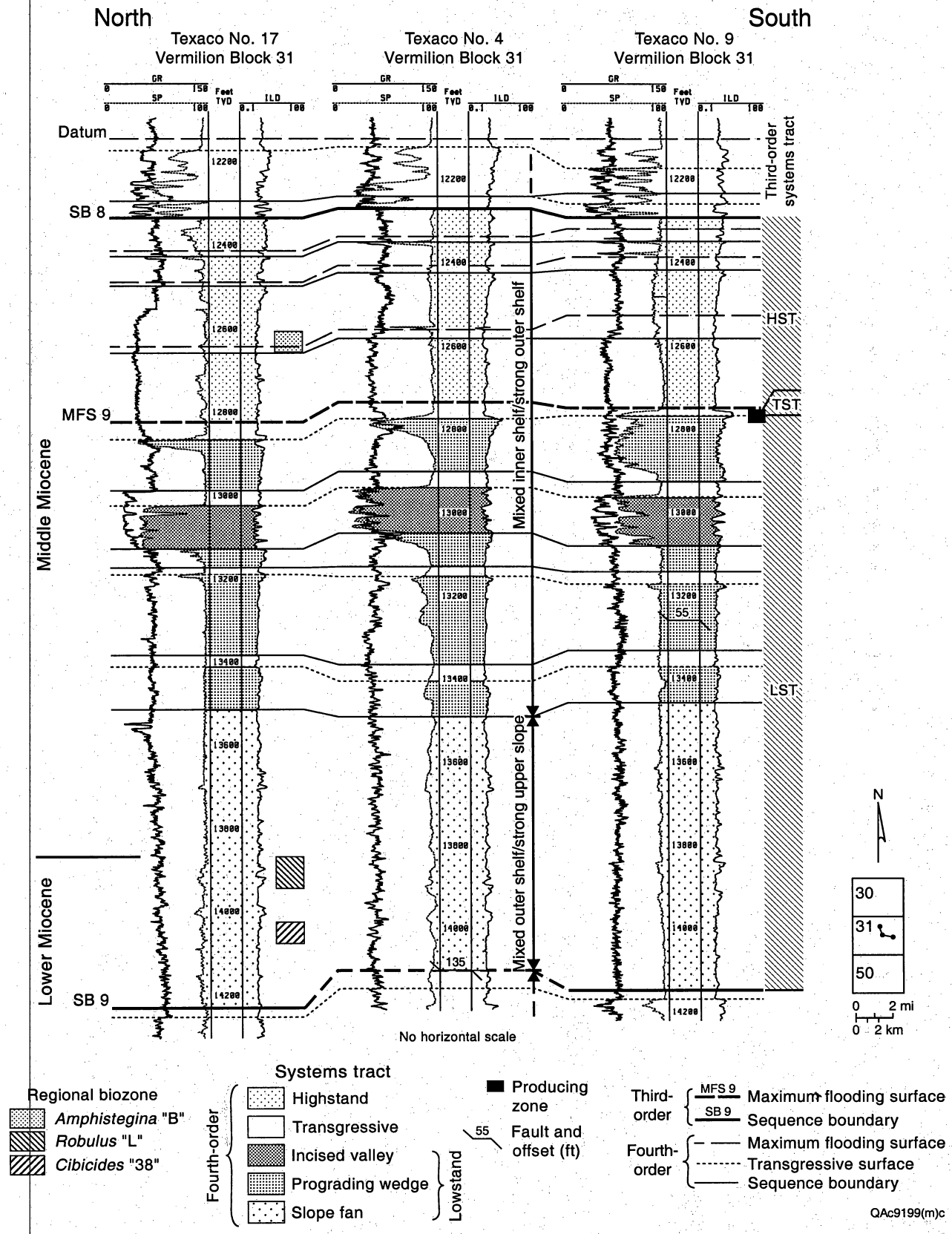

Figure 6. Cross section of third-order Cycle 9, Starfak field, showing all third- and fourth-order chronostratigraphic surfaces, precise positions of regional biozones, third- and fourth-order systems tracts, and general depositional settings as deduced from indicator fossils. Inner shelf=inner and outer neritic, outer shelf=outer neritic, upper slope=upper bathyal (table 1).

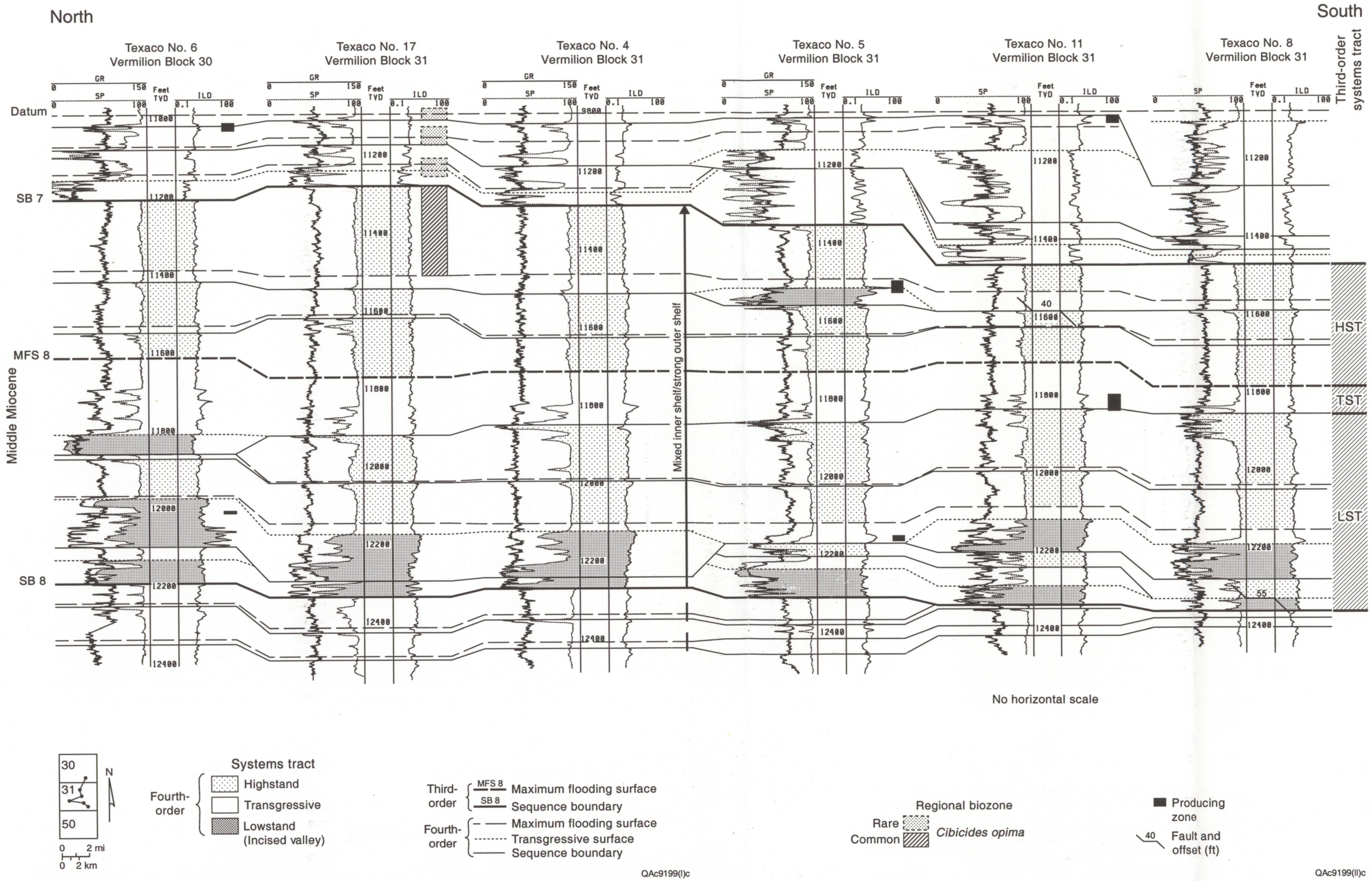

Figure 7. Cross section of third-order Cycle 8, Starfak field, showing all third- and fourth-order chronostratigraphic surfaces, position of the regional biozone, third- and fourth-order systems tracts, and general depositional setting as deduced from indicator fossils. Inner shelf=inner and outer neritic, outer shelf=outer neritic, upper slope=upper bathyal (table 1).

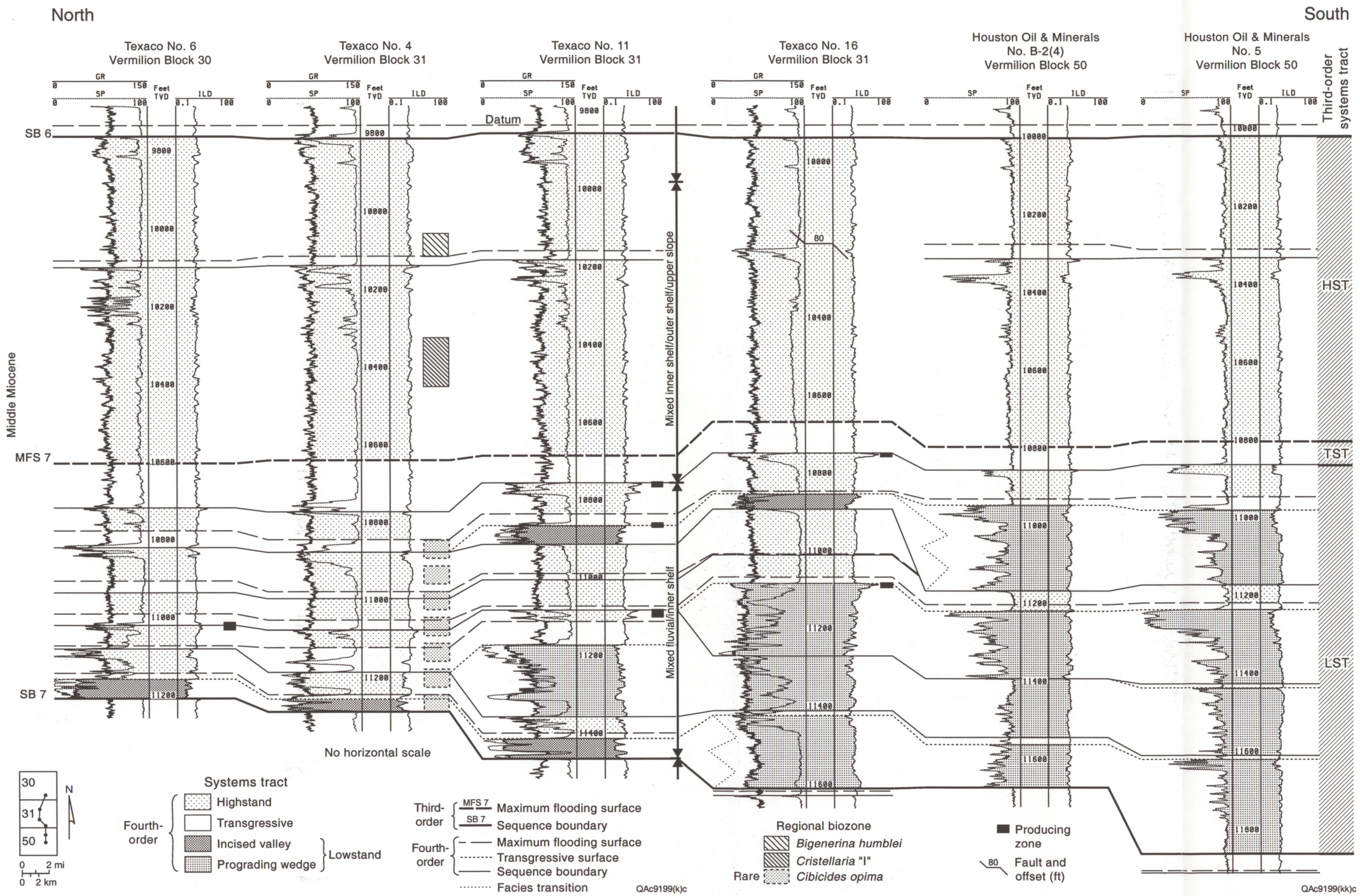

Figure 8. Cross section of third-order Cycle 7, Starfak field, showing all third- and fourth-order chronostratigraphic surfaces, position of the regional biozone, third- and fourth-order systems tracts, and general depositional setting as deduced from indicator fossils. Inner shelf=inner and outer neritic, outer shelf=outer neritic, upper slope=upper bathyal (table 1).

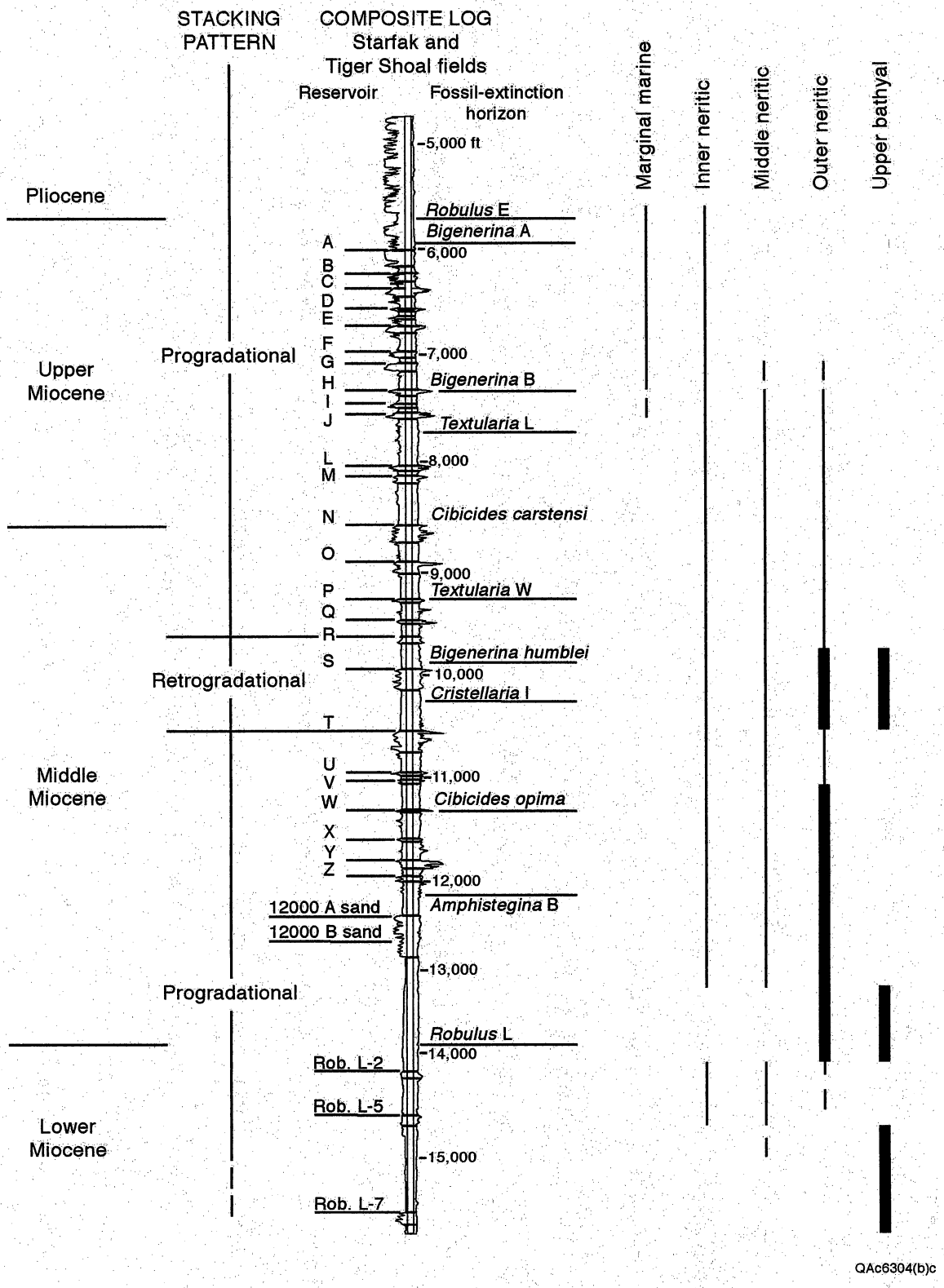

Figure 9. Generalized vertical variation in paleobathymetric conditions as recorded by benthic indicator fossils from 15 wells in Starfak and Tiger Shoal fields. See table 1 for water depths associated with each water-depth zone.

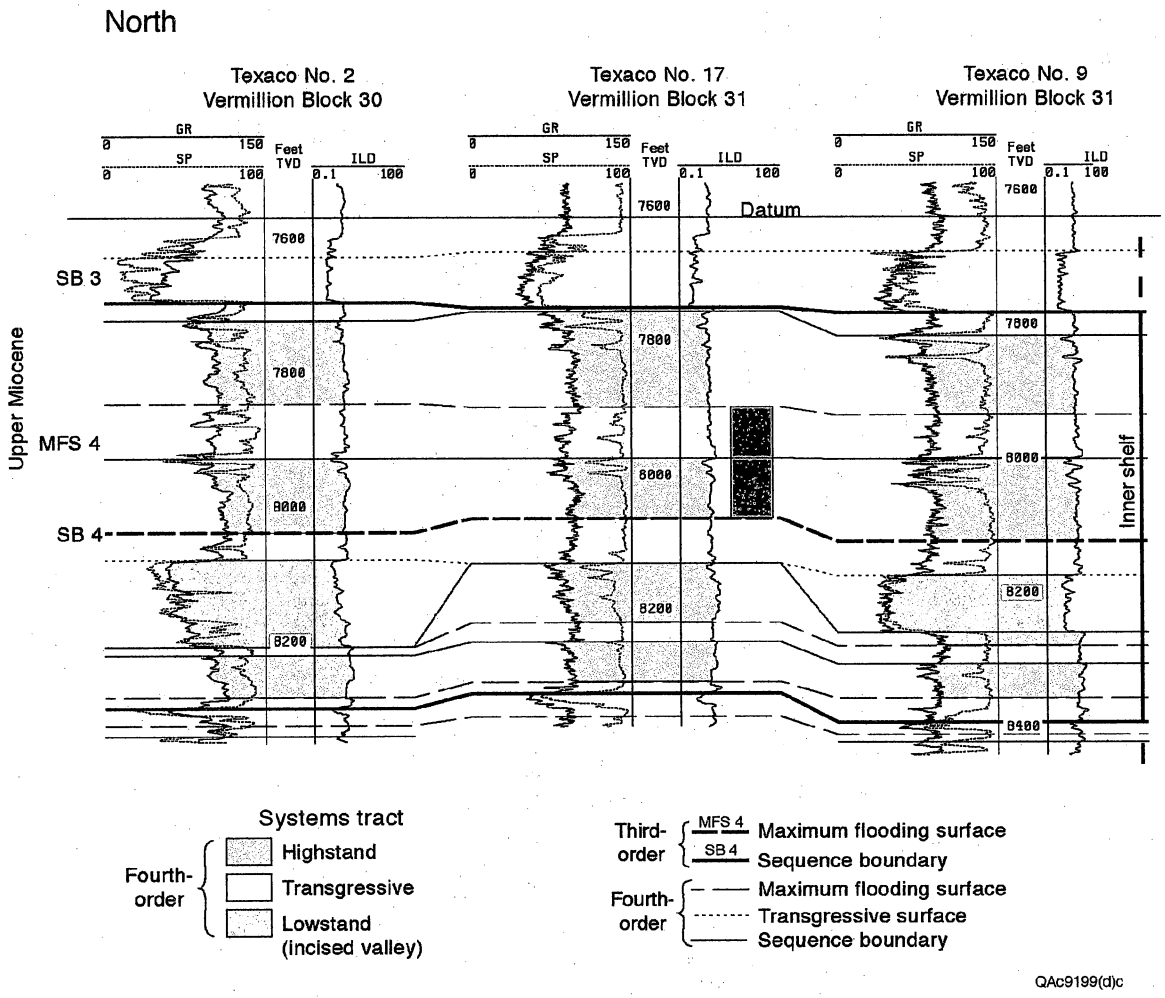

Figure 10. Isochore map and amplitude stratal slice of a productive incised-valley-fill sandstone within the third-order lowstand systems tract of Cycle 2, Starfak field. This figure illustrates the precision of facies and reservoir imaging that can be achieved using the stratal-slicing technique. Such seismic imaging provides excellent resolution over thin (~15-ft) stratigraphic intervals and supports facies interpretations from wireline-log cross sections.

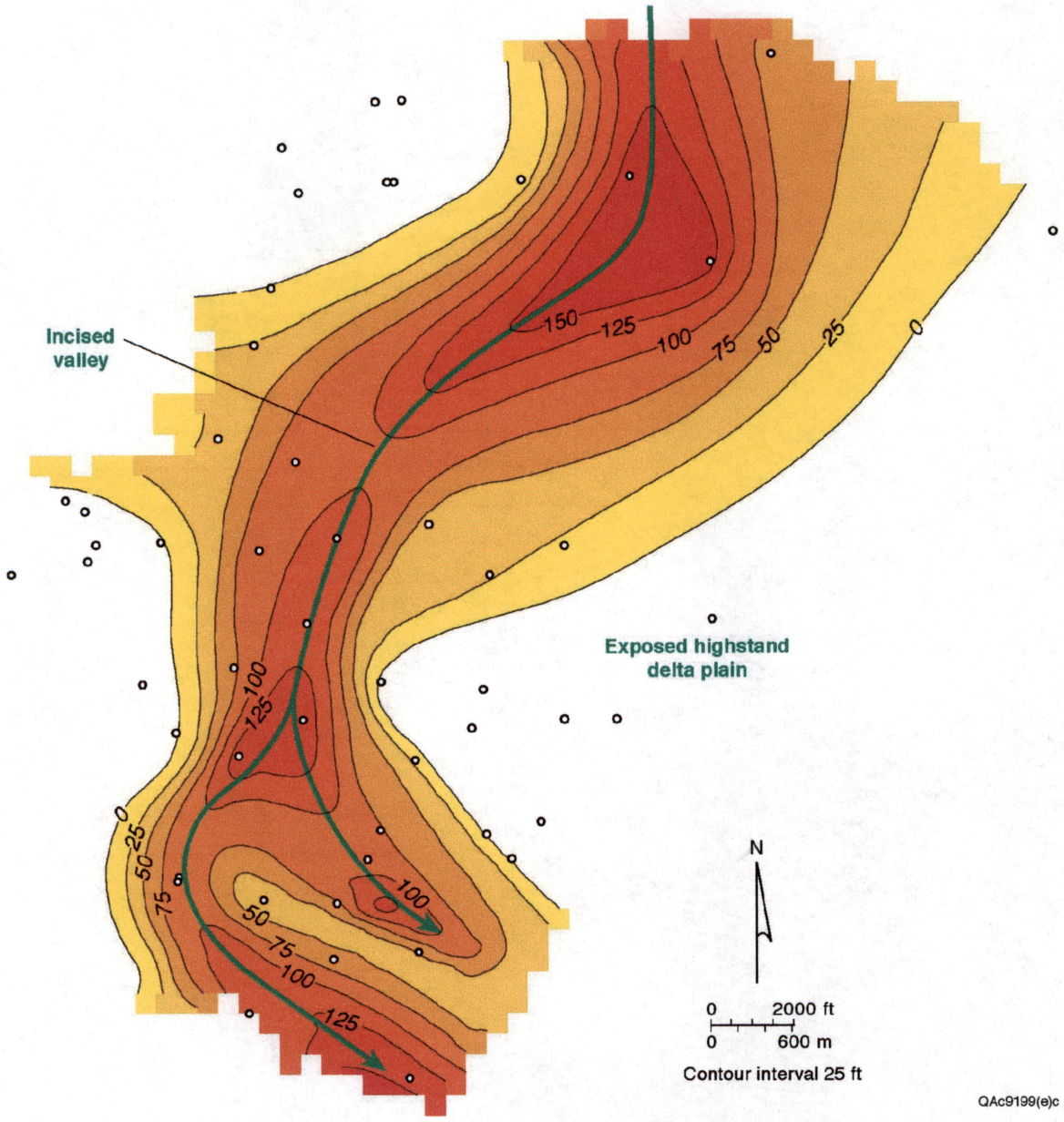

Figure 11. Isochore map of the proximal portion of a well-developed incised-valley system that rests on the third-order sequence boundary of third-order Cycle 5. Stratal slices show that incision by this system occurred over a broad area of the middle Miocene shelf.

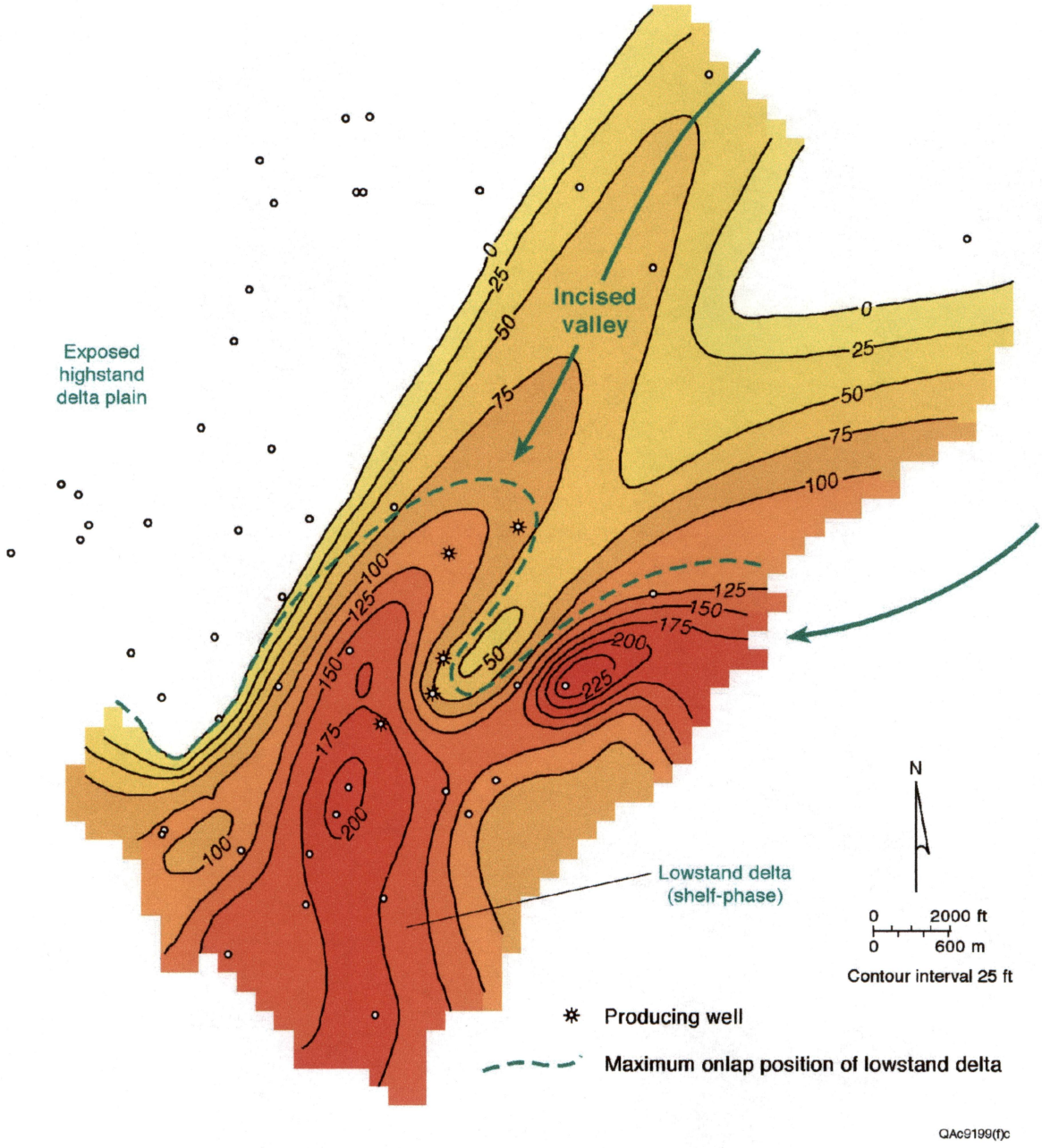

Figure 12. Isochore map of the incised-valley-to-prograding-wedge transition of a lowstand systems tract in third-order Cycle 7 in Starfak field. There is no evidence of fault control of a shelf break. Instead, this shelf-phase lowstand delta formed basinward of the depositional-shoreline break of the underlying highstand delta platform (fig. 13).

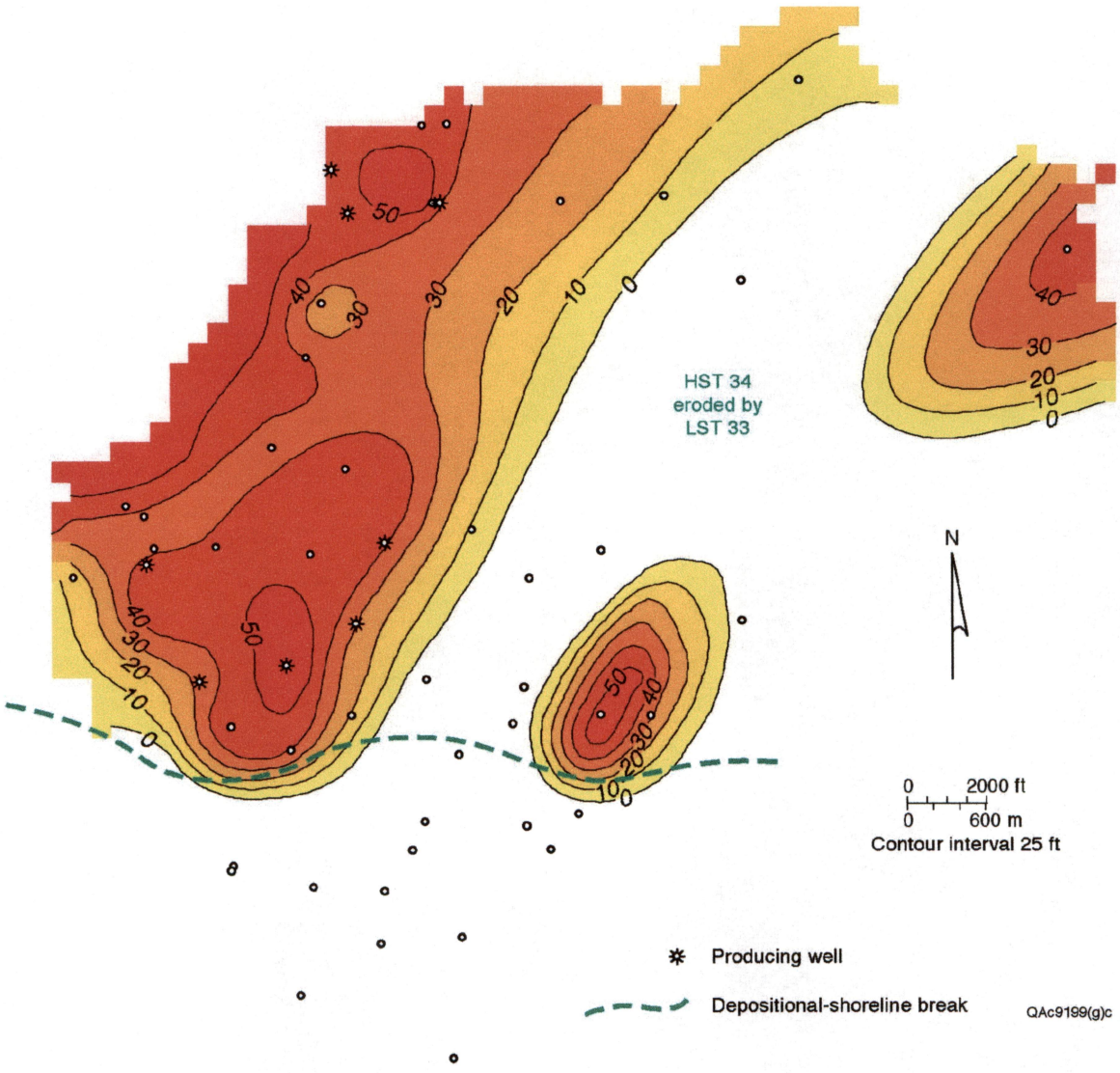

Figure 13. Isochore map of the fourth-order highstand systems tract (Cycle 7) that underlies, and was partially incised by, the valley/wedge complex shown in figure 12. Both intervals contain productive sandstones; reservoir-scale petrophysical and engineering analyses indicate that sandstones of the two systems tracts form separate reservoir compartments.

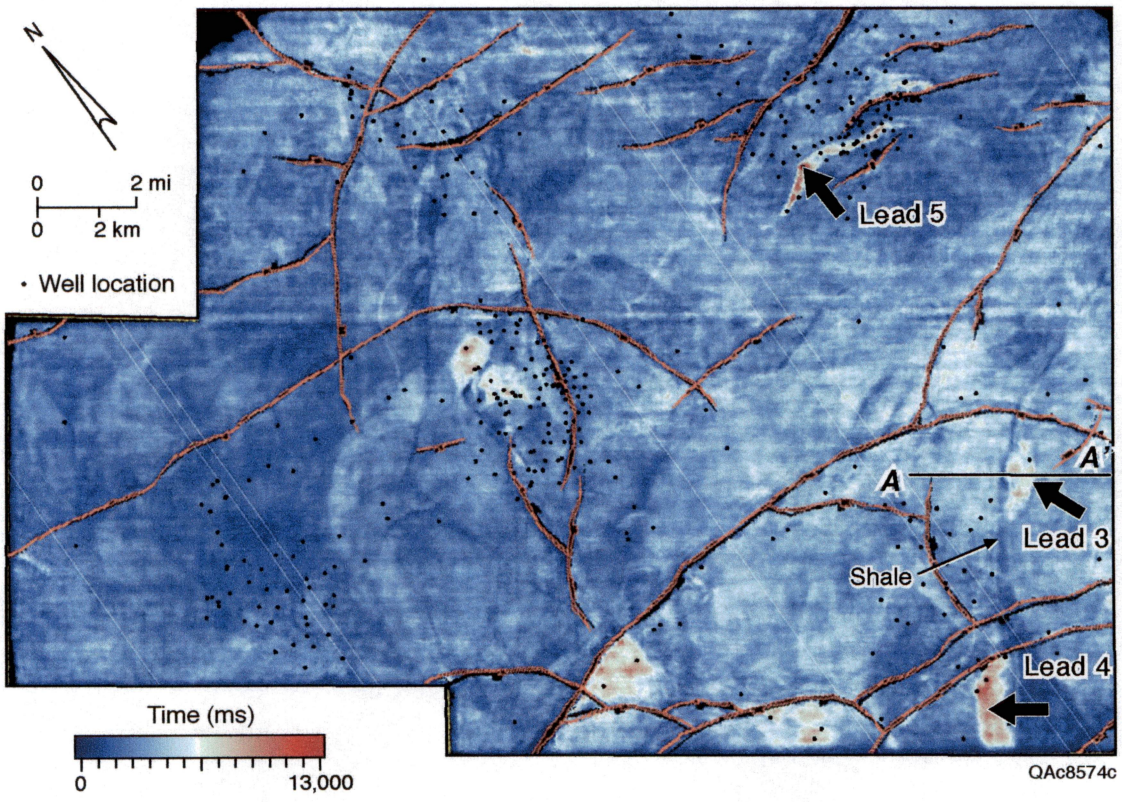

Figure 16. Root-mean-squared (RMS) amplitude map from the F Sand interval extracted from the 3-D seismic data set over the study area. The thin orange lines are down-to-the-southeast normal faults. Several stratigraphic incised distributary-channel leads are pointed out, including the Lead 3 opportunity. This accumulation (bright red) is limited on its west side by shaly (dark) facies. Seismic section A–A' shown in figure 14.

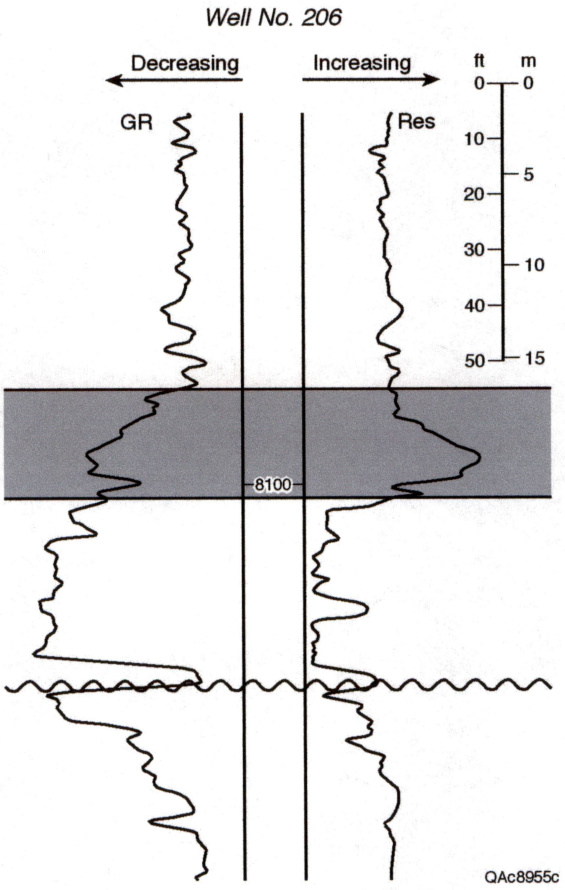

Figure 17. Gamma-ray and resistivity log from Well 206 drilled by Texaco in 2001 to test the Lead 3 stratigraphic trap. Note the sharp-based upward-fining signature of the stacked channel-fill sands and the high resistivity in the top of the unit denoting gas saturation.

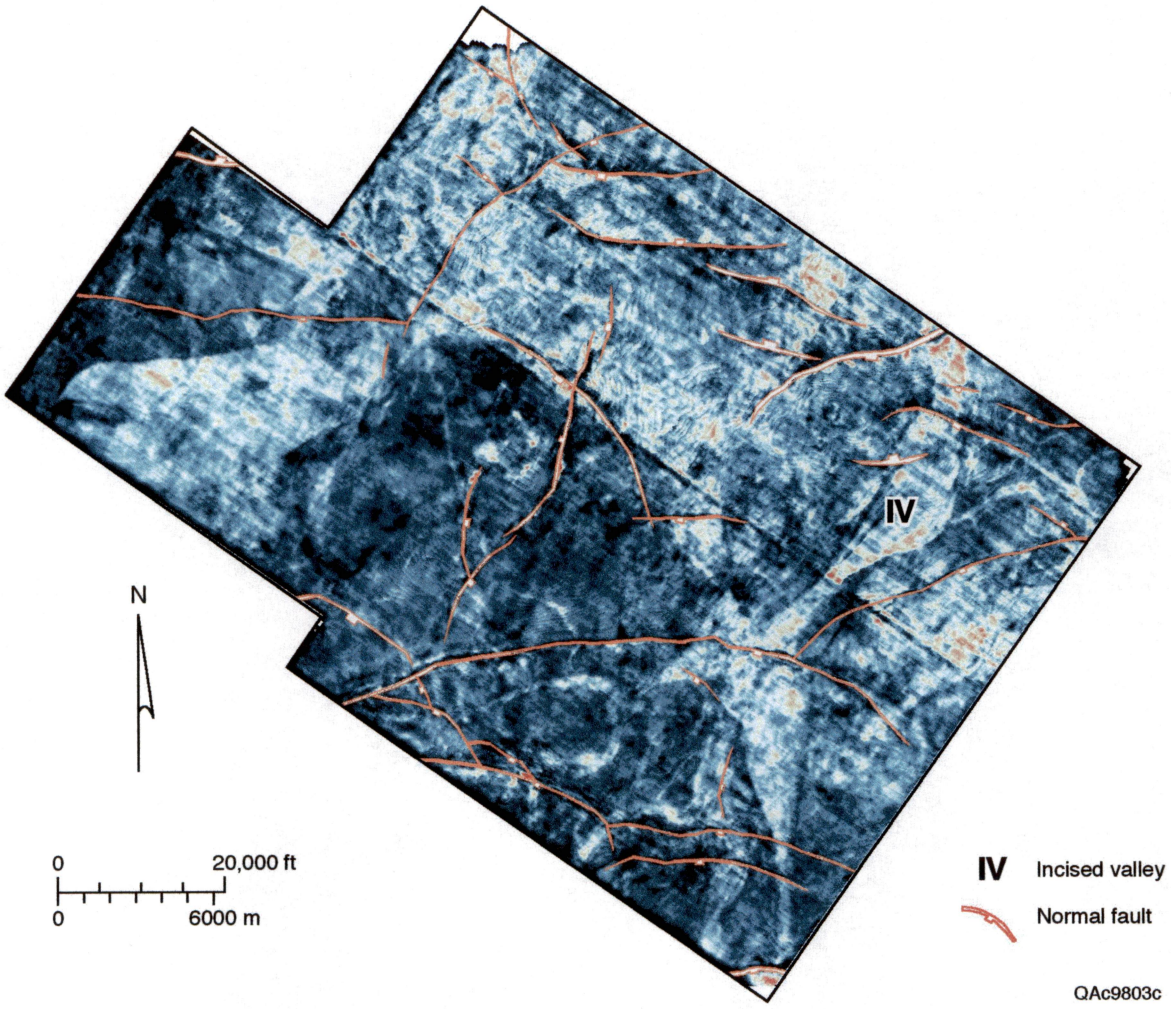

Figure 18. Root-mean-squared (RMS) amplitude map of the B sand reveals subtle stratigraphic features in Starfak field that may be associated with a large incised-valley system. Tiger Shoal field indicates that there is little or no sand associated with this reservoir interval. Farther to the east of the study area, there are clear indications of incised-valley sands and incised-valley-fill sands; however, most have been penetrated by previous drilling.

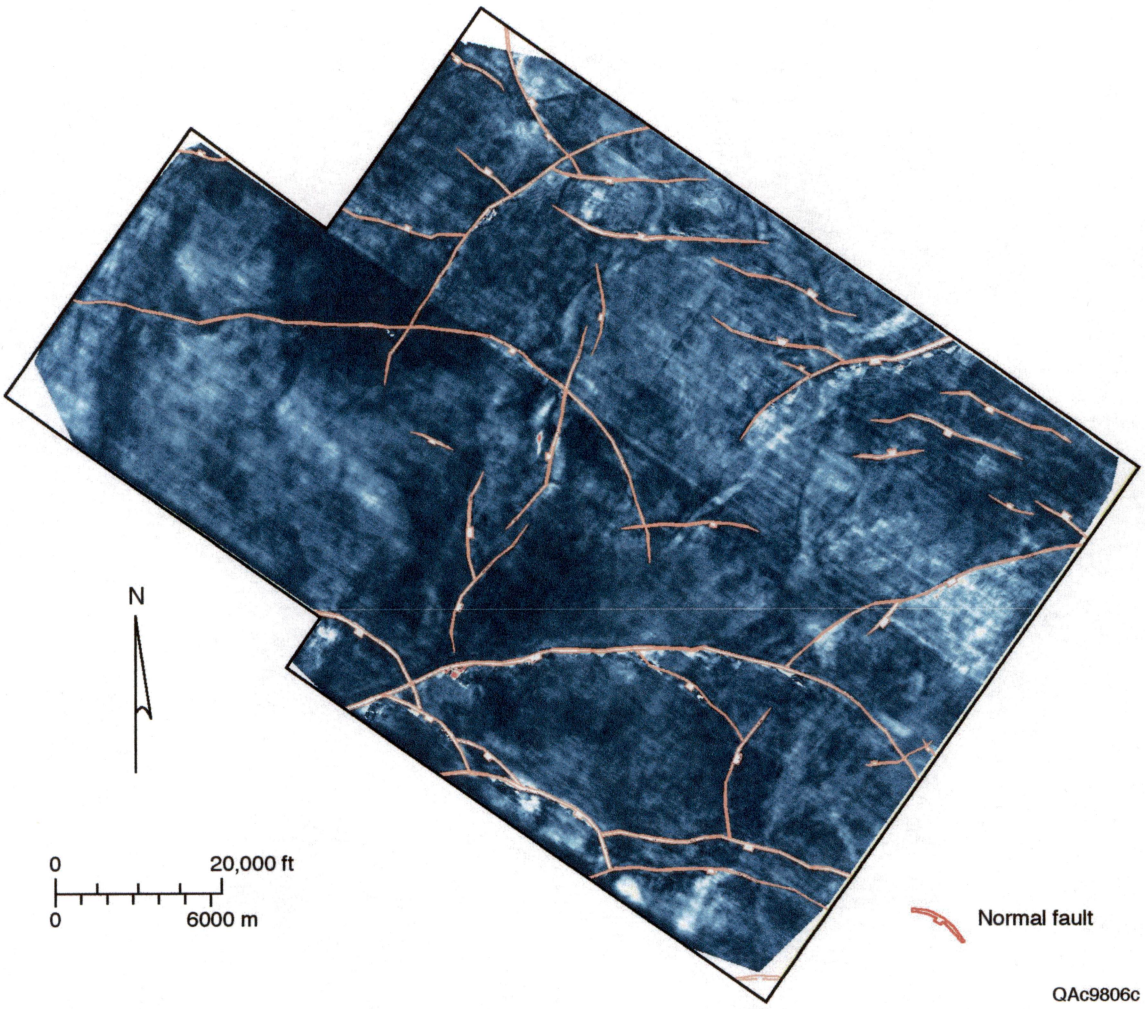

Figure 19. Root-mean-squared (RMS) amplitude map of the G sand interval depicting a depositional environment dominated by shales. No leads were generated from this map.

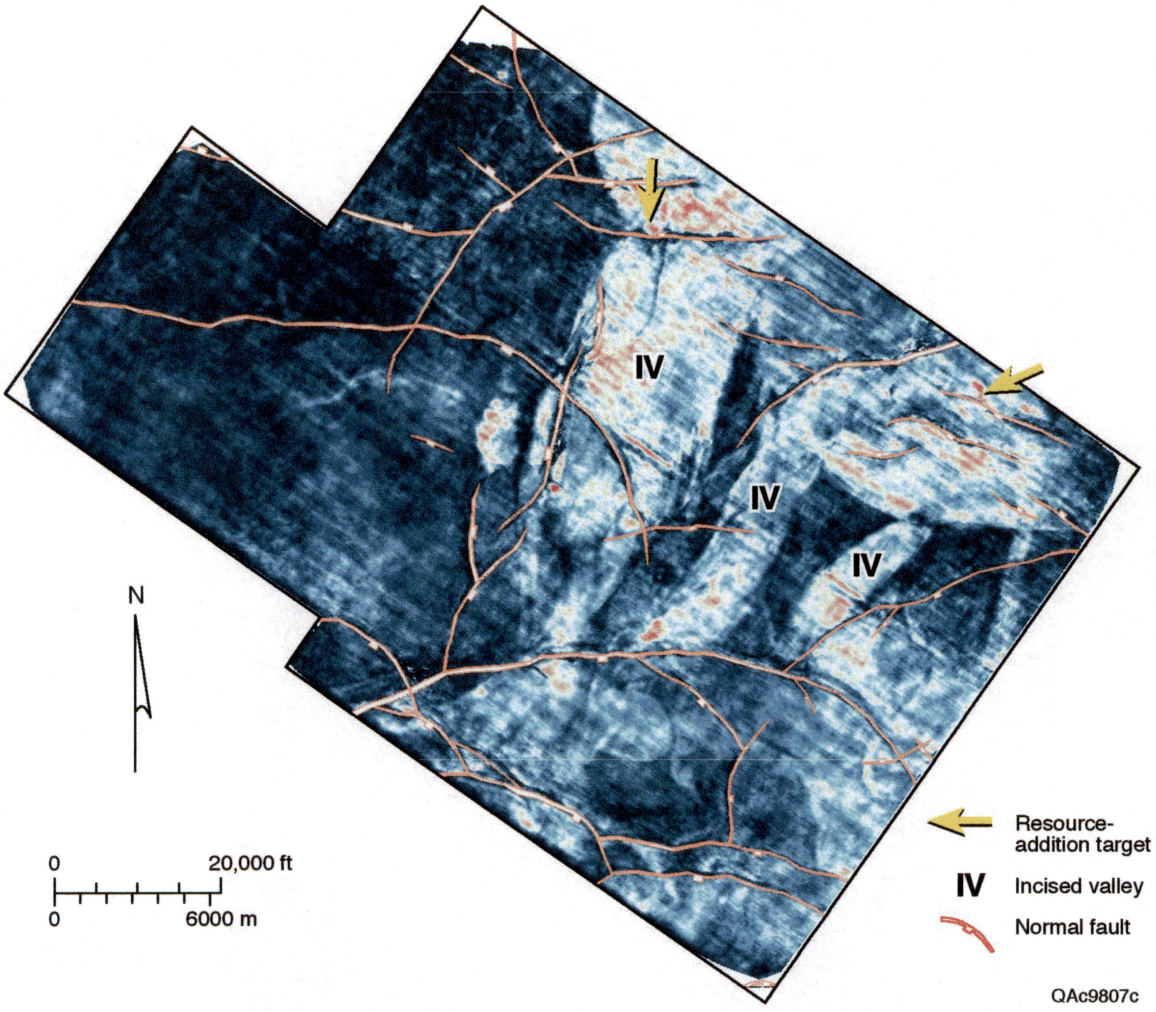

Figure 20. Root-mean-squared (RMS) amplitude map of the H sand interval depicting an incised-valley system that dominates the saddle area between Lighthouse Point field and Mound Point field. Additional valley-fill sands are evident throughout the eastern half of the study area. Starfak field has amplitudes indicative of shale-dominated sequences.

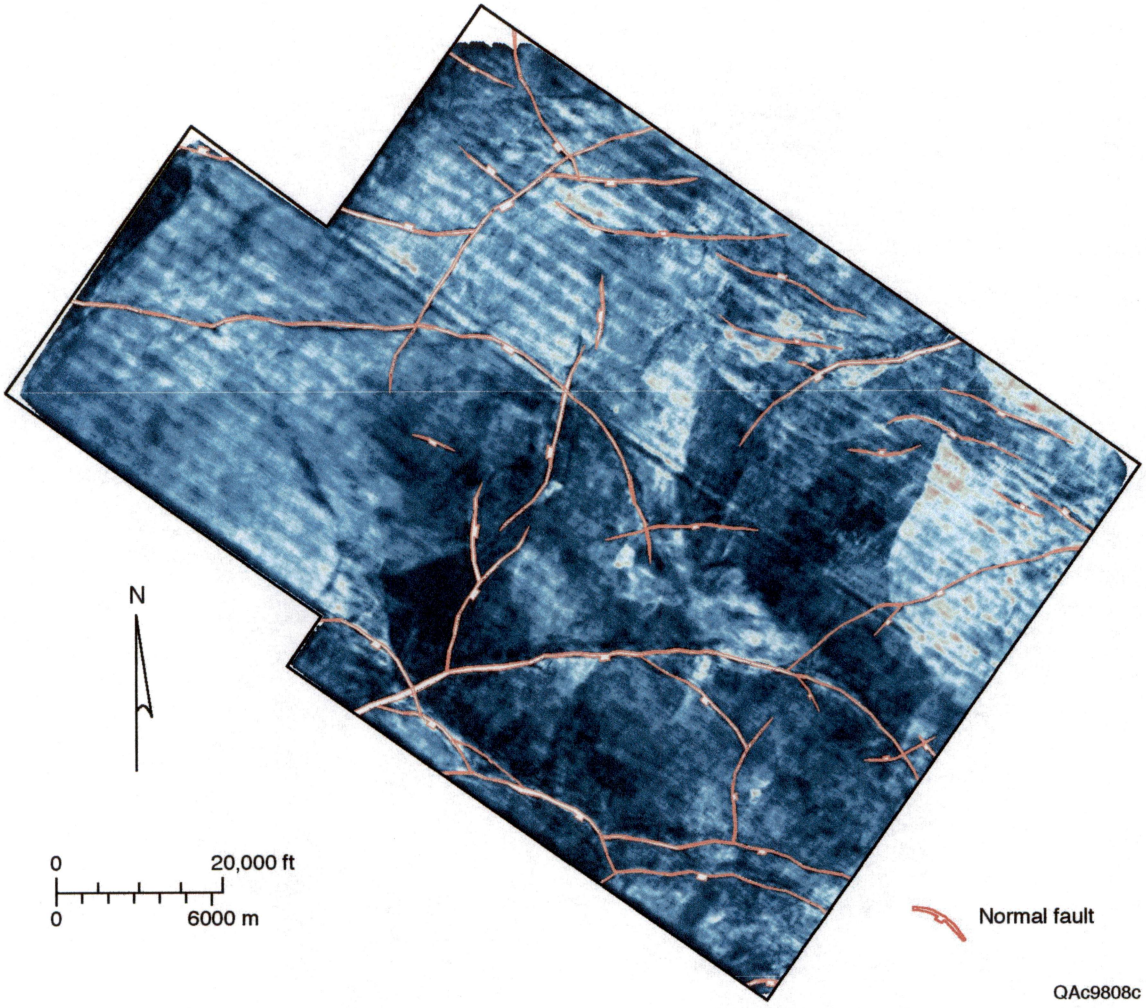

Figure 21. Root-mean-squared (RMS) amplitude map of the J sand interval illustrating few features of interest. One prospect was identified on this map, a fault-bounded graben with a significant strong amplitude anomaly in the North Lighthouse field. Tiger Shoal field is interpreted to be dominated by deep marine sediments at this interval.

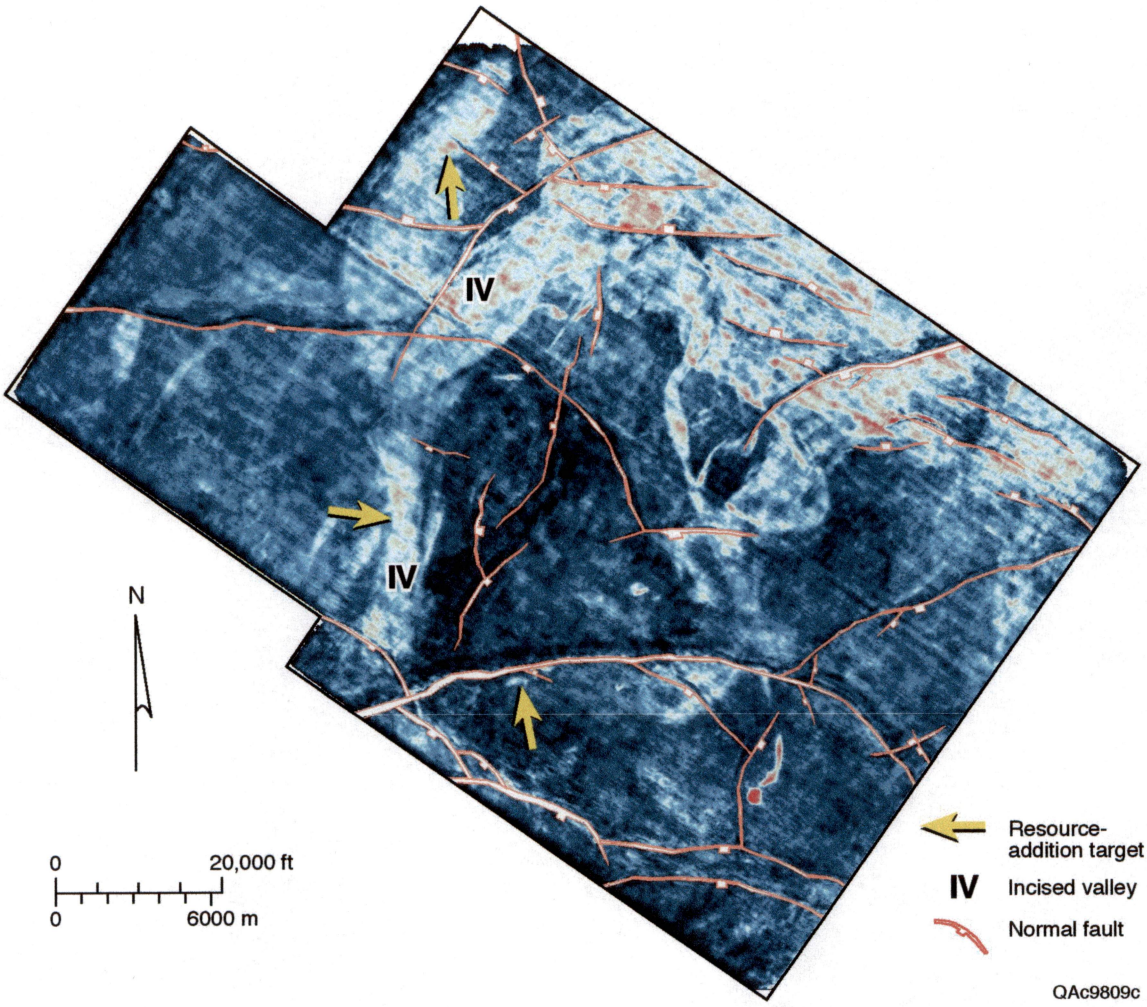

Figure 22. Root-mean-squared (RMS) amplitude map of the L sand illustrating a prominent lowstand incised-valley system traversing Lighthouse field and the saddle area between Starfak and Tiger Shoal fields. In addition, several sinuous features in the east portion are interpreted to be remnants of an ancient fluvial system. Tiger Shoal shows little evidence of reservoir-quality sand deposits. Two structural prospects are associated with deeper "rollover" features on the downthrown (hanging wall) side of a first-order growth fault.

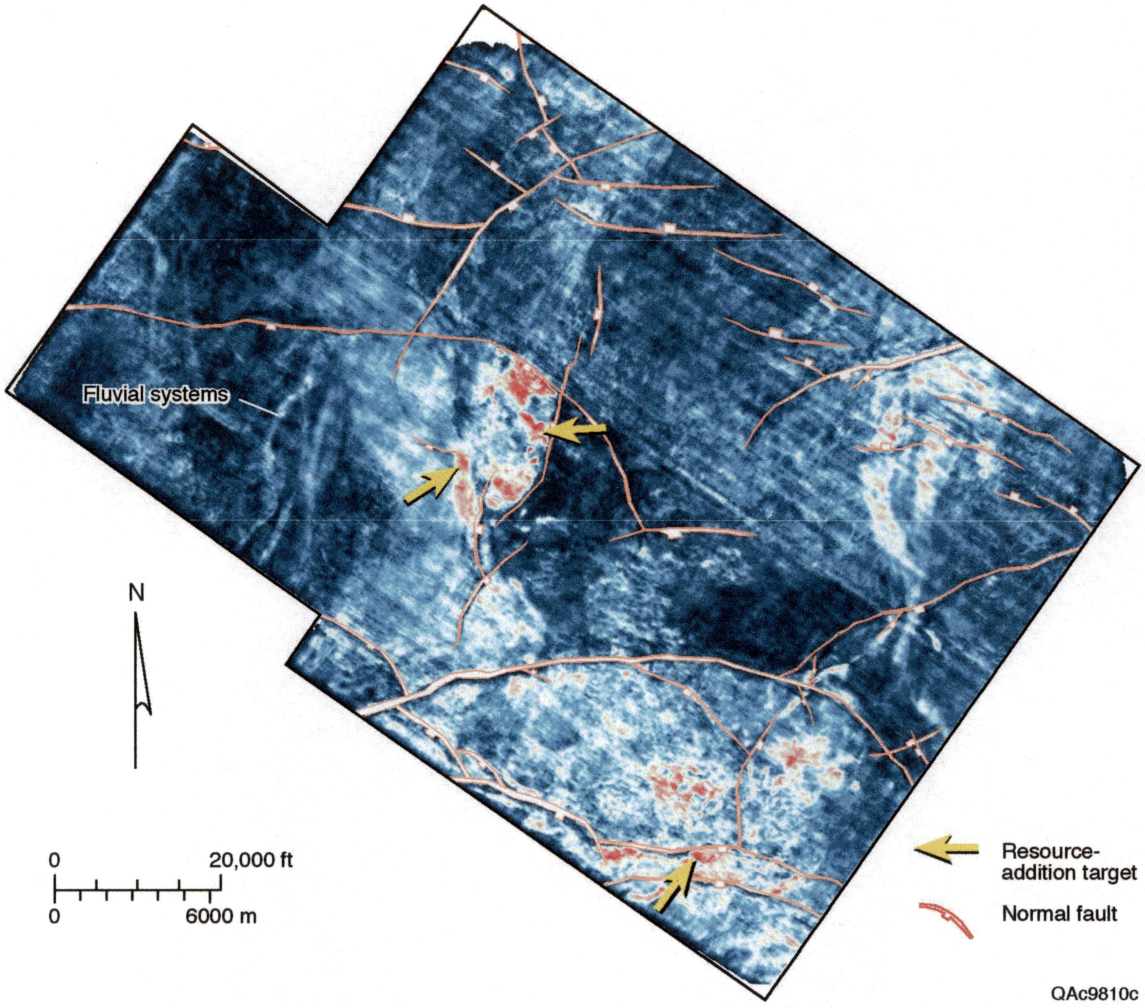

Figure 23. Root-mean-squared (RMS) amplitude map of the M sand revealing a large lowstand incised valley system dominating the Tiger Shoal field and the adjacent saddle area to the west, providing two excellent prospects missed by previous drilling programs. Similar features pervade the Mound Point field; however, these features have already been exploited. Starfak field has several sinuous features that meander through the area. Each of these features needs to be examined closely for hydrocarbon potential.

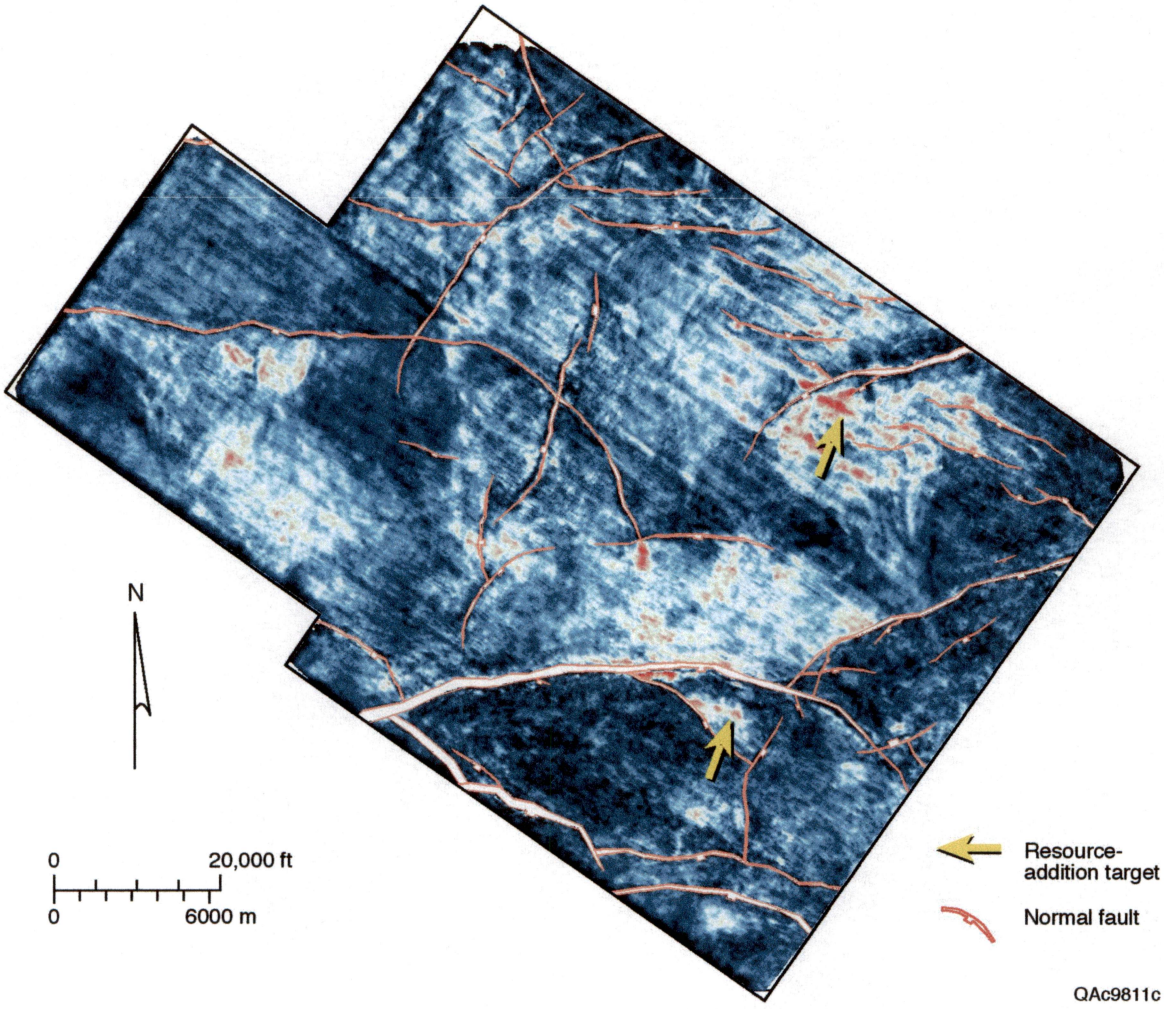

Figure 24. Root-mean-squared (RMS) amplitude map of the N sand interval illustrating massive depositional sequences dominating the northern two-thirds of the study area. Syndepositional subsidence along the first-order growth faults probably contributed to the creation of accommodation for the thick, lowstand-deltaic sands.

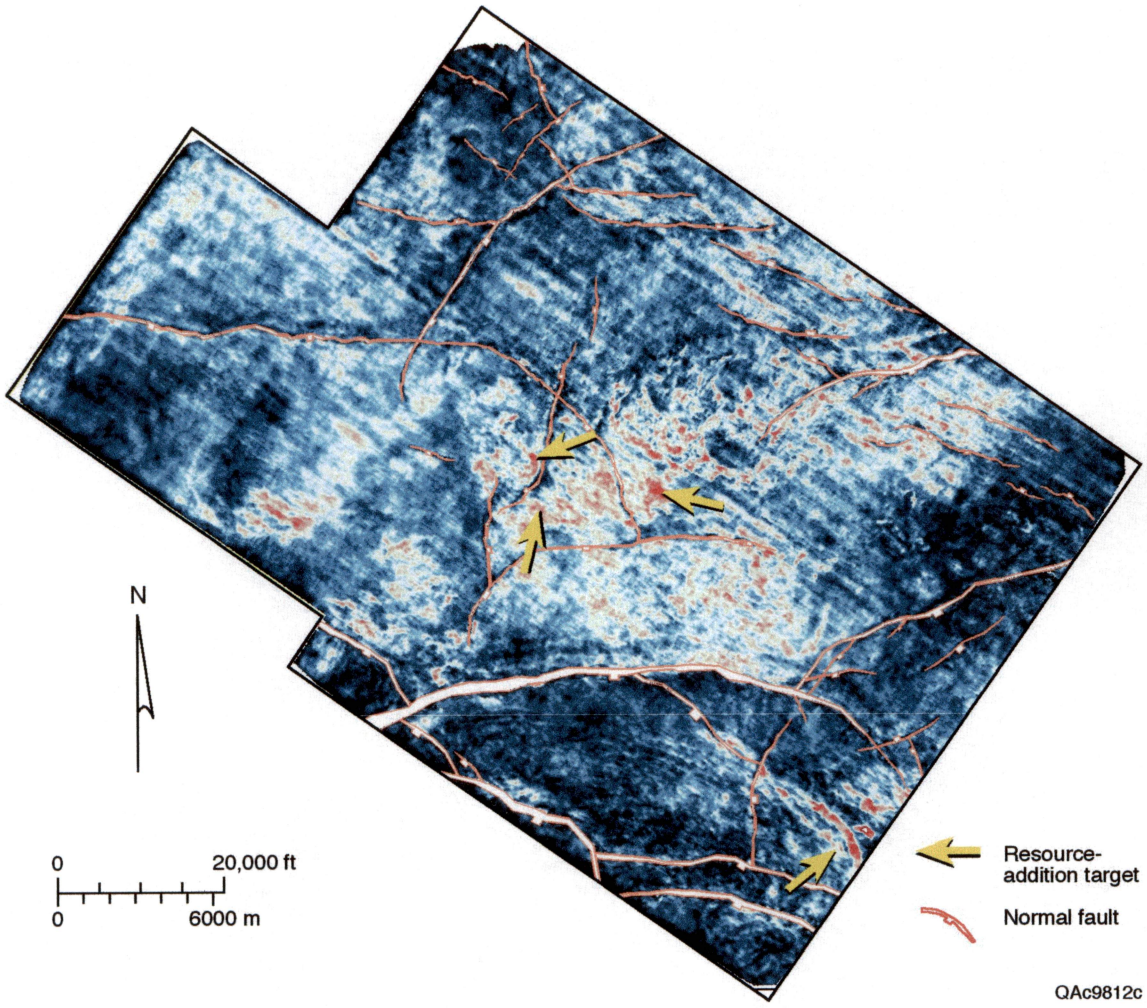

Figure 25. Root-mean-squared (RMS) amplitude map of the O sand interval depicting a dominant highstand systems tract that caused significant deposition of sand units through most of the study area. Several prospect were identified in the Tiger Shoal field.

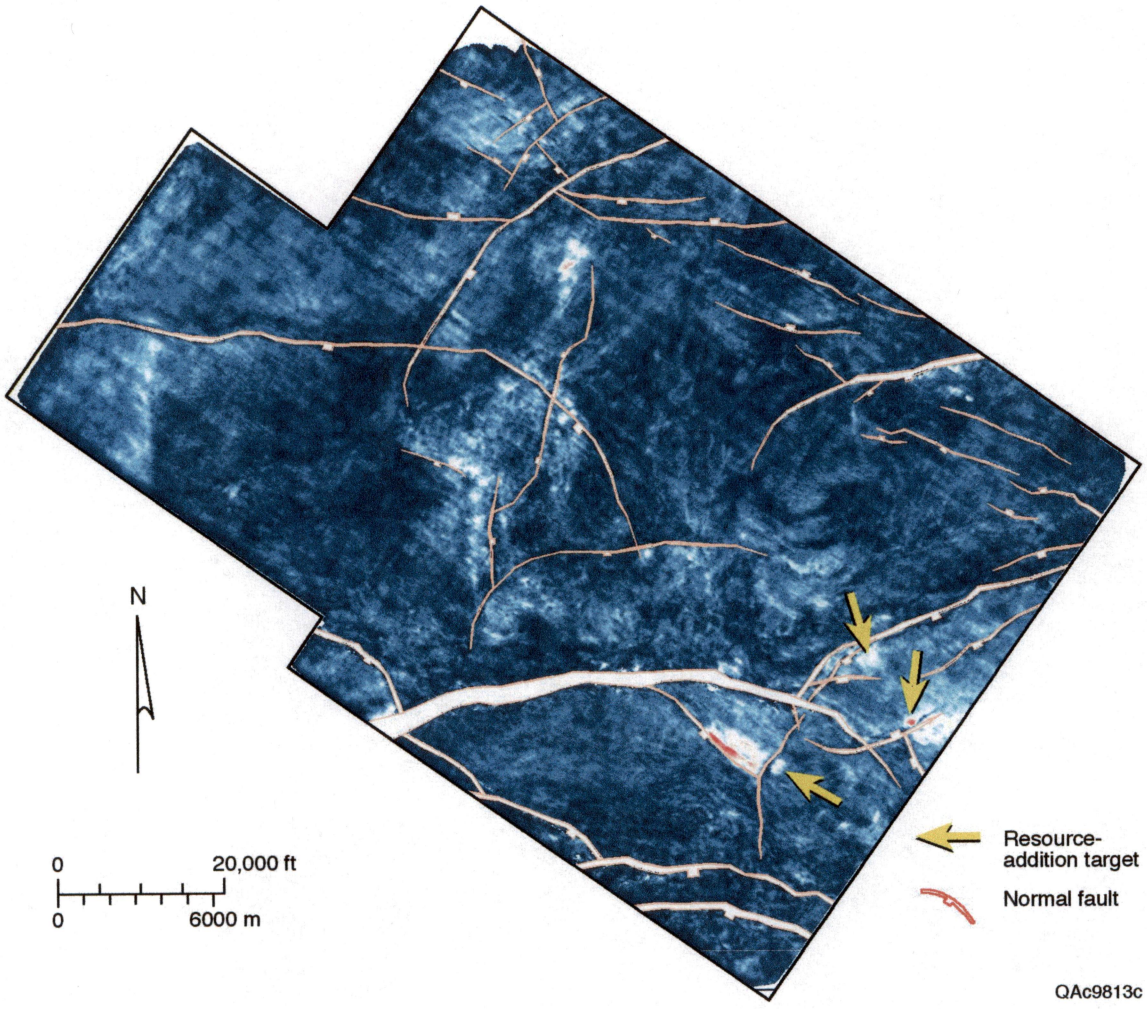

Figure 26. Root-mean-squared (RMS) amplitude map of the Q sand interval showing predominantly shale rich environment. The southeastern Amber Complex has several possible deposits (slope fan?) that may prove to be productive.

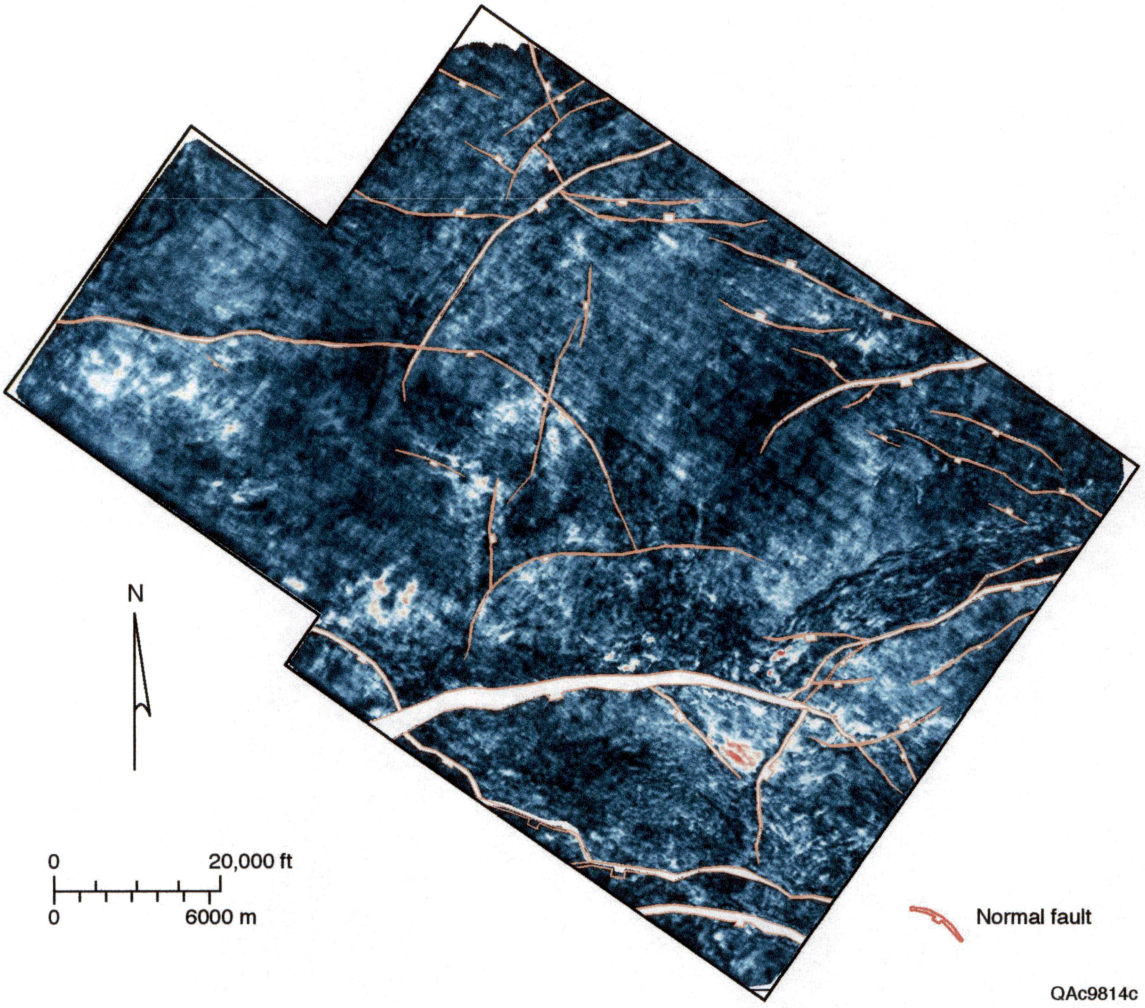

Figure 27. Root-mean-squared (RMS) amplitude map of the R sand interval that may depict the beginnings of a highstand systems tract sequence. Note the "ripples" in the eastern portion of the study area. This feature is indicative of "lap-out" depositional sequences common in this type of depositional environment.

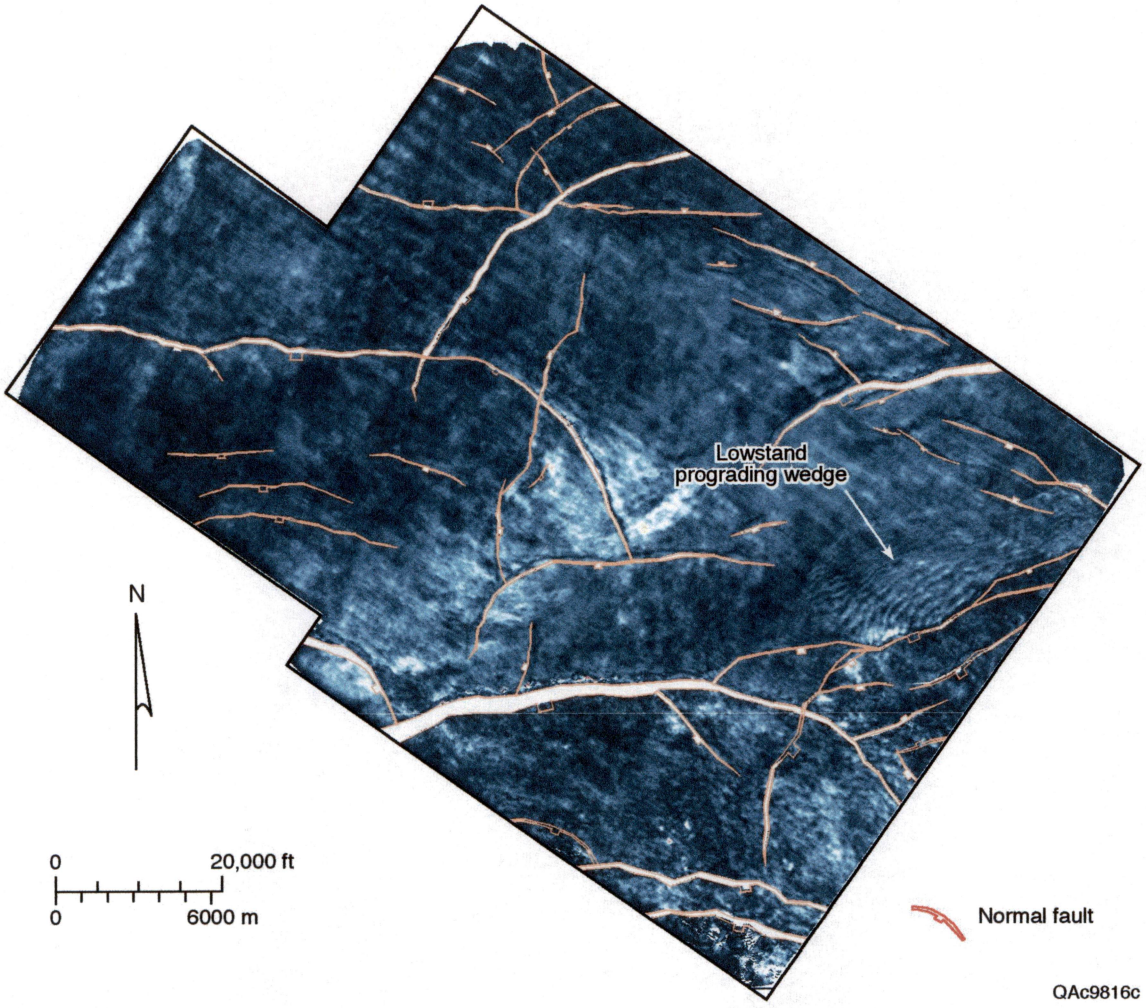

Figure 28. Root-mean-squared (RMS) amplitude map of the S sand reservoir system. The depositional environment is indicative of an early highstand systems tract. Note the "rippling" on the eastern extremity of the study area. These features are commonly associated with progradational/retrogradational depositional systems and should be examined carefully for stratigraphic target potential.

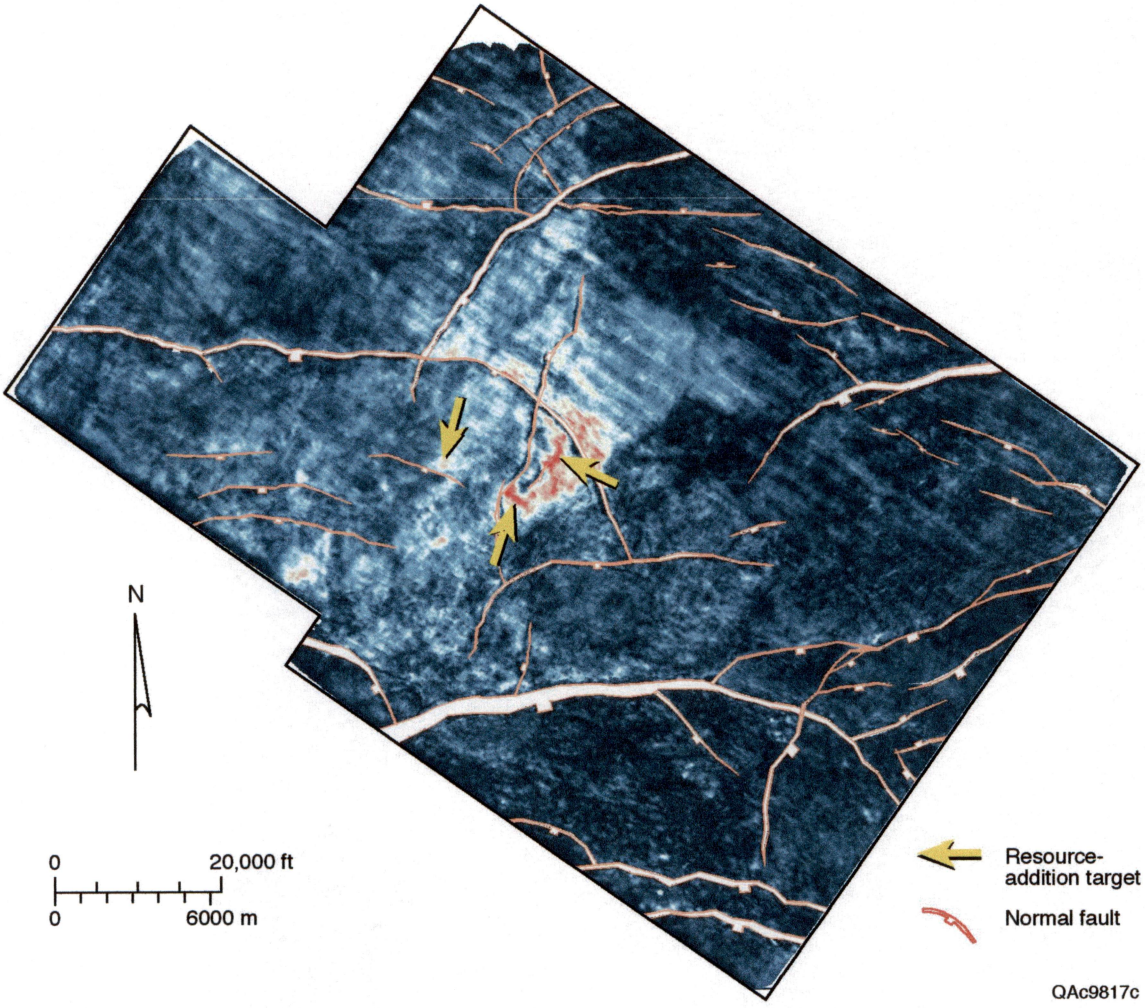

Figure 29. Root-mean-squared (RMS) amplitude map of the T sand reservoir. Note the incised valley system cutting through Tiger Shoal field. The high amplitudes (red) correspond to thick incised-valley-fill sands, which have already been heavily exploited. However, several additional prospects were located by analysis of this map. The eastern half of the study area is interpreted to dominated by deepwater shales.

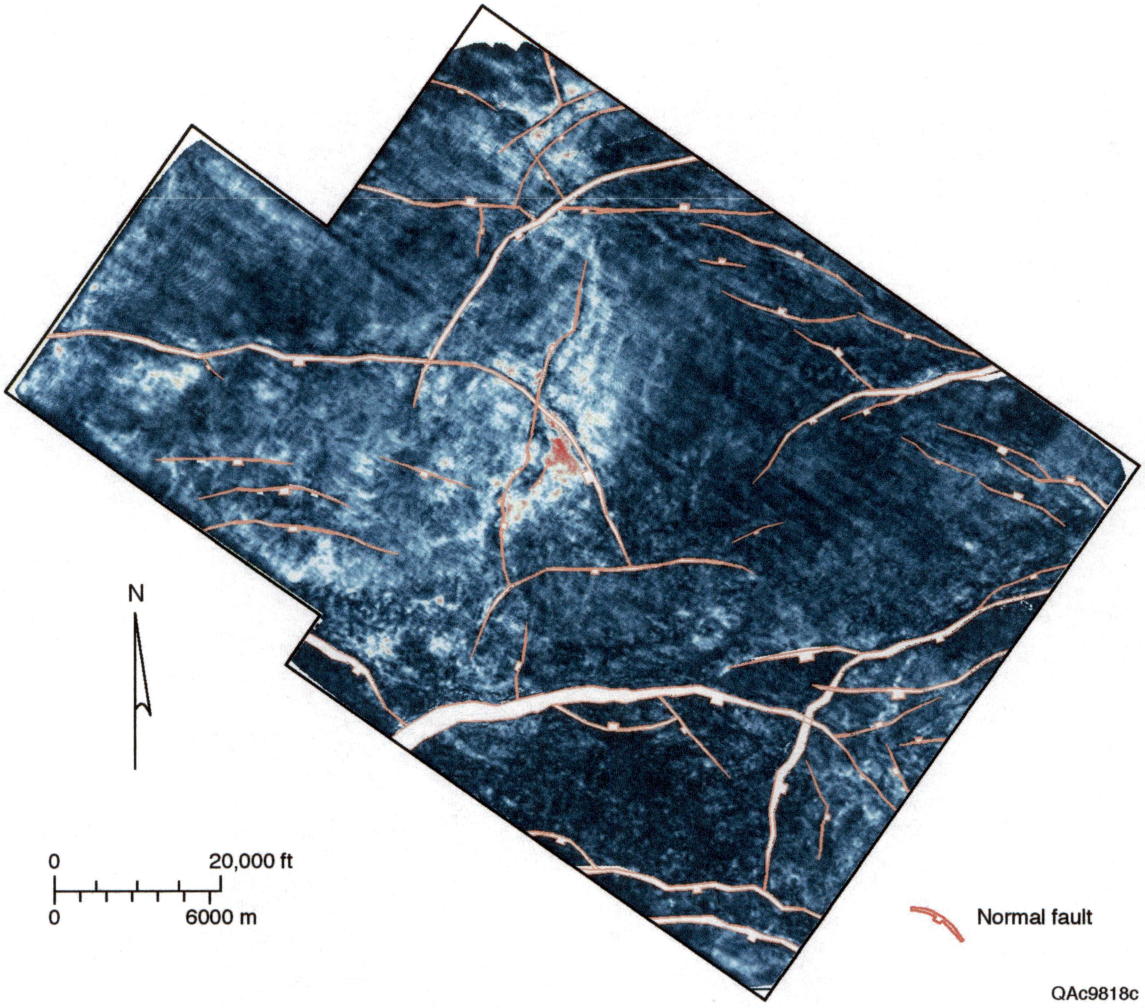

Figure 30. Root-mean-squared (RMS) amplitude map of the U-sand interval illustrating a late lowstand, incised-valley system that caused deposition of the U-sand in Lighthouse and Tiger Shoal fields. Areas outside this incised valley represent the underlying shaly transgressive sequences incised by this valley.

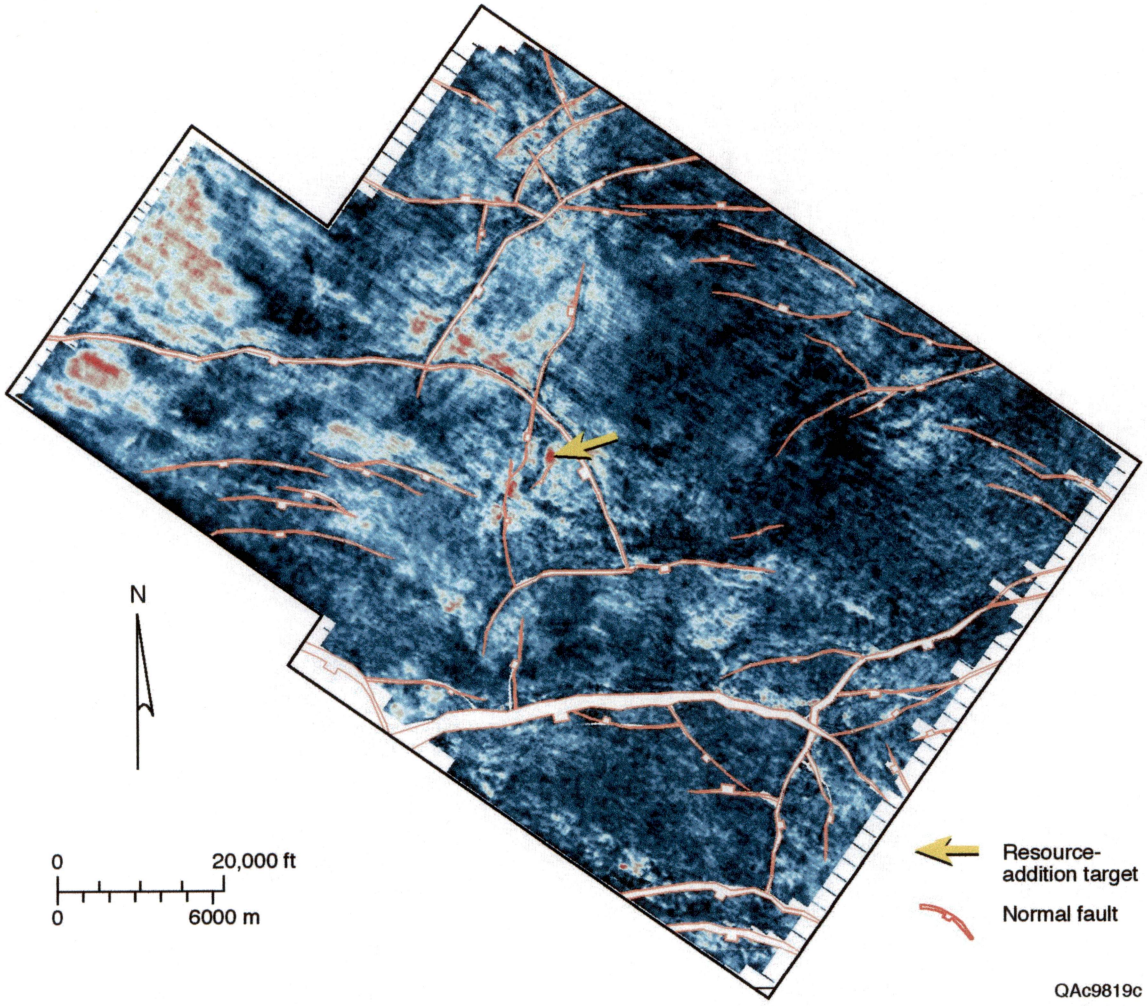

Figure 31. Root-mean-squared (RMS) amplitude map of the V sand that successfully illuminated a prospect in the Tiger Shoal field missed by previous drilling. The strong (red) amplitude characteristics associated with the western half of the study area may outline the extent of the ancient paleoshelf at that time.

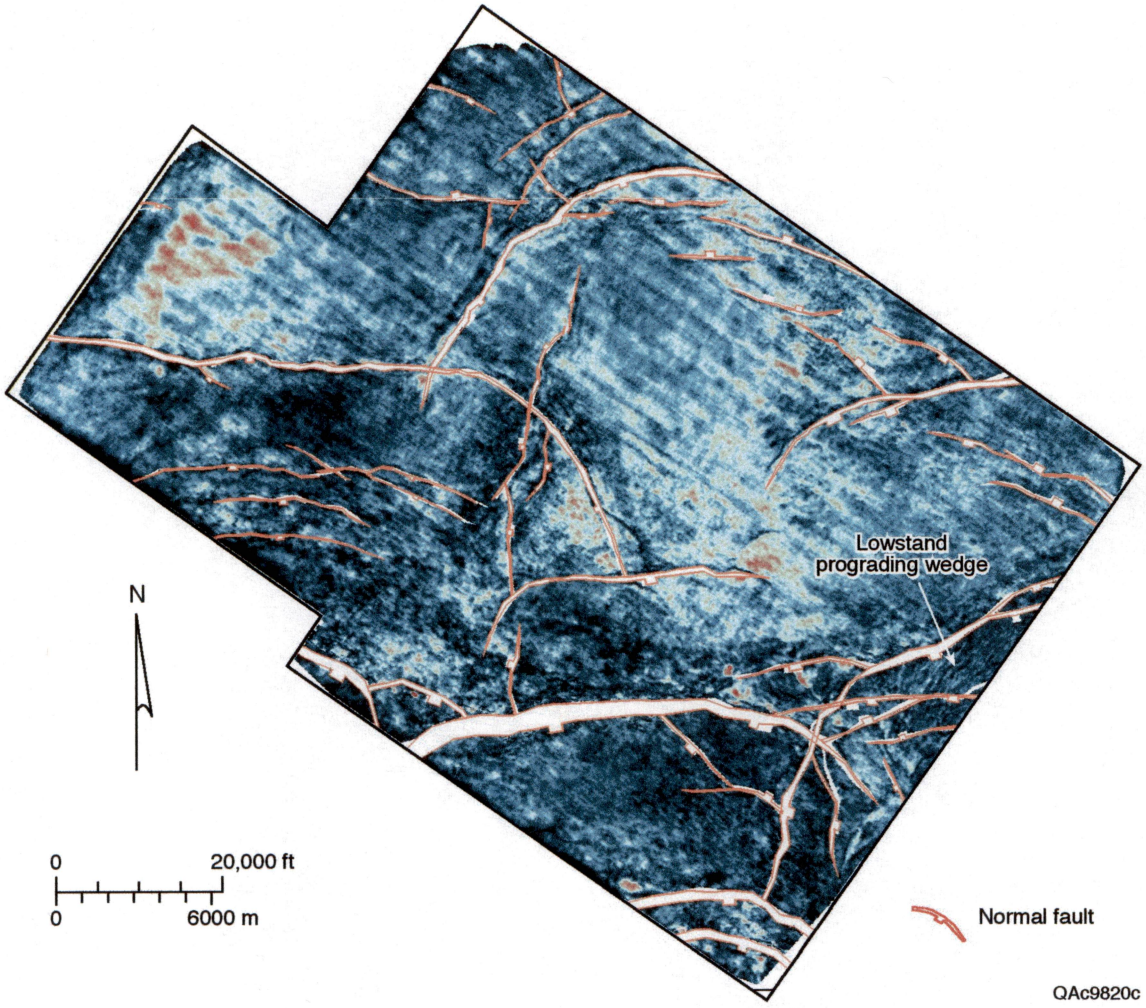

Figure 32. Root-mean-squared (RMS) amplitude map of the X sand reservoir interval illustrating chaotic depositional patters indicative of a highstand/transgressive systems tract, perhaps at its maximum seaward extent. Amplitudes indicate thick sand sequences in the saddle area between Lighthouse and Mound Point fields. Tiger Shoal appears to have some reservoir-quality sands on the eastern flank. Starfak field, however, is dominated by shale. Significant sands should be encountered in the saddle area between Starfak and Tiger Shoal fields.

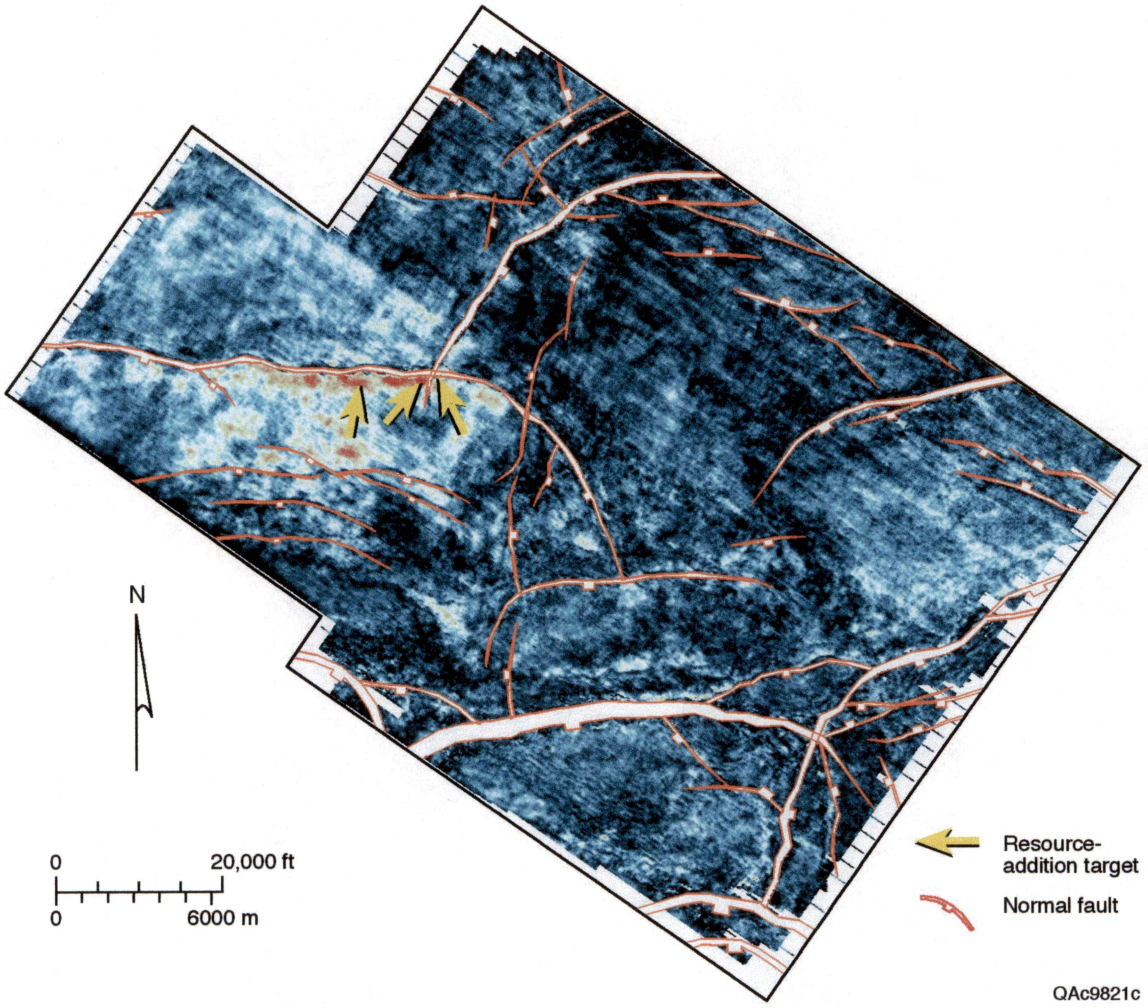

Figure 33. Root-mean-squared (RMS) amplitude map of the Y sand. Strong amplitudes (red) along the hanging wall (downthrown) are associated with rollover structural features and are excellent prospect targets. The remainder of the study area is pervaded by deepwater shale at this interval.

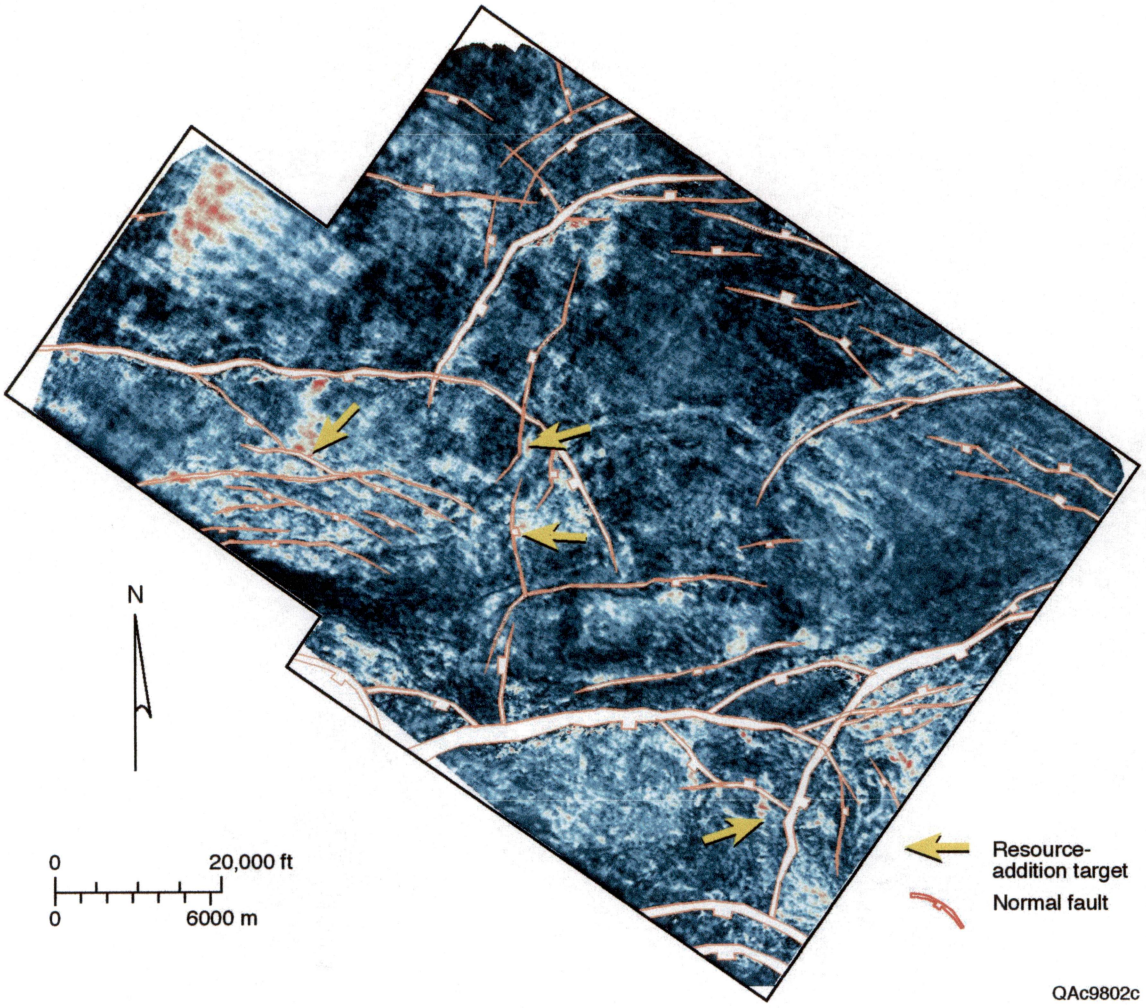

Figure 34. Root-mean-squared (RMS) amplitude map of the 12000A sand illustrating a prominent lowstand deltaic wedge within Starfak field. Note the second-order, east-west-trending faults that cut the wedge. Prospects (arrows) were identified by high-amplitude (red) anomalies imaging geological features (deltas, meanders, etc.) that were missed by previous drilling programs.

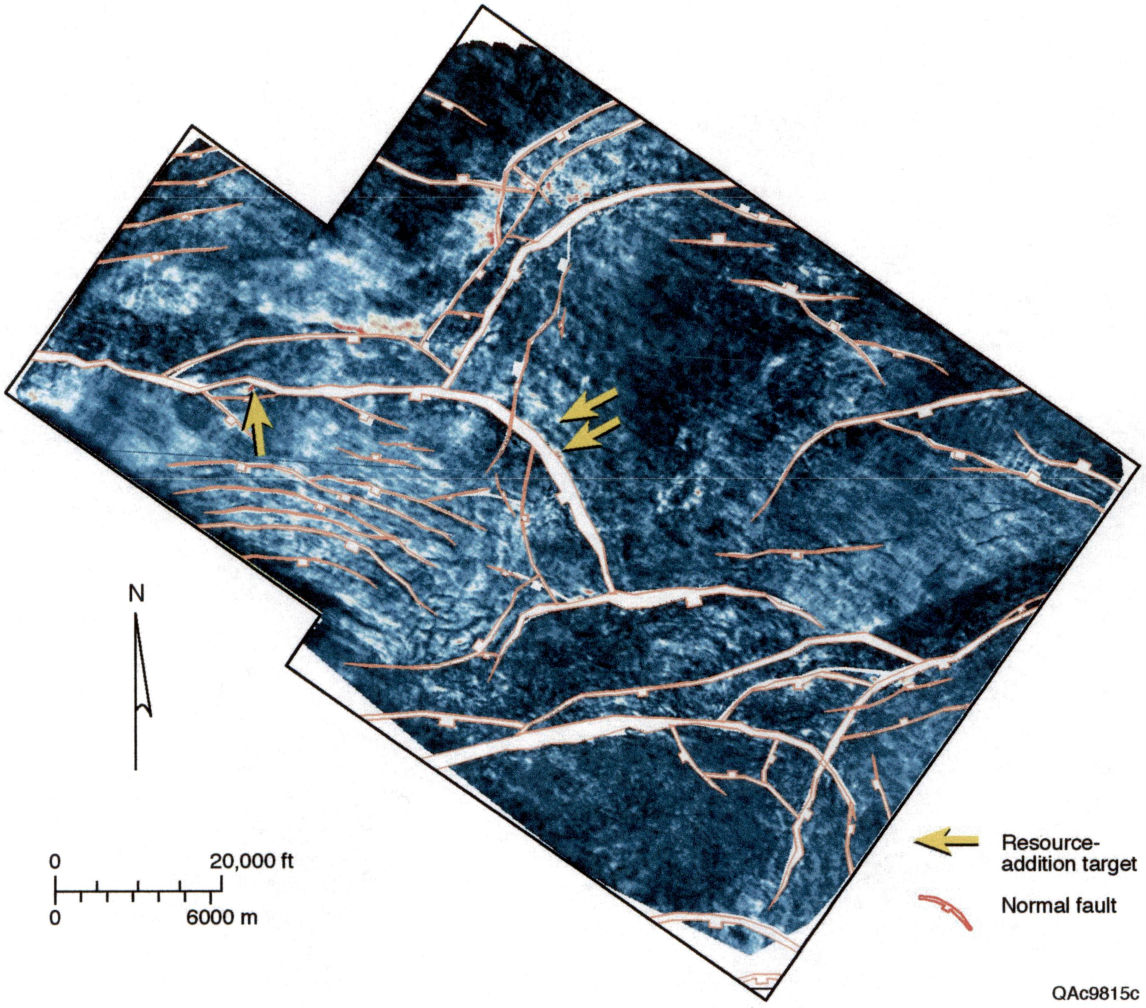

Figure 35. Root-mean-squared (RMS) amplitude map of the deep *Robulus* 2 sand interval illustrating a prograding wedge commingled with second-order faults. This feature is a classic stratigraphic target; however, amplitudes at this level do not necessarily correspond to the level of reservoir sand quality as with shallower intervals. Note the complexity of the structure increases with depth, where first-order fault offset increases dramatically and associated second-order faulting increases as a result.

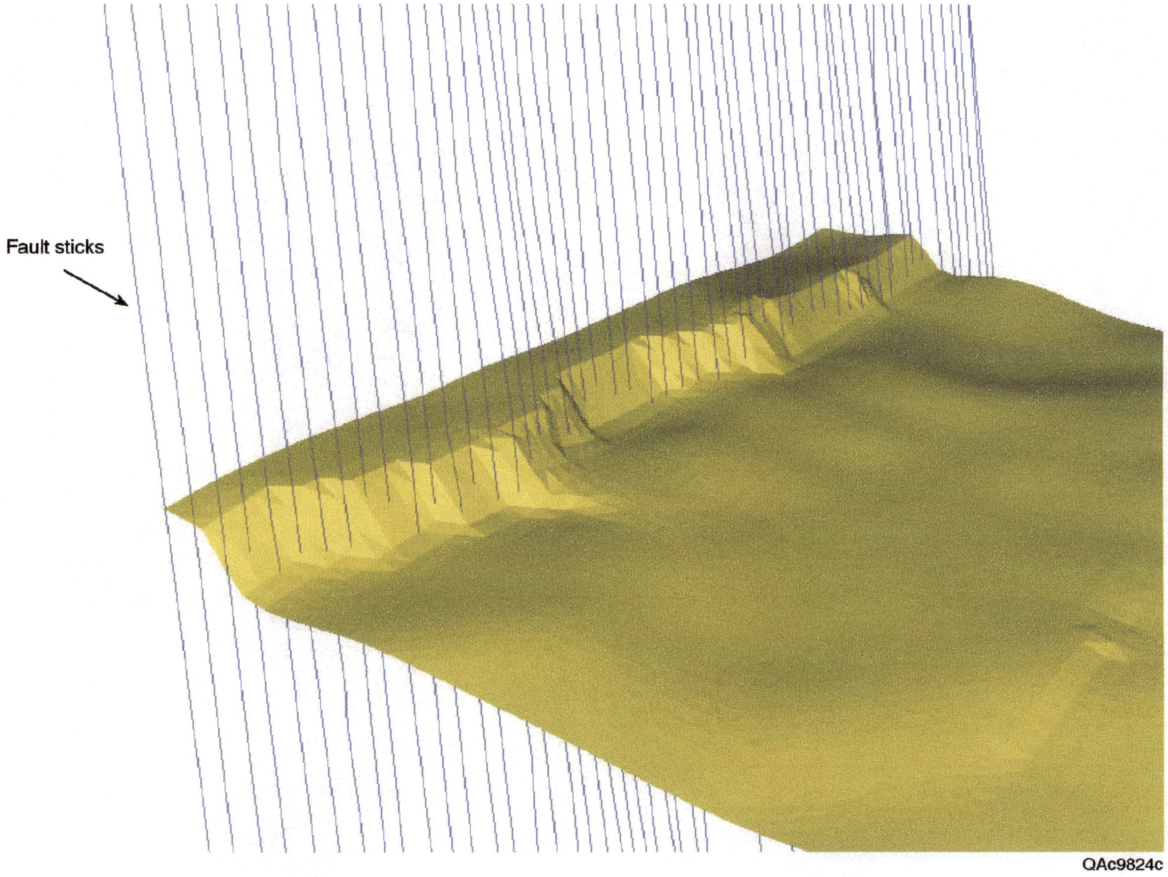

Figure 36. Depth fault sticks for the EW4 fault showing penetration through the MFS30 surface.

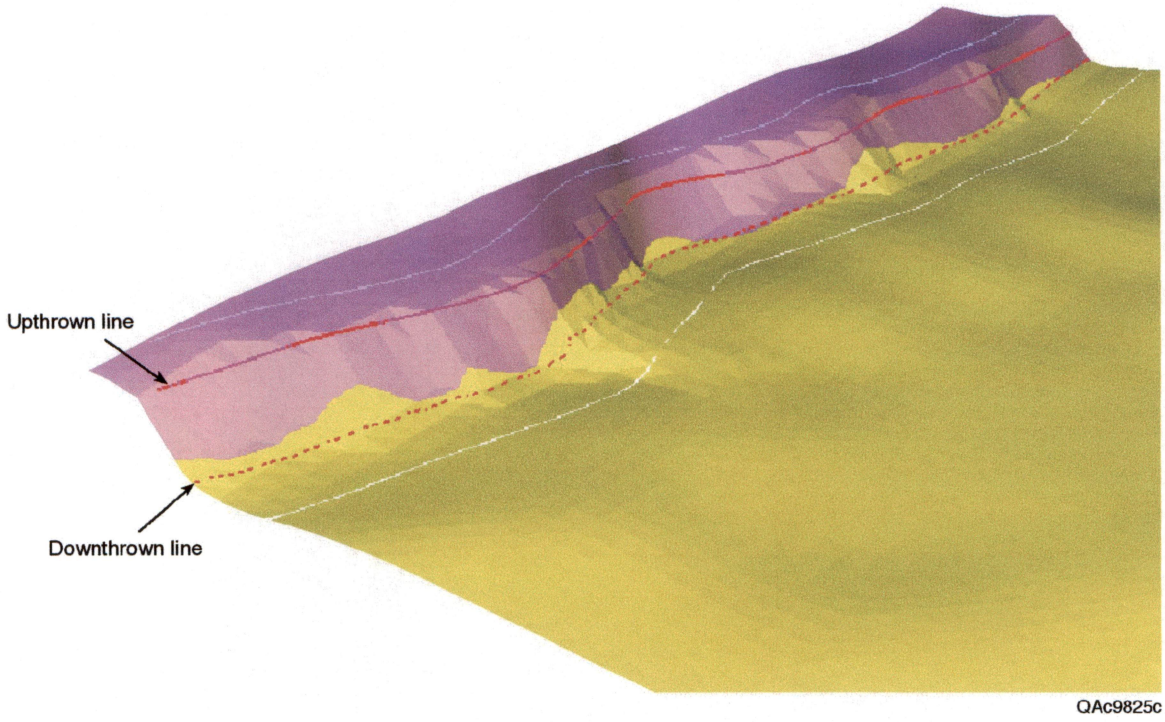

Figure 37. Derivation of MFS30 fault lines for EW4 by extrapolating the associated cutoff lines (white) onto to the fault surface.

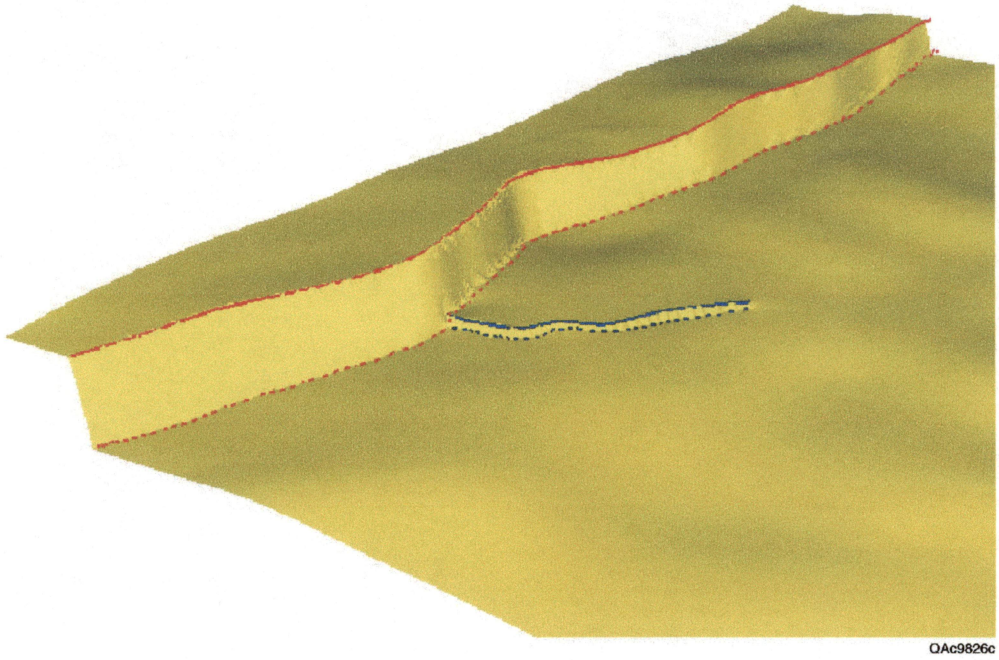

Figure 38. Results of truncating fault D2 (blue) against the first-order fault EW4.

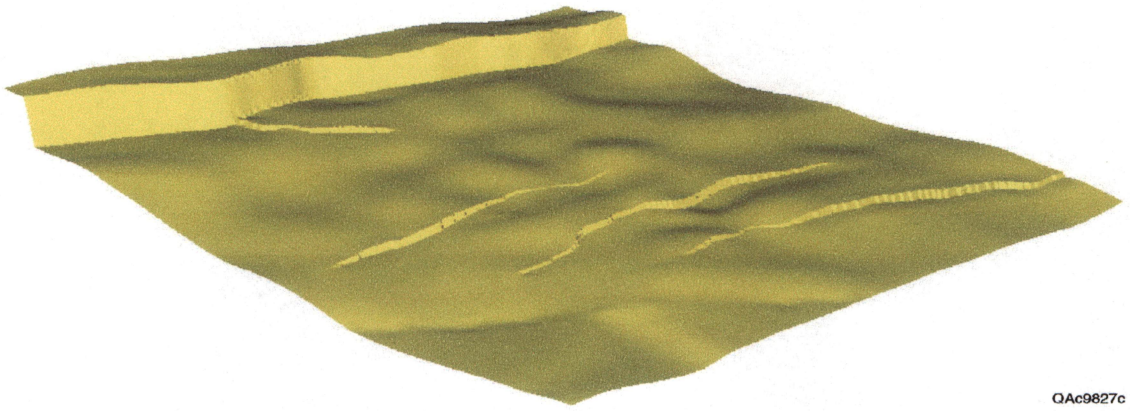

Figure 39. Interpolated and quality-checked MFS30 structural surface that is consistent with both the fault model and the surface picks from well logs.

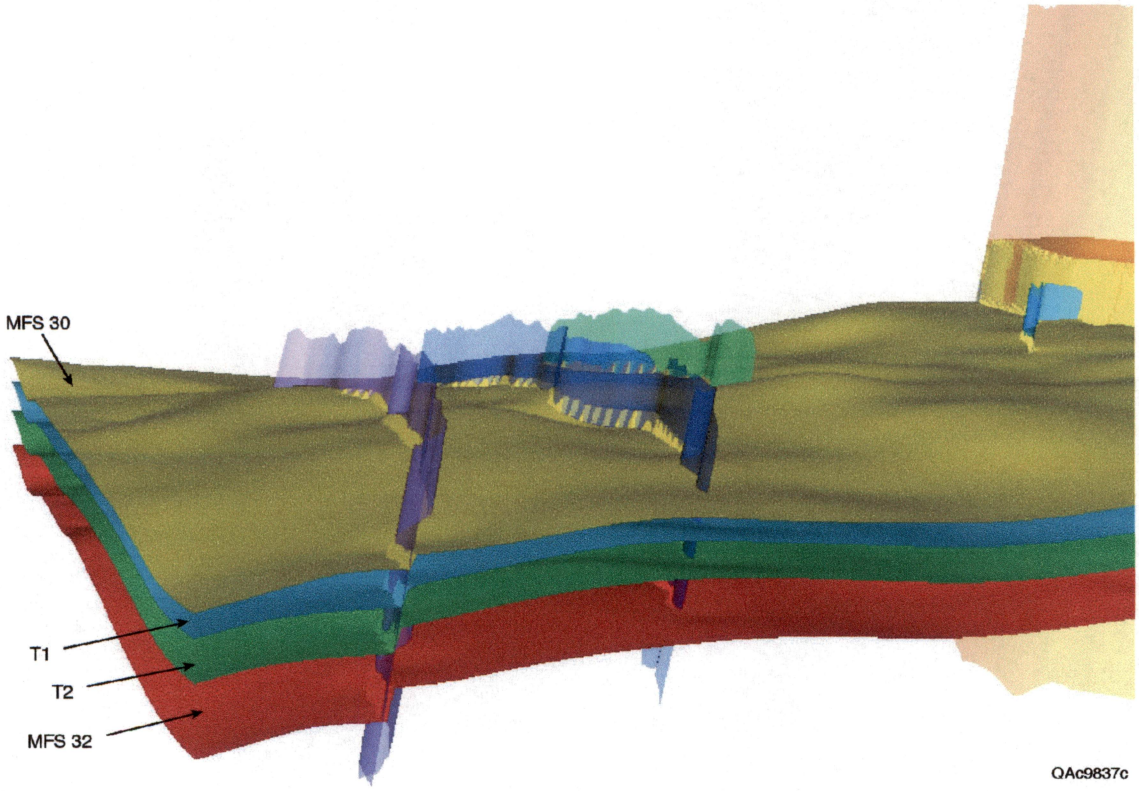

Figure 40. Revised MFS30 and MFS32 surfaces used for stratigraphic modeling inputs.

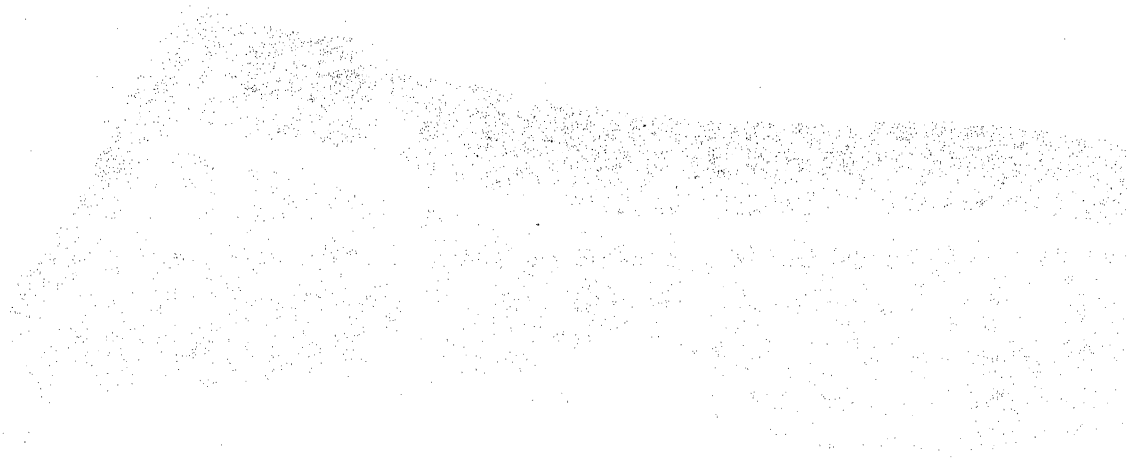

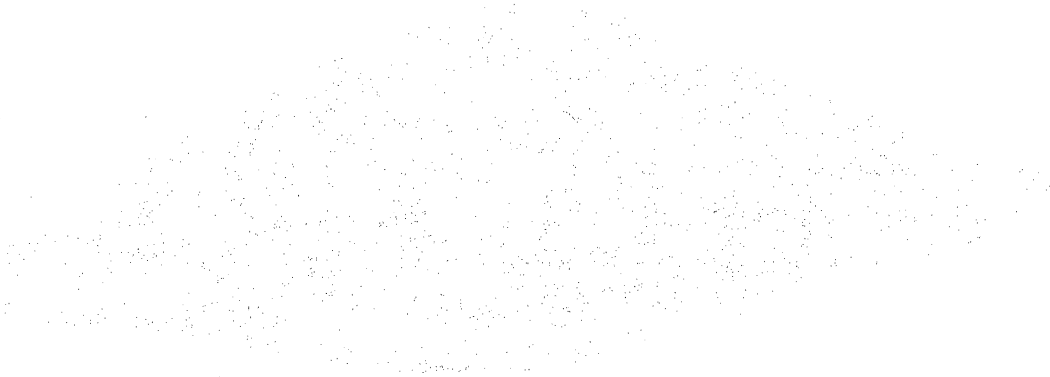

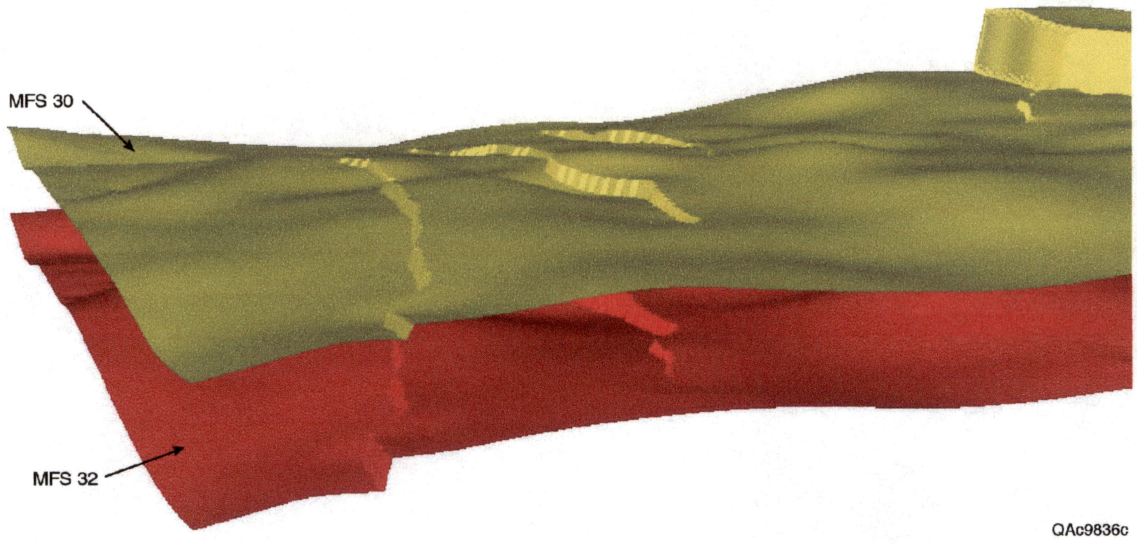

Figure 41. Final MFS30, T1, T2, MFS32 surfaces used for stratigraphic modeling inputs.

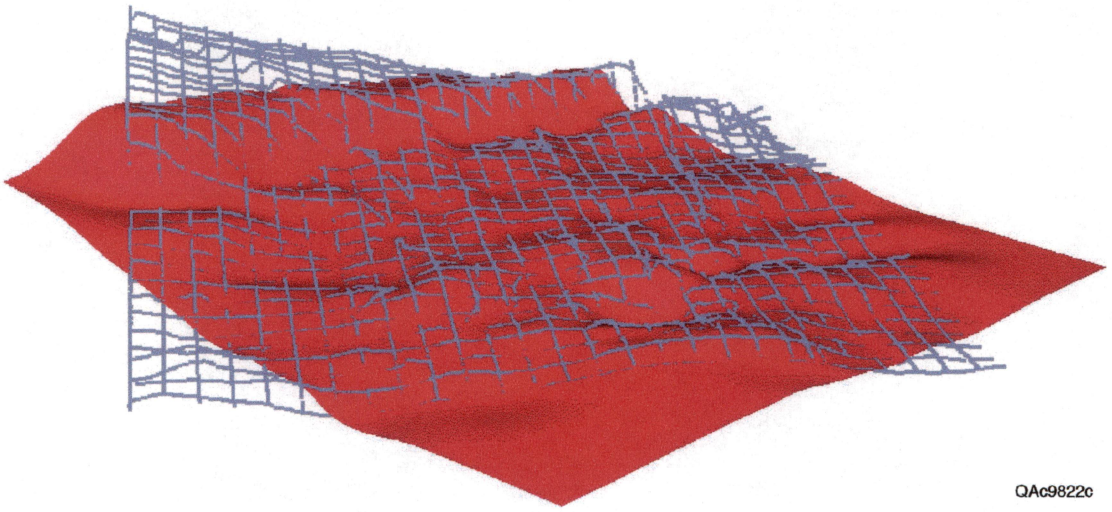

Figure 42. T1 surface (gray) picked from the 3-D seismic shown overlain on the T1 seismic surface.

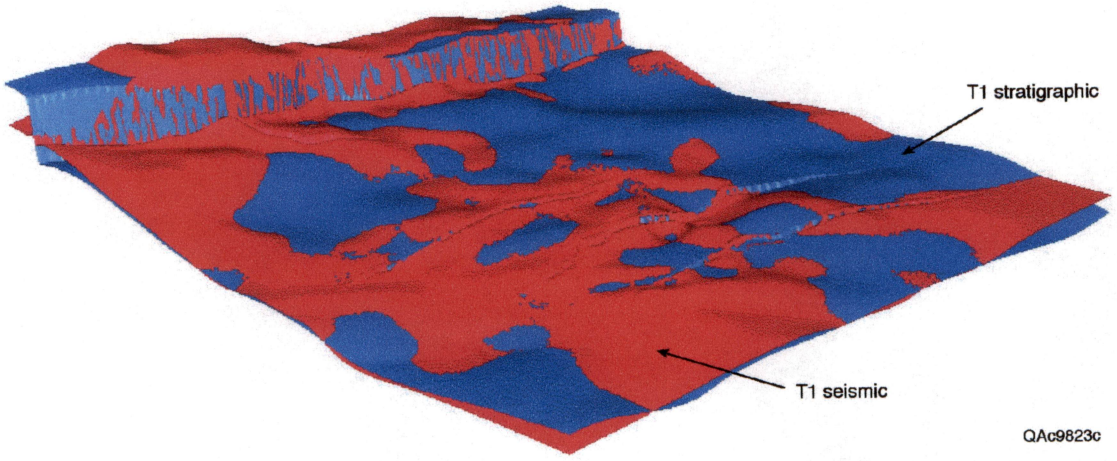

Figure 43. Stratigraphically calculated versus seismically interpreted T1 surface showing the differences between the two approaches.

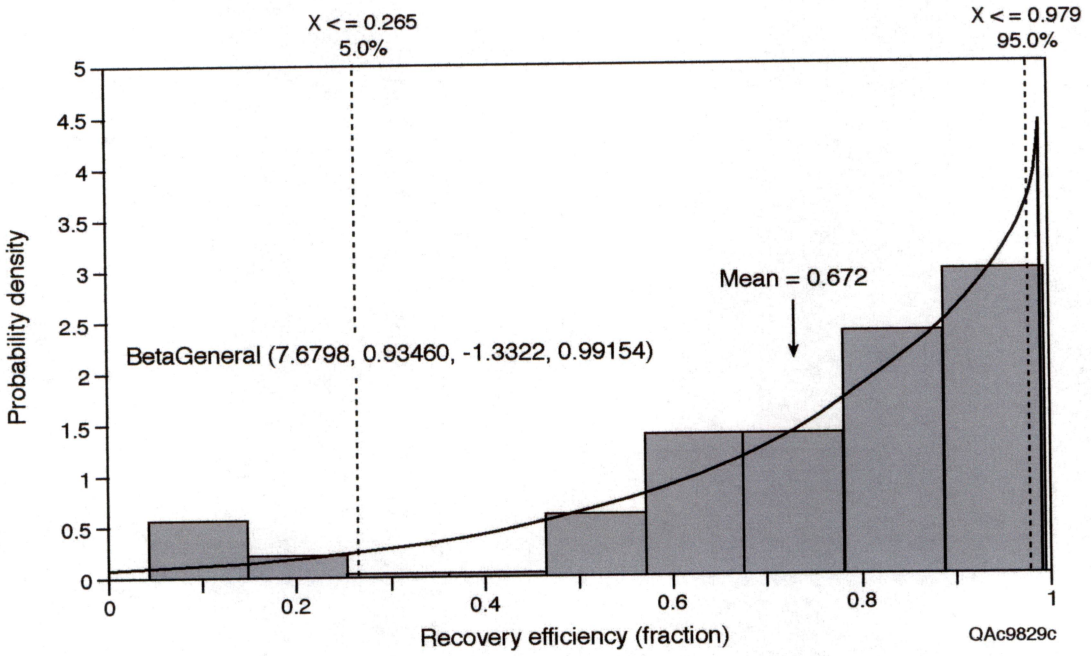

Figure 44. Pressure-depletion, gas-reservoir, ultimate-recovery efficiency for U.S. reservoirs based on data from the Department of Energy's Gas Information System (GASIS) database.

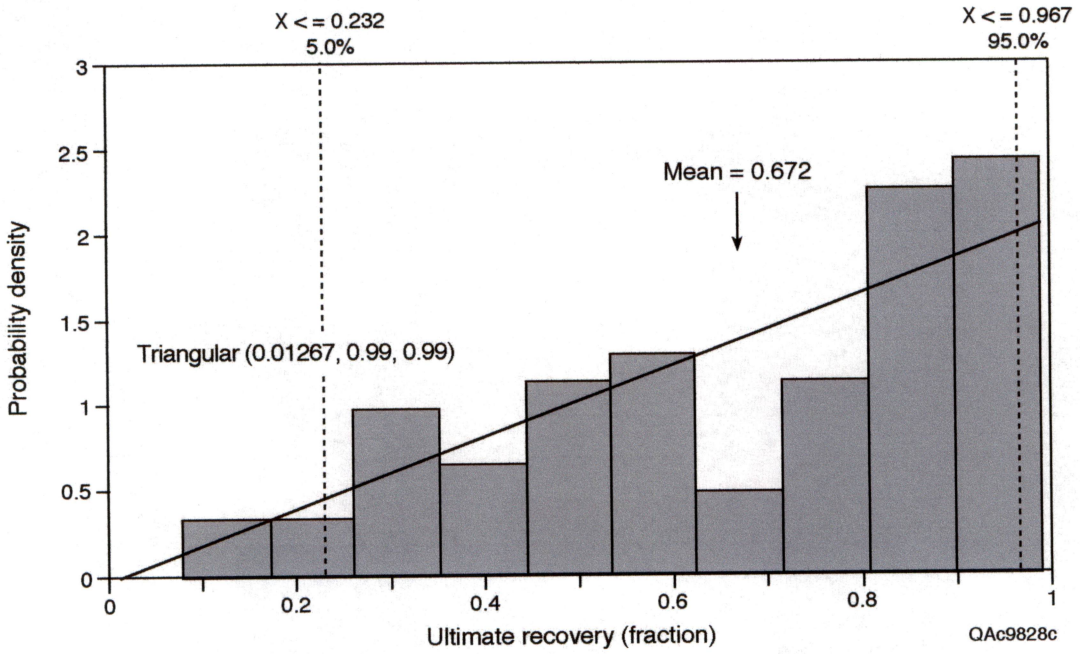

Figure 45. Aquifer-drive, gas-reservoir, ultimate-recovery efficiency for U.S. reservoirs based on data from the Department of Energy's Gas Information System (GASIS) database.

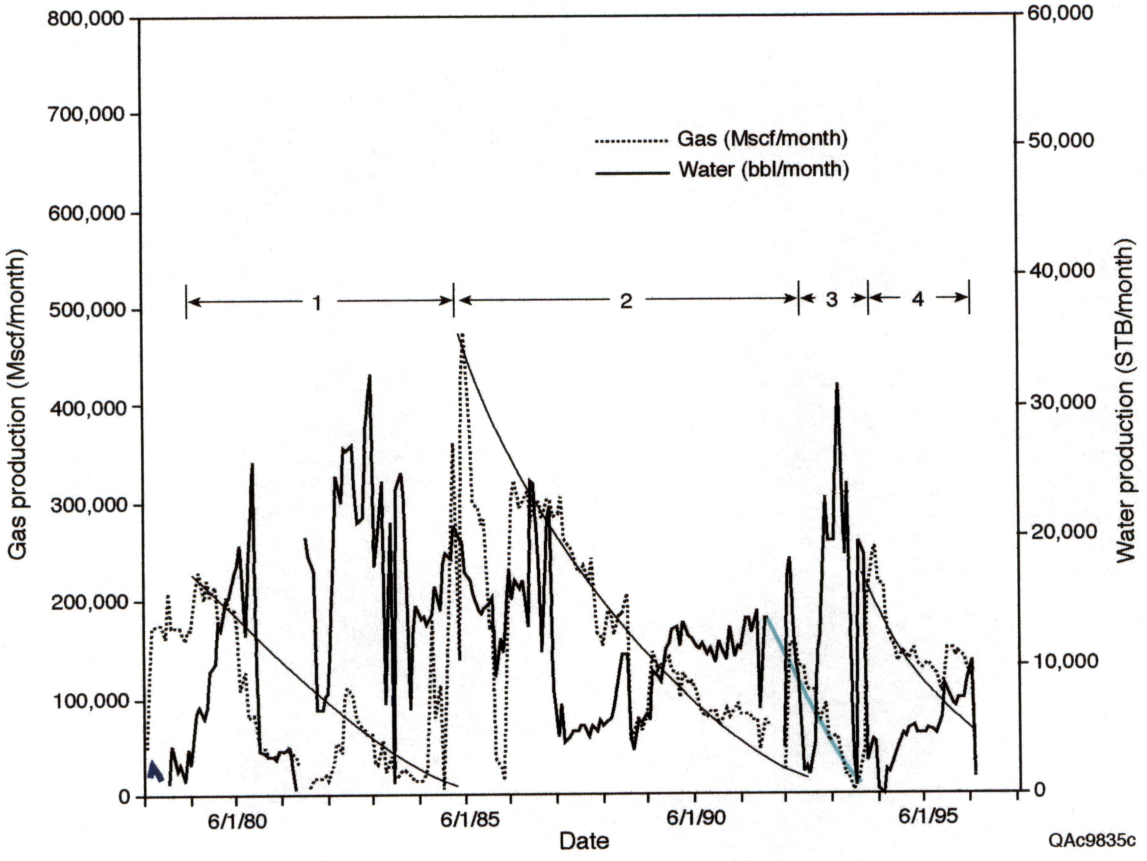

Figure 46. Production history of the Starfak T1 reservoir showing multiple pulses of decreasing gas production rate and increasing water production rate.

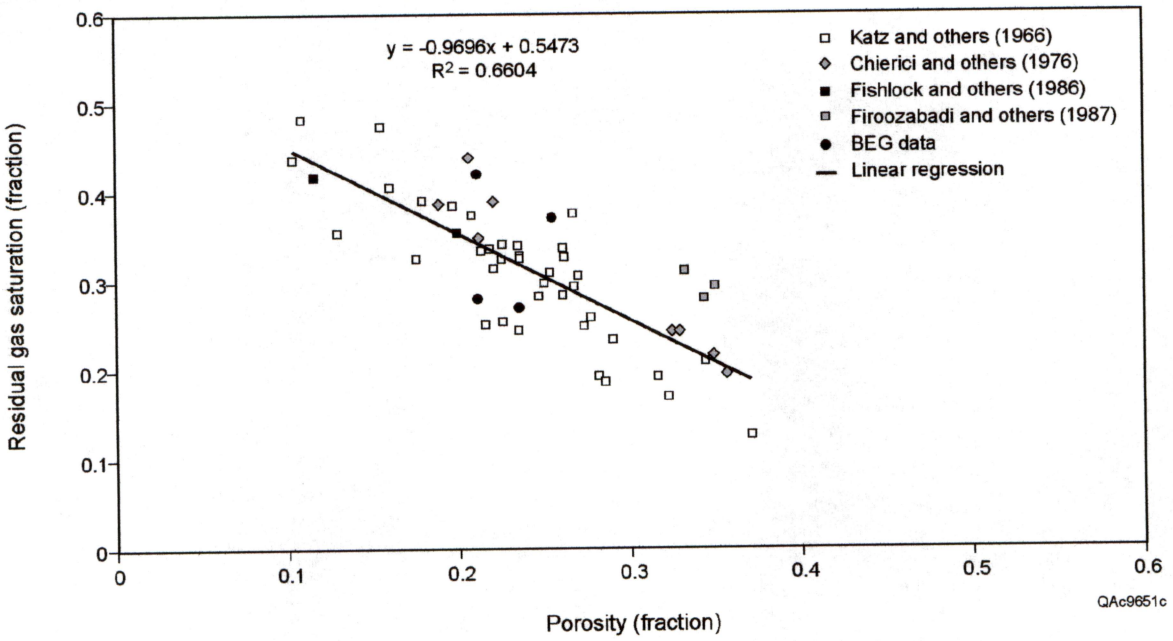

Figure 47. Residual gas saturation can be predicted from porosity and can therefore be varied throughout a 3-D geocellular model.

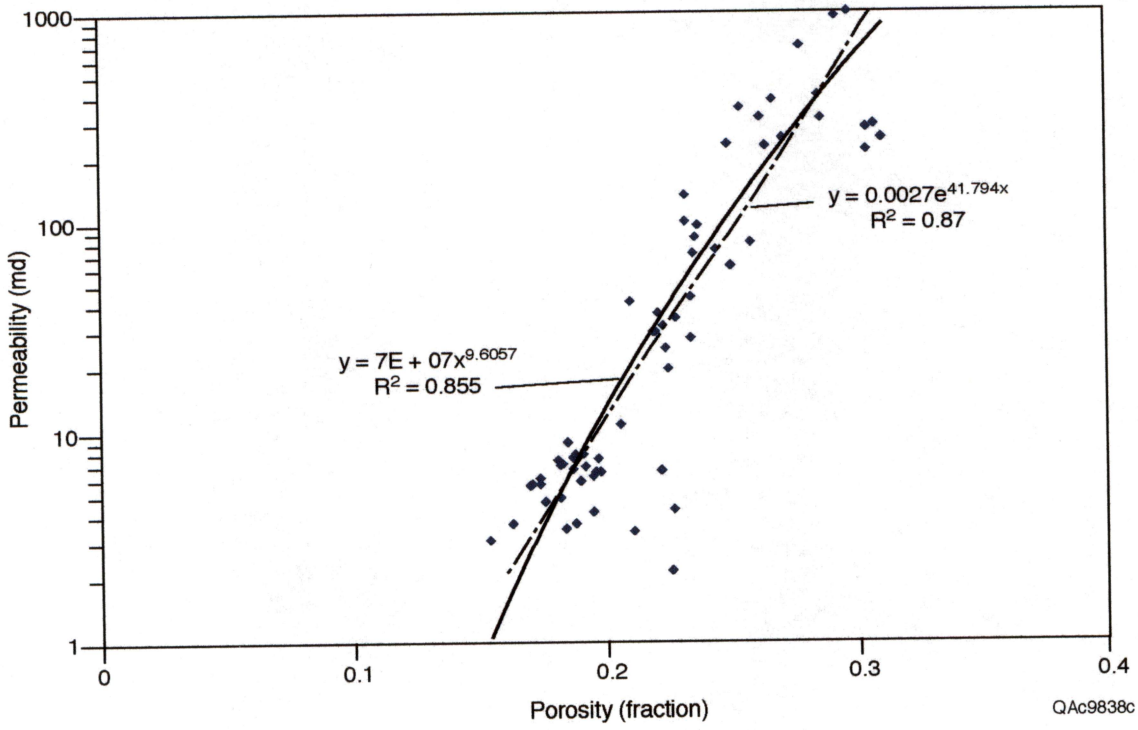

Figure 48. Ambient condition porosity displays a strong correlation with permeability.

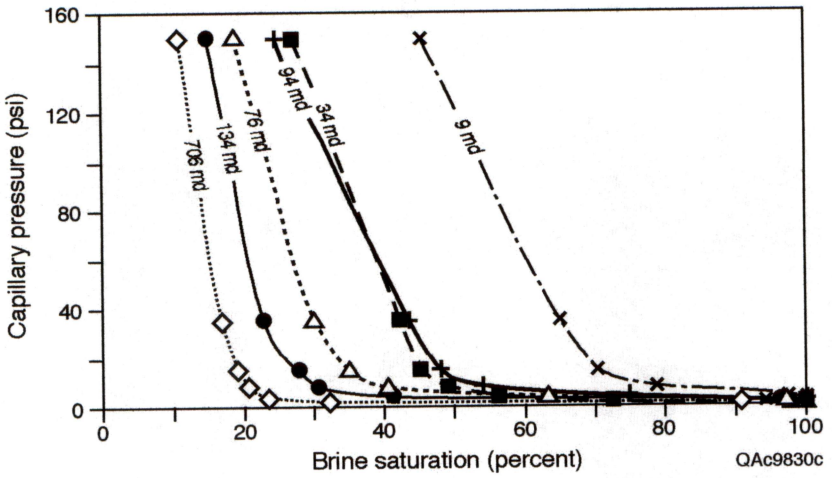

Figure 49. Capillary pressure character displays a correlation with permeability.

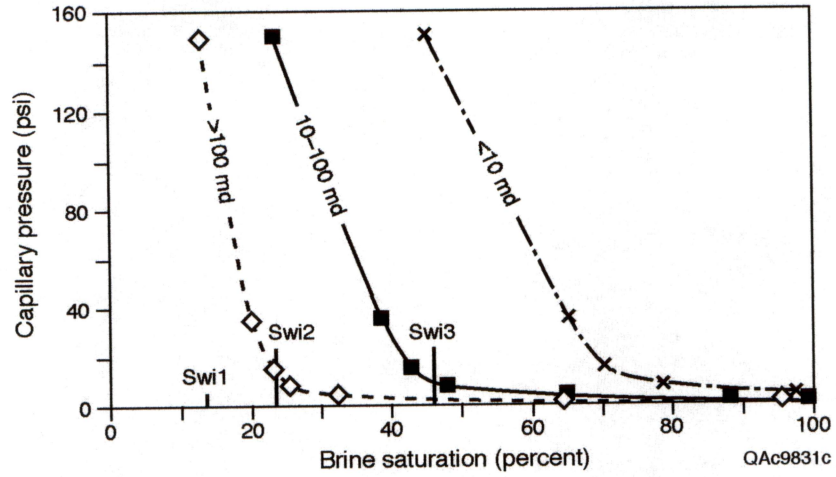

Figure 50. Average capillary pressure curves displaying the variation of irreducible water saturation with permeability.

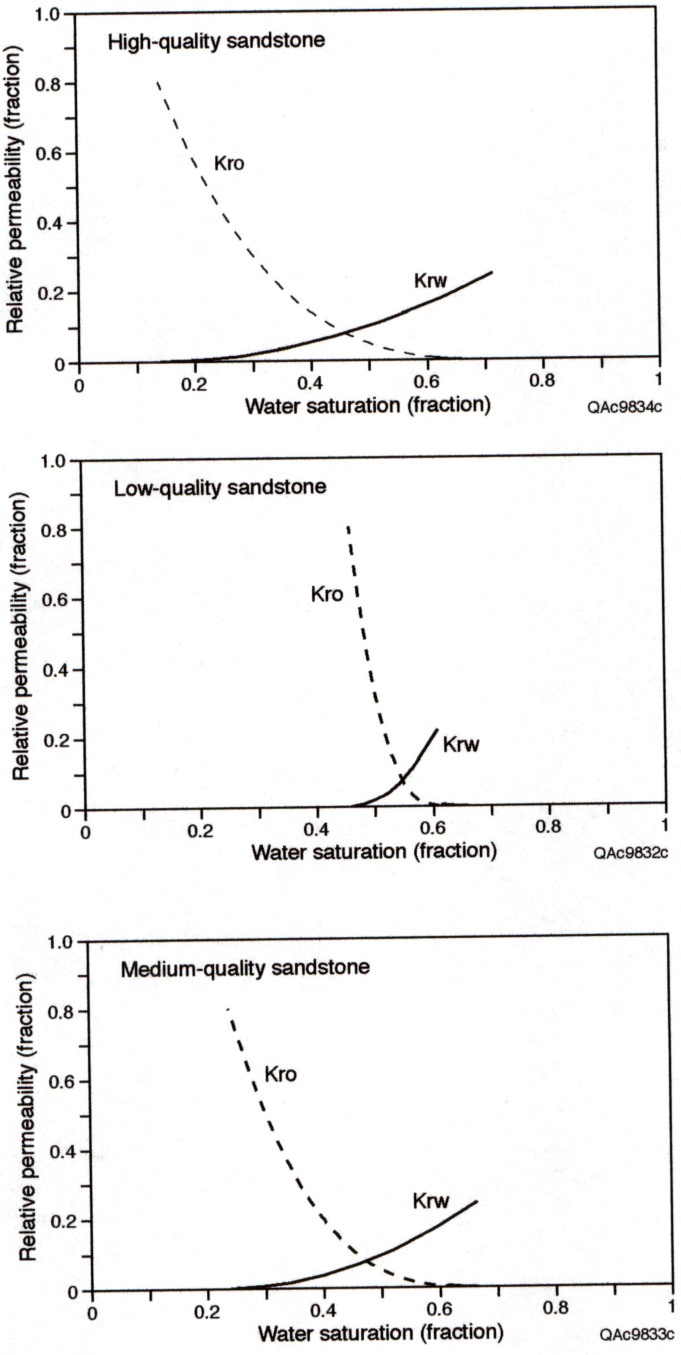

Figure 51. Relative permeability curves for each of the three rock-quality classes: (a) low quality, (b) medium quality, and (c) high quality.

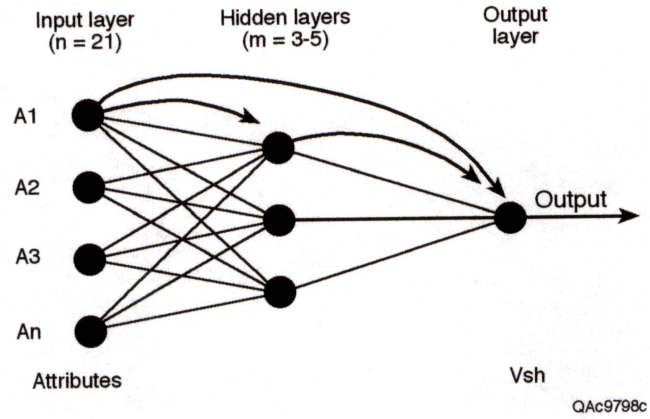

Figure 52. Generalized forward-feed model used in the neural network training for this study.

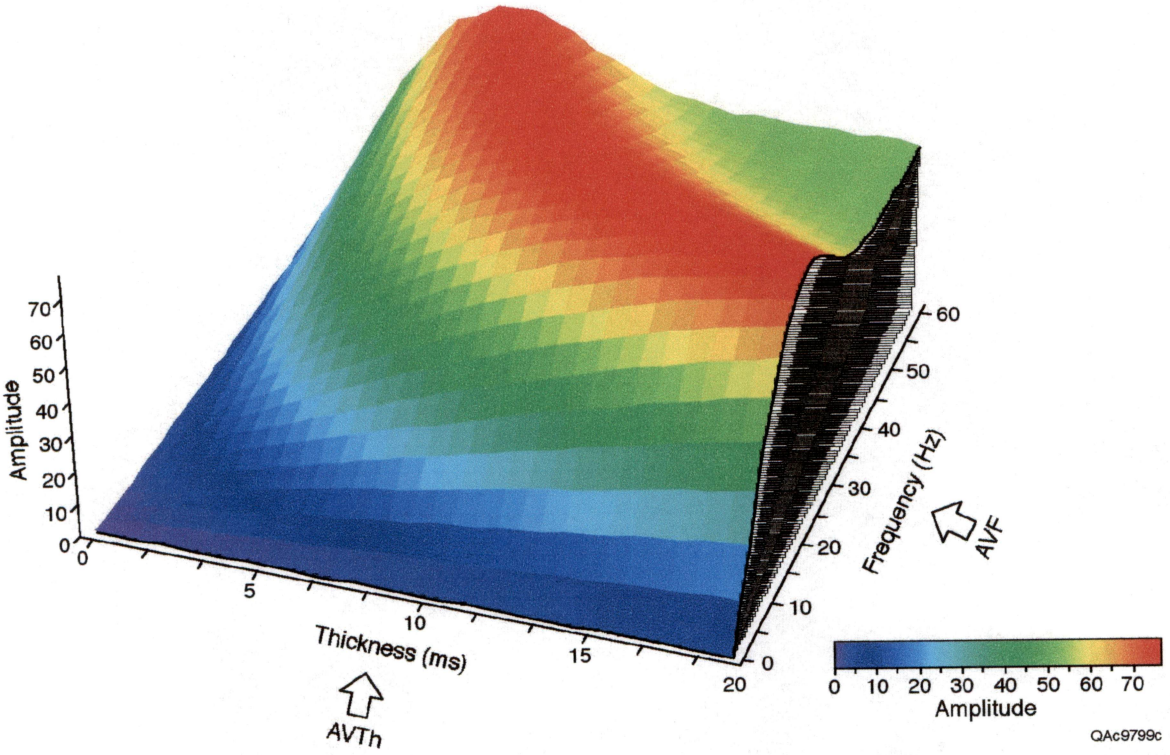

Figure 53. Seismic amplitude as a function of thickness (AVTh) and frequency (AVF).

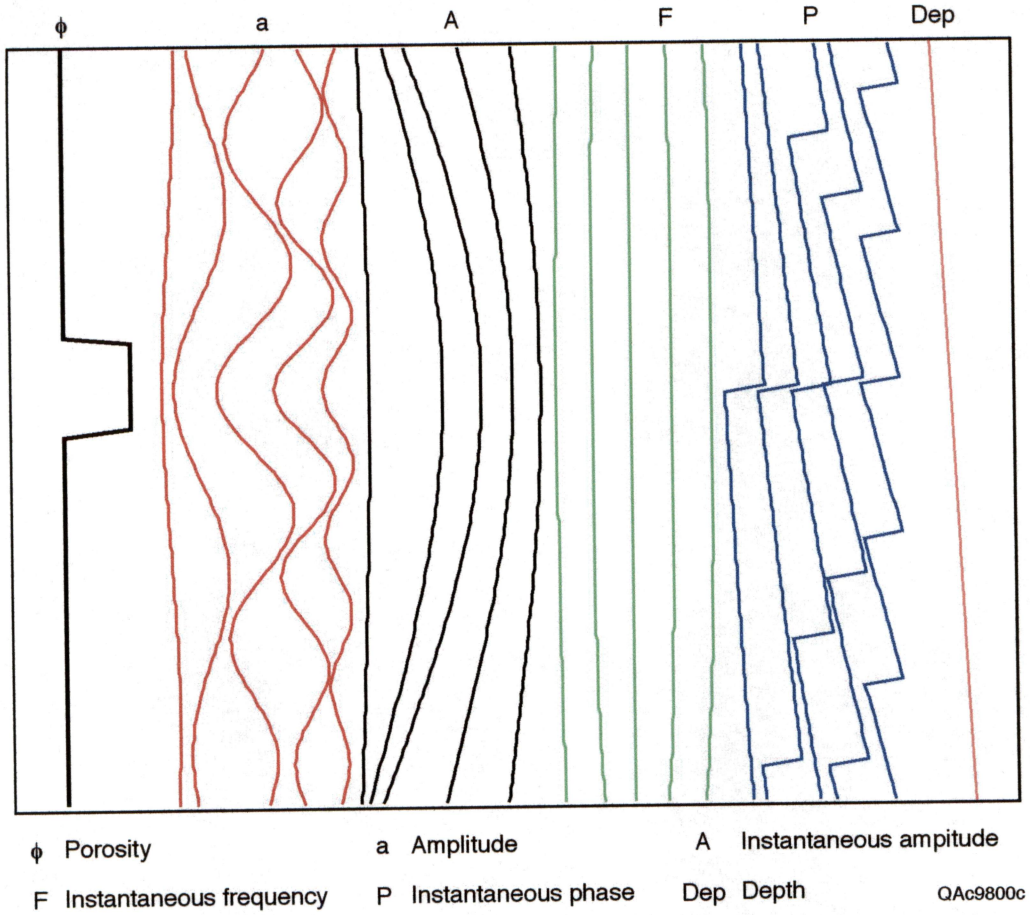

Figure 54. A synthetic example of multiple seismic attributes generated by panel-filtering of seismic data.

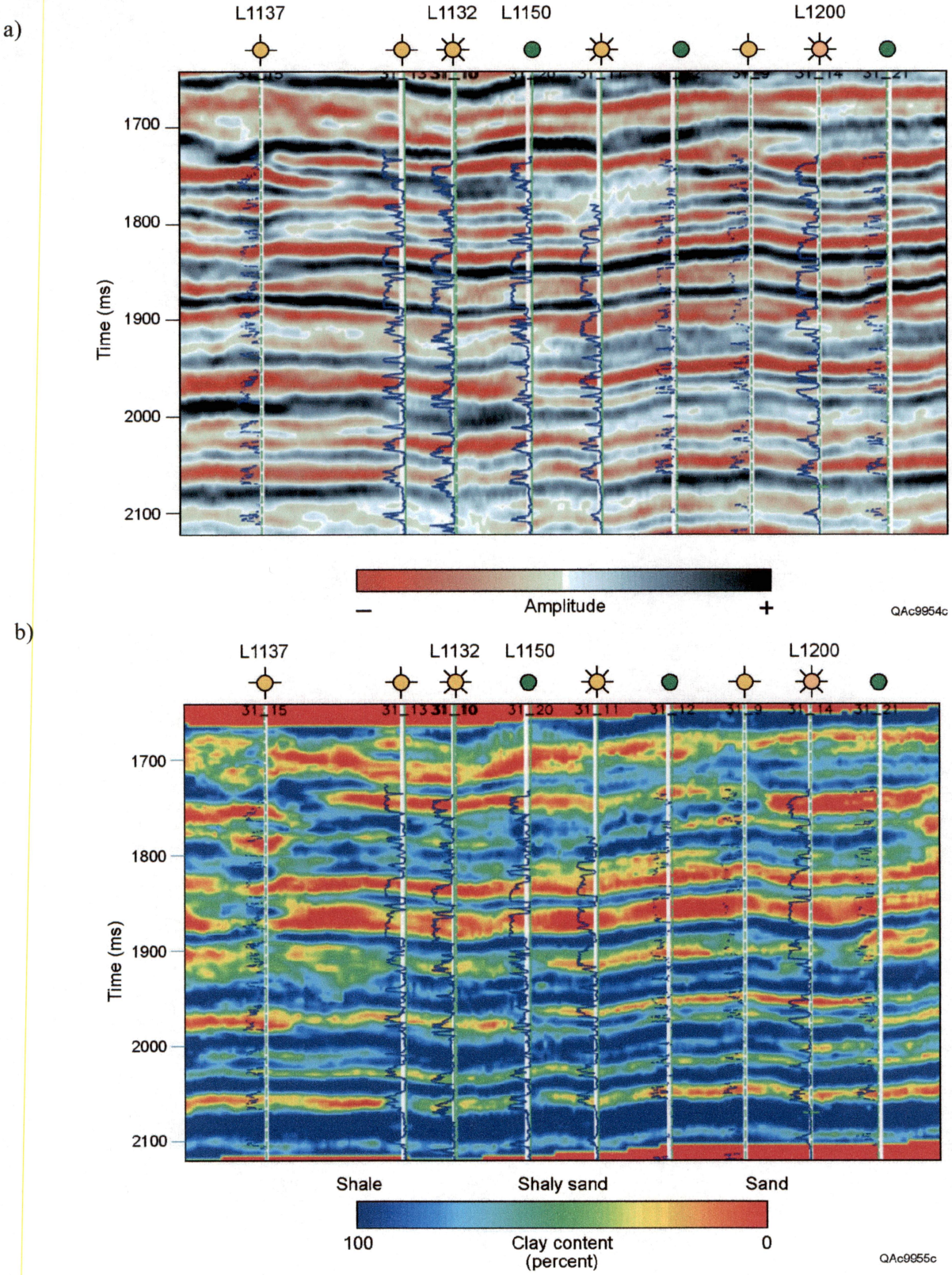

Figure 55. Neural network-assisted log property (Vsh) inversion. (a) Original seismic data section tied to nine wells in A-H sand interval. (b) Same section after inversion.

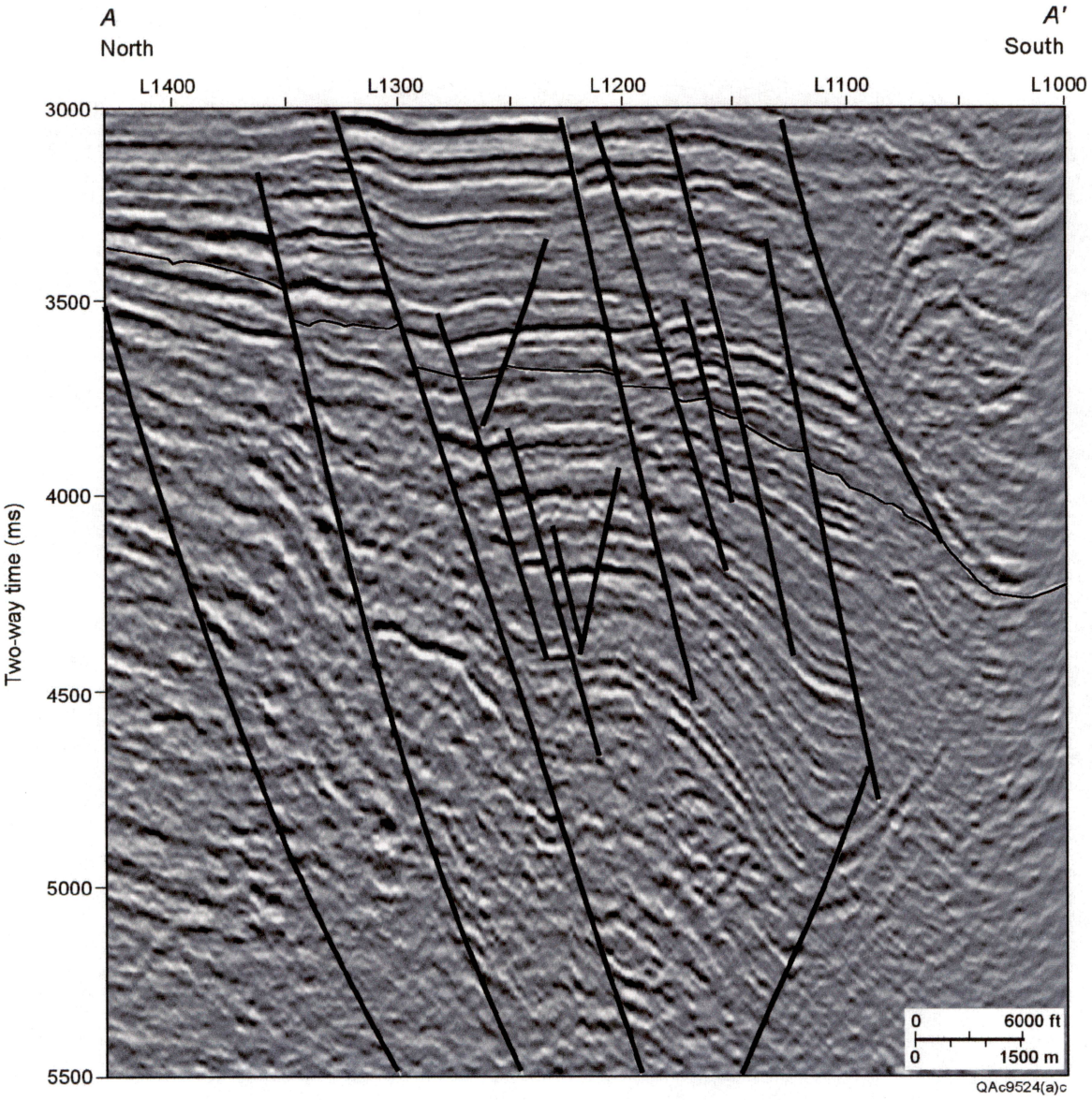

Figure 56. Seismic line with location shown in figure 57 that illustrates the structural nature of the sections below 3.0 s (approximately below 15,000 ft subsea). Several large deep structural closures exist. Reservoir facies are middle-to-late Miocene-age deep marine fan and slope deposits. The black horizon represents approximate top of overpressure conditions.

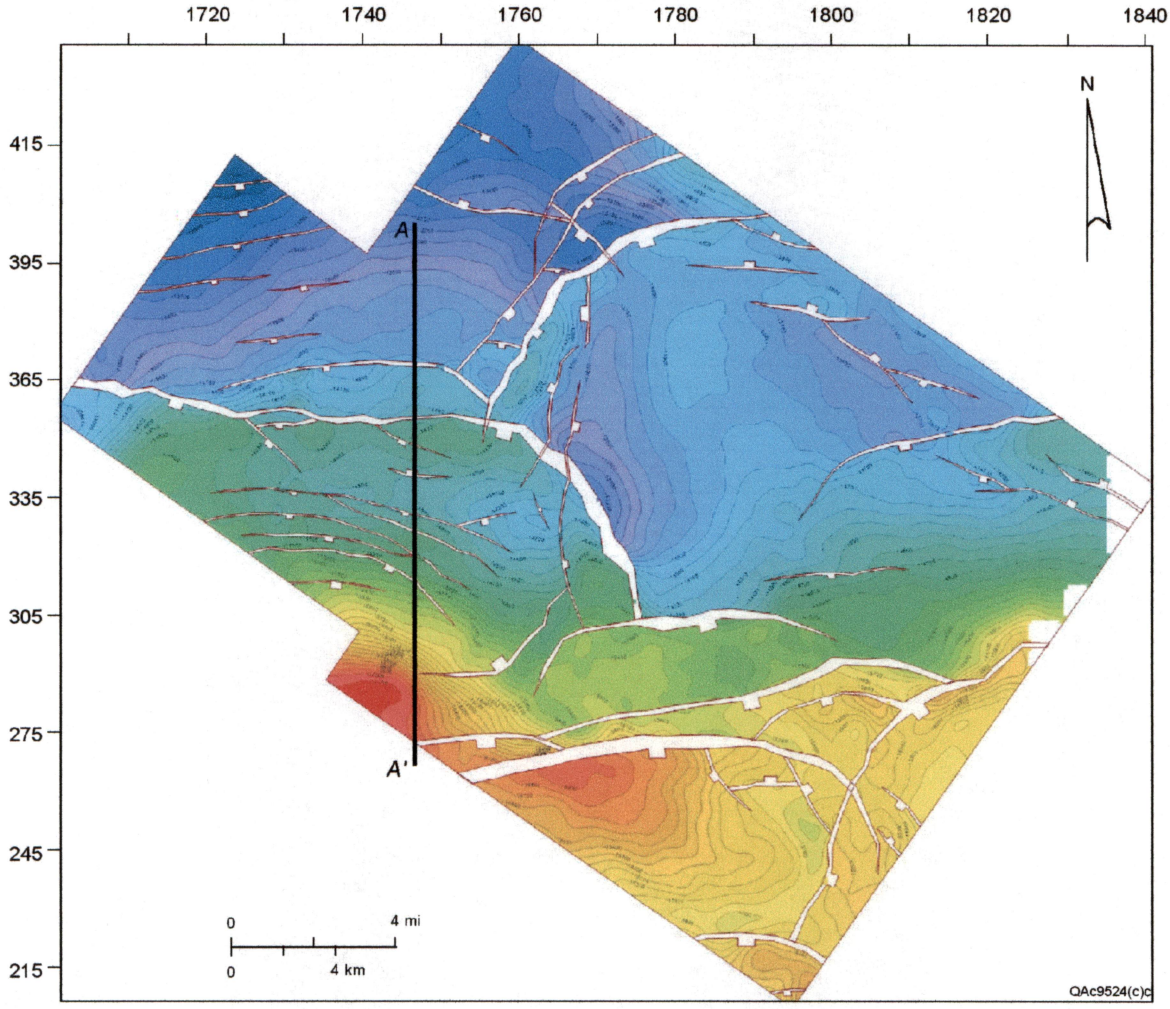

Figure 57. Structure map of maximum flooding surface (MFS) 48 and well below 15,000 ft, showing several deep structural closures. Secondary fault swarms form multiple deep fault traps and untested fault blocks. Seismic section A–A' is shown in figure 56.